Yash Tambi | MSc. Sustainable Energy Technology | May 2019

Exergy-Gravimetric Design Approach to Determine Optimal Fuel Cell – Battery Hybrid Powerplant Configuration for All-Electric 2-Seater Aircraft

Hybrid Powerplant Design for Pipistrel Alpha-H_2

TU Delft

Exergy-Gravimetric Design Approach to Determine Optimal Fuel Cell - Battery Hybrid Powerplant Configuration for an All-Electric 2-Seater Aircraft

Hybrid Powerplant Design for Pipistrel Alpha-H_2

by

Yash Tambi

to obtain the degree of Master of Science
at the Delft University of Technology,
to be defended on Wednesday May 29, 2019 at 8:30 AM.

Faculty of Electrical Engineering, Mathematics and Computer Science

Faculty of Mechanical, Maritime and Materials Engineering

Student number: 4723708

Project duration:	August 1, 2018 – May 29, 2019	
Thesis committee:	Assc. Prof. Dr. P.V. Aravind,	Main supervisor
	Prof. Dr. D. J. E. M. Roekaerts,	Committee member
	Assc. Prof. Dr. Nandini Bhattacharya,	Committee member
	Dr. Vikrant Venkataraman,	Supervisor
	Ir. Theo. Woudstra,	Supervisor

This thesis is confidential and cannot be made public until May 31, 2024.

TU Delft

Abstract

As all industries move towards sustainable fuels to reduce emissions, aircraft industry is still at its nascent stages. The adoption of clean energy sources has been slow particularly due to low energy density of commercially available batteries, and high volumetric density of hydrogen as a fuel. Electric aircrafts have been demonstrated but only a few are available commercially. Hydrogen powered flights have also been demonstrated, but only for experimental purposes. As the move towards clean aviation furthers, it is necessary to indicate an approach for designing a mass-minimized aircraft powerplant.

The aim of this thesis was to indicate exergy-gravimetric approaches towards designing an optimal minimized-mass powerplant for aircraft applications. This thesis work also aimed to use this approach to size a mass-minimized powerplant for the Pipistrel Alpha Electro aircraft. The exergy analysis of fuel cell was carried out on CycleTempo through which sources of exergy destruction were identified. A mass-minimized model was developed on MATLAB. Using these tools, a number of system configurations for varying battery combinations, endurance requirements, and fuel cell types were analysed.

Overall, an exergy-gravimetric approach towards mass minimization was developed in this thesis work. Multiple fuel cell - battery hybrid powerplants were sized for the Pipistrel Alpha Electro. It was demonstrated that at least three system configurations using commercially available batteries and PEM fuel cells exist which would perform superior than the existing battery system on the aircraft, reducing the powerplant weight by as much as 30 kg from the existing battery system, while increasing endurance by about 15 minutes.

Acknowledgement

This project has been a learning experience that I have enjoyed very much and the perfect closure of my masters in Sustainable Energy Technology. First off, I would like to thank my thesis supervisor Prof. Aravind for providing the opportunity to work on a thesis on sustainable aviation, an industry most challenging to transform.

I would also like to thank Dr. Vikrant Venkataraman for helping me shape this thesis work, and being available whenever needed. Theo Woudstra deserves special thanks for helping me with CycleTempo and solving my technical queries at any given time. I thank Dr. Vikrant, Prof. Aravind and Theo for going the extra mile to ensure I graduate in time. I would also like to thank my friends Saloni Luhadia, Suvansh Kasliwal, Ajinkya Krishnakumar, Mihir Mehta, Neel Nagda Sukanya Prabhudesai, Philipp Essle, and David Oort for helping me with my thesis writing, being there when needed, and providing moral support.

Special mention to Project Talaria, where I have been working for the past 18 months. This project deserves credit for sparking my interest in sustainable aviation, and helping me gain theoretical understanding of flying vehicles, as well as hands-on experience on the same. I thank all my colleagues there for being ever-so-supportive and sharing my responsibilities while I worked on my thesis.

Finally, I would like to thank my mom, my dad my sister, my girlfriend and my grand parents for being always there for me, advising me and supporting me throughout all these years in the Netherlands. I love you all with all my heart.

Thank you all.

Contents

List of Figures

List of Tables

List of Symbols

α	Charge transfer coefficient	
ΔG	Molar Gibbs free energy	kJ/mol
ΔH	Molar enthalpy	kJ/mol
η	Efficiency	
$\lambda_{Parallel}$	No. of components in parallel	
λ_{Series}	No. of components in series	
C_{exp}	Exponential zone capacity of Li-Ion cell	V
C_{max}	Max capacity of Li-Ion cell	V
C_{nom}	Nominal capacity of Li-Ion cell	V
En	Energy	kJ/mol
Ex	Exergy	kJ/mol
F	Faraday's constant	
j_0	Exchange current density	A/cm^2
j_{lim}	Limiting current density	A/cm^2
j_{ext}	External current density	A/cm^2
j_{loss}	Loss current density	A/cm^2
M	Mass of component	kg
n	No. of electrons exchanged per mole of reactants	
P	Electrical power	W
p_{H_2O}	Partial pressure of water	bar
p_{H_2}	Partial pressure of hydrogen	bar
p_{O_2}	Partial pressure of Oxygen	bar
R	Universal gas constant	
R_i	Area-specific resistance	$\Omega - cm^2$
T	Temperature	K
V_{OCV}	Open circuit voltage	V

List of Abbreviations

ACELL	Active Area per Cell
AGL	Above Ground Level
BATT	Battery
BOP	Balance of Plant
DC	Direct Current
DOH	Degree of Hybridization
EDENS	Energy density
FC	Fuel Cell
HHV	Higher Heating Value
LHV	Lower Heating Value
LSA	Light Sport Aircraft
MEA	Membrane-Electrode Assembly
MSL	Mean Sea Level
OCV	Open Circuit Voltage
PDENS	Power Density
PINAN	Anode Inlet Pressure
PEM	Proton Exchange Membrane
SOC	State of Charge
SOFC	Solid Oxide Fuel Cell
SOH	State of Health
SSE	Sum-of-Squared Errors
TFCELL	Fuel Cell Temperature
UFL	Fuel Utilization Factor
UOX	Oxidant Utilization Factor

Chapter 1

Introduction

The Intergovernmental Panel on Climate Change (IPCC) estimates that aviation is responsible for around 3.5% of anthropogenic climate change. With growing air traffic, this number could go as high as 15% by 2050 [1]. Thus, aircraft manufacturers are increasingly exploring more sustainable and emission-free powerplant designs for aircrafts. With fuel cell and battery technologies evolving rapidly, they are becoming more feasible for motive and aircraft applications. Small fully electric aircrafts like the Pipistrel Alpha Electro are already flying in the skies.

However, electric aircrafts (Pipistrel Alpha Electro for example) suffer from a decreased endurance of only about an hour flight-time, compared to its conventional counterpart Pipistrel Alpha Trainer boasting over three hours flight-time. This is due to the low energy density of even the state-of-the-art lithium batteries available commercially, compared to aviation fuel. To shift away from conventional fuels, sustainable sources of energy (and power) should be able to match the specific power and specific energy density of conventional fuels and powertrains.

State-of-the-art rechargeable batteries used in electric vehicles have specific energy density of up to 0.25 kWh/kg [2] and latest batteries for aviation claim up to 450 Wh/kg [3]. This however is no match to the energy density of gasoline, which is about 12.7 kWh/kg [4], i.e. more than 2 order of magnitude higher. Hydrogen, with a specific energy density of about 39 kWh/kg [4] is far superior than even gasoline[1]. With regards to specific power density, the internal combustion engines used for small 2-seater aircrafts is about about 1.3 kW/kg [5], the specific power density of fuel cells is under 1 kW/kg, and Li-Ion cells which have a power density of over 5 kW/kg. Aircrafts require much higher power during takeoff and climb (about 65 kW in case of Pipistrel Alpha Electro), but only a fraction of this power is required during cruise flight (about 18 kW when cruising at 140 kmph). Hence, fuel cell - battery hybridization provides the opportunity to maximize both,

the specific power density and the specific energy density of the powerplant. Such hybrid powerplants hence have the potential to provide a clean alternative to conventional versions. The Ragone plot in Figure 1.1 shows a comparison of specific power and specific energy density of batteries and fuel cells [6].

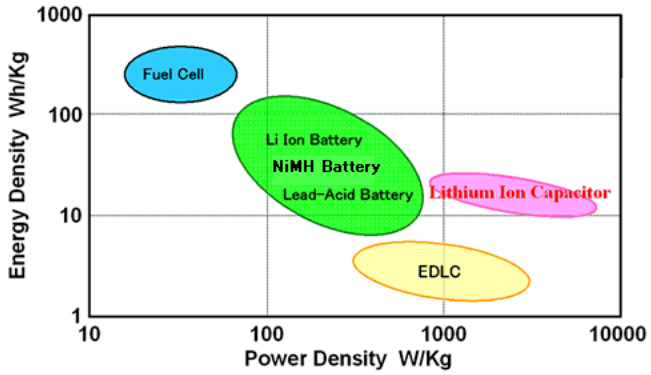

Figure 1.1: Comparing fuel cell and battery power and energy density [6]

Hydrogen, with its high energy density, is being explored in several projects to enable extending range of such fully electric aircrafts. Several fuel cell powered manned aircrafts have already been demonstrated, with the first one being Boeing Fuel Cell Demonstrator in 2009, a 2-seater motor glider flown for about 18 minutes on level flight. Other demonstrators include the ENFICA-FC, and the Antares DLR-H2.

The electrical efficiency of a fuel cell is a function of terminal voltage, which is a function of fuel cell's current density. The electrical efficiency thus is higher when the fuel cell is operated at higher terminal voltage, i.e. low current density. Consequently as the fuel cell is operated at higher power density, the efficiency decreases. This is shown in images Figure 1.2 and Figure 1.3.
It can be seen from Figure 1.2 that fuel cells suffer from low electrical efficiencies due to various irreversibilities. Apart from these, the system level efficiency is also dependant on the efficiency of other balance-of-plant (BOP) components, like cooling fans and DC-DC converters. First law of thermodynamics can be used to analyse the losses and inefficiencies, but it does not provide any information about the quality of energy available, or quality of energy lost. Second law analysis is more powerful in giving the true "losses" and better identifying the quality of these losses and potential for improvement. There is a trade-off between fuel cell power density (and electrical efficiency) with the fuel and fuel tank weight. However, an optimum can be found between these extremes to achieve the lowest

[1]Energy density excludes the weight of storage and regulation components.

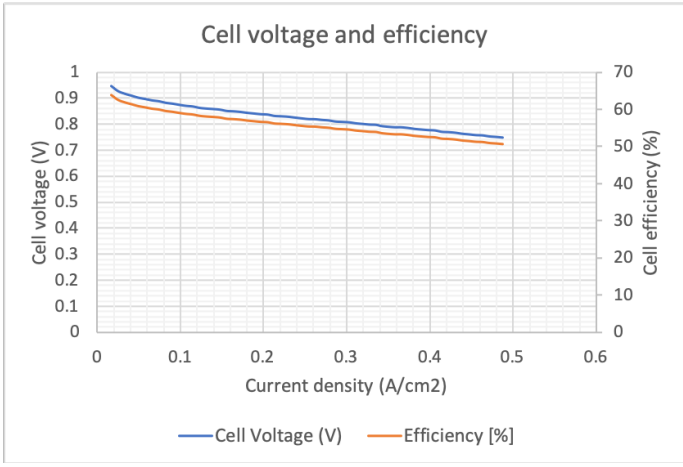

Figure 1.2: Cell voltage and efficiency for a sample fuel cell.

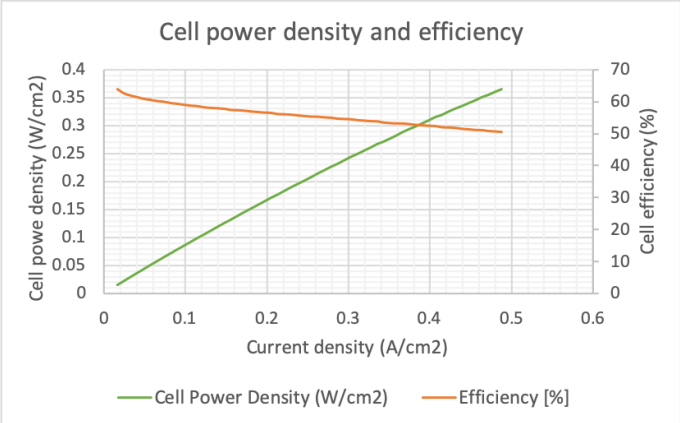

Figure 1.3: Cell power density and efficiency for a sample fuel cell.

system mass. Implementing such mass-minimization while accounting for exergy provides deeper insights on the ”cost” of exergy losses on the overall system mass. Such study where exergy analysis is used to design mass-minimized systems is called an ”exergy-gravimetric analysis”.

The aim of this Master’s thesis was to further an exergy-gravimetric approach, which was originally introduced by US Air Force. This approach attempts at an exergy-aided weight reduction of advanced energy systems, inclusive of fuel [7]. This thesis work also aimed to use this approach to design a mass-minimized fuel cell - battery hybrid powerplant for the 2-seater aircraft Pipistrel Alpha Electro using commercially available systems. Focus was laid on reducing irreversibilites and power consumption of auxiliary components, and its impact on the minimized system mass. The choice of battery and endurance requirements are also taken into account. The approach and the models developed in this thesis can be easily applied to develop mass-minimized systems for any application.

The goal of this thesis can be achieved by answering the following questions:

- What approach can be used to design mass-minimized fuel cell - battery hybrid powerplants for mass-sensitive applications?
- Is it possible to design a powerplant for Pipistrel Alpha Electro with currently available technologies, to reduce the powerplant mass, or increase endurance?
- If possible, suggest some likely powerplant configurations for the Pipistrel Alpha-H_2

This report starts with the *Background Information* provided in chapter 2 where underlying concepts about fuel cell operation, specifications of the aircraft, and the exergy-gravimetric approach are explained. The next chapter *Literature Review* mentions some of the previous work done in this field. Chapter 4 explains the modeling approach taken on MATLAB and CycleTempo for exergy and energy efficiency analysis. The results of this modeling are used to theoretically size numerous mass-minimized configurations, which are presented in Chapter 5. This chapter also analyses the effects of various variables like fuel cell type, cruise endurance requirement, type of battery, and fuel cell power density on mass-minimized configuration. Chapter 6 is about *Practical System Sizing* where system configuration for three hybrid system combinations is determined and analysed. Finally *Conclusion and Future Work* is presented in the last chapter.

Chapter 2

Background Information

This chapter introduces the basics of all the components used in this work. Basic working principles of fuel cells, batteries, and power converters are explained. Towards the end, information is provided about Pipistrel Alpha Electro, the aircraft in consideration for sizing the fuel cell hybrid system. This chapter also introduces the terminologies used throughout this thesis work.

2.1 Fuel cells

A fuel cell converts chemical energy directly into electrical energy via electrochemical processes. While batteries store energy as well as supply power, fuel cells are only electrical power production units, and the energy is derived from fuel stored separately.

A variety of fuel cells are available commercially. These can be categorized broadly on the basis of their operating temperatures.

- Low temperature fuel cells (up to 100 °C)

  Permeable Electrolyte Membrane (PEM)

- Medium temperature fuel cells (up to 600 °C)

  Phosphoric Acid Fuel Cells (PAFC)

  Alkaline Fuel Cells (AFC)

  Solid Acid Fuel Cells (SAFC)

- High temperature fuel cells ($\geq$ 650 °C)

  Solid Oxide Fuel Cells (SOFC)

  Molten Carbonate Fuel Cells (MCFC)

The type of fuel also varies with type of fuel cell. While PEM strictly requires pure H_2, SOFCs can work with organic fuels like propane as well. In this study, PEM fuel cells and propane fuelled SOFCs are explored for sizing the aircraft hybrid power systems.

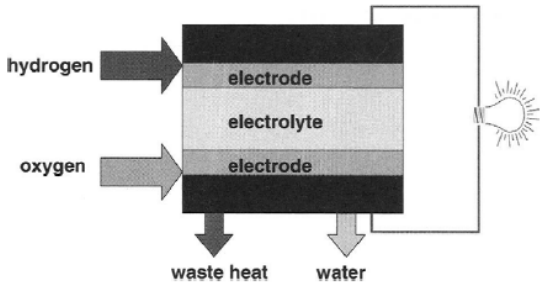

Figure 2.1: A typical fuel cell construction. A hydrogen fuel cell needs fuel and oxidant supply to generate electricity, heat and exhaust gases [8].

2.1.1 PEM fuel cells

The PEM fuel cells fall in the category of low temperature fuel cells. This type of fuel cells use a thin ($\leq 50\mu m$) proton conductive polymer exchange membrane as the electrolyte. The electrodes are made out of various materials, but Platinum is used as a catalyst on the electrodes. Operating temperatures are low, typically under 100 °C [9]. This is because the electrolyte membrane needs to be hydrated to conduct protons, and water evaporates faster as the temperature increases due to the increase in saturation pressure, and consequently the water carrying capacity of air [10, 11].
The anode is fed by H_2, while the cathode can be either air-fed or oxygen-fed. The electro-chemical reactions in the fuel cell happen simultaneously on both the anode and cathode. These reactions are shown in equation below [12].

$$\begin{aligned} \text{Anode} \quad & H_2 \rightarrow 2H^+ + 2e^- \\ \text{Cathode} \quad & \frac{1}{2}O_2 + 2H^+ + 2e^- \rightarrow H_2O \end{aligned} \tag{2.1}$$

The overall reaction results in release of energy, the enthalpy of formation of water. For this reaction taking place at standard state, i.e. 25°C and 1.01325 bar, the energy released is 286 kJ/mol of water produced (enthalpy of formation of liquid water).

$$H_2 + \frac{1}{2}O_2 \rightarrow H_2O(l) + 286kJ/mol \tag{2.2}$$

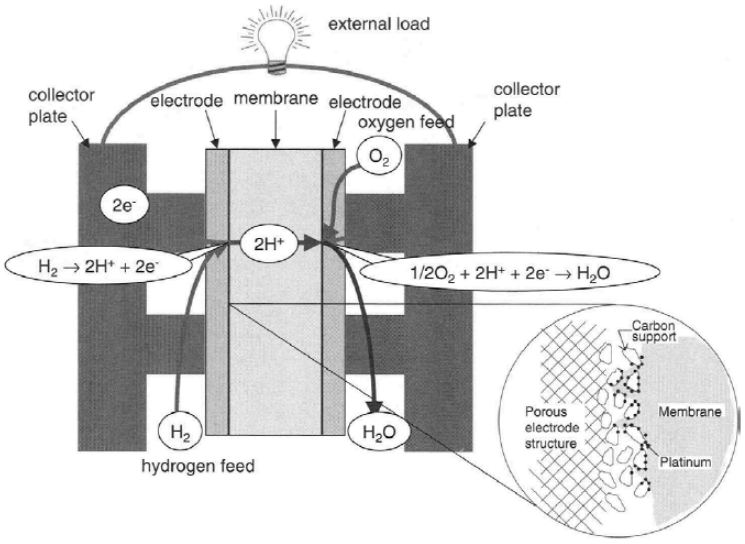

Figure 2.2: The basic operation principle of PEM fuel cell [8].

Higher and lower heating value

The enthalpy of water formation in the above reaction is also called hydrogen's heating value. It is the amount of energy released on complete combustion of a mole of hydrogen gas at standard state temperature and pressure conditions, i.e. at 25 °C and 1.01325 bar, and then products are allowed to cool down to 25 °C, i.e. the product water is in liquid state. This is the Higher Heating Value (HHV) of hydrogen combustion, and has a value of 286 kJ/mol [12]. However, if the product water is in vapor state, energy is used in phase conversion of water. This energy is equal to the enthalpy of evaporation of water at 25 °C (= 45 kJ/mol). Hence consequently the energy released by the reaction when water vapor is formed as a product is called the Lower Heating Value (LHV) of hydrogen combustion reaction. This value is equal to 241 kJ/mol at 25 °C and 1.01325 bar [12].

Losses and Polarization Equation

Gibbs free energy ΔG is the maximum amount of work that can be performed by a system at constant temperature and pressure [9]. The Gibbs free energy is related to the enthalpy and entropy via:

$$\Delta G = \Delta H - T\Delta S \tag{2.3}$$

Where T (K) is the reaction temperature, ΔH (J/mol) is the change in enthalpy at the reaction temperature, and ΔS (J/mol-K) is the change in entropy at the reaction temperature. The theoretical reversible voltage of the fuel cell is related

to Gibbs free energy of the reaction via the equation [12]:

$$V_{rev} = \frac{-\Delta G}{nF} \tag{2.4}$$

Where n is the number of electrons exchanged per mole of fuel consumed, and F is Faraday's constant. The reversible voltage at a non-standard state, i.e. variation with molar concentrations and pressures is given by the equation [12]:

$$V_{Nernst} = \frac{-\Delta G^{\circ}}{nF} + \frac{RT}{nF} ln \left(\frac{y_{H_2} * y_{O_2}^{0.5}}{y_{H_2O}} \left(\frac{p}{p_0} \right)^{0.5} \right) \tag{2.5}$$

Where T is the reaction temperature (K), p is the pressure of the reactants and the products, and p_0 is the reference pressure, i.e. 1.01325 bar, and y is the molar concentration of the reactant and product species.

Three types of losses determine the output potential of the fuel cell: activation losses, ohmic losses, and mass transport losses [9]. These loss mechanisms are described below.
Activation losses represent the proportion of voltage generated that is lost in driving the chemical reaction that transfers electrons to or from the electrode [9].

$$\Delta V_{Activation} = \frac{RT}{nF\alpha} ln \left(\frac{j_{ext} + j_{loss}}{j_0} \right) \tag{2.6}$$

Ohmic loses occur due to the ohmic resistance of the fuel cell components (eg. membrane, electrodes, electrolyte etc.). These losses are given by Equation 2.7.

$$\Delta V_{Ohmic} = (j_{ext} + j_{loss}) R_{i,ohmic} \tag{2.7}$$

Mass transport losses arise due to the change in concentration of the reactants at the surface of the electrodes as fuel is consumed [9]. These losses are given by the Equation 2.8.

$$\Delta V_{MassTransport} = \frac{RT}{nF} ln \left(\frac{j_{lim} - j_{ext} - j_{loss}}{j_{lim}} \right) \tag{2.8}$$

The overall voltage, after accounting for all losses, is given by

$$V_{FC} = V_{Nernst} - \Delta V_{Activation} - \Delta V_{Ohmic} - \Delta V_{MassTransport} \tag{2.9}$$

Where j is current density given by $j = I/Aa$, Aa is the active area per cell. j_{ext} is the external current density, i.e. the current drawn from the fuel cell by the connected load, divided by the active area per cell. The loss current density

j_{loss} is the current density attributed to losses due to fuel or oxidant crossovers, i.e. "leakages" in the electrolyte membrane. The limiting current density j_{lim} is defined as the maximum current density that can be used to get a desired electrode reaction without undue interference, such as may come from polarization [12]. j_0, the exchange current density is the forward (or backward) reaction current density when no current is being drawn from the system. For a high value of j_0, the electrode surface can be said to be more "active", leading to low activation losses when external current is drawn [9]. A generic IV curve of a fuel cell depicting the regions of IV where these losses are most prominent is shown in Figure 2.3 [13].

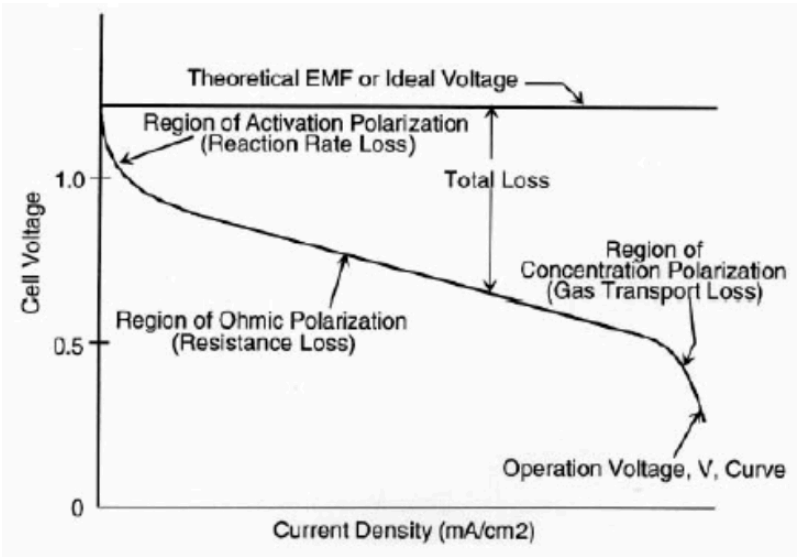

Figure 2.3: IV curve of a generic fuel cell showing various losses

2.1.2 Solid oxide fuel cells

Solid Oxide Fuel Cells use solid and non-porous metal oxide as the electrolyte. These electrolytes do not allow permeation of any ions at low temperatures, but become conductive for O^{2-} ions at higher temperatures, and hence these fuel cells typically operate between 800 °C to 1000 °C, although SOFCs at lower temperatures, 400 °C to 650 °C have been demonstrated at cell level [14].
The basic operation principle of Solid Oxide Fuel Cell is the same as that of PEM fuel cell. There are certain differences however. While in PEM, H^+ ions are transported via the electrolyte membrane, O^{2-} anions are transported via electrolyte in SOFC. In other words, water is produced at the anode in SOFCs. The Solid Oxide Fuel Cells are also more flexible in terms of inlet fuel: the choice of fuel can vary from pure H_2 to ammonia, to hydrocarbons. Besides, the anodic and cathodic reactions are also different. For an H_2 fuelled SOFC, the reaction

equations are

$$\begin{aligned} &\text{Anode:} && H_2 + O^{2-} \rightarrow H_2O + 2e^- \\ &\text{Cathode:} && \frac{1}{2}O_2 + 2e^- \rightarrow O^{2-} \end{aligned} \tag{2.10}$$

While for Carbon Monoxide fueled SOFC, the reaction equation is given by

$$\begin{aligned} &\text{Anode:} && CO + O^{2-} \rightarrow CO_2 + 2e^- \\ &\text{Cathode:} && \frac{1}{2}O_2 + 2e^- \rightarrow O^{2-} \end{aligned} \tag{2.11}$$

These processes are represented in Figure 2.4 [9].

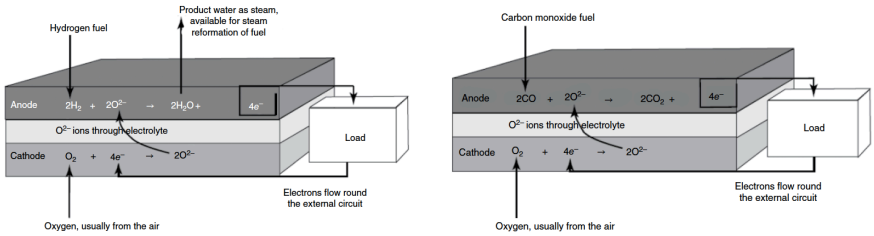

Figure 2.4: Anode and Cathode reactions for SOFC, when using H_2 and CO as fuels respectively [9].

The voltage of an SOFC is governed by the same equations as those of PEM described in section 2.1.1. However, the gibbs free energy will be different depending on the fuel used reaction temperature.

2.1.3 Balance of Plant (BOP) components

Balance of Plant (BOP) components include all components other than the fuel cell stack required to ensure proper functioning of the fuel cell. Smaller PEM fuel cells generally do not need any balance of plant components, just fuel and oxygen supply. However, balance of plant (BOP) components are required for larger fuel cells. This section describes some of the BOP components for PEM fuel cells.

Cooling systems

All irreversibilites mentioned above result in losses released as heat. This heat needs to be dissipated to maintain the fuel cell at the required temperature. PEM are differentiated mainly into two categories depending on how cooling is achieved:

1. Air cooled
2. Liquid cooled

In air cooled fuel cells, heat is dissipated via forced air convection. Fans / compressors are used to drive the air at the required flow rate. Some fuel cells [15, 16] use the fan to cool the fuel cell, as well as to provide sufficient air flow through the cathode. Air cooled fuel cells are generally < 5 kW power output [17, 18].
In liquid cooled fuel cells, the fuel cell temperature is maintained by the flowing liquid in the cooling channels. Since heat capacity of water is > 4 times that of air, liquid cooled fuel cells are often found in higher output capacities, up to 100 kW stacks are commercially available. Liquid cooled stacks require coolant pumps, heat exchangers, flow pipes, and coolant reservoirs.

Humidifier

PEM fuel cells rely on the proton conductivity of the electrolyte membrane to complete the reaction. Nafion membranes, or their variants are typically used as these electrolyte membranes. These membranes need to be humidified to increase / maintain their proton conductivity [19]. However, the fuel and air flow through the anode and cathode respectively have drying effect on the membrane as the water is evaporated, and could cause the membrane to dry out if sufficient humidity is not maintained. Humidifiers are used to humidify the inlet gases when sufficient humidity cannot be maintained at the membrane otherwise.

DC-DC converter

Voltage requirements vary depending on the application. Sometimes, the output voltage of the fuel cell does not match the required voltage. In such cases, DC-DC converters are used to convert the output voltage of the fuel cell to the required voltage level. Hence, while DC-DC converters are not exactly essential for functioning of the fuel cell system, they may be required at a system level.

2.2 Component research

This section lists commercially available powerplant components, i.e. the fuel cells, fuel storage, batteries, and DC-DC converters. This data is used for theoretical and practical system sizing in the later chapters.

2.2.1 Fuel cells

A list of commercially available PEM fuel cells for motive applications is presented in Table 2.1 [16, 20, 15, 21, 22]. The specific and volumetric power densities

mentioned are at a system level. These power and energy densities are only for the fuel cells (including BOP components), and do not include the fuel storage.

Table 2.1: List of commercially available PEM fuel cells for motive applications [16, 20, 15, 21, 22].

System name	Nominal Power [W]	Weight [kg]	Volume [L]	Specific Power Density [W/kg]	Volumetric Power Density [W/L]	BOP	Cooling
HES A250	250	0.73	1.63	342.47	153.37	Included	Air
HES A500	500	1.30	3.38	384.62	147.93	Included	Air
HES A1000-50	1000	2.04	5.39	490.20	185.53	Included	Air
HES A1000-65	1000	1.80	4.76	555.56	210.30	Included	Air
HES A1500	1500	2.80	5.25	535.71	285.71	Included	Air
HES A2000	2000	3.80	10.56	526.32	189.39	Included	Air
IE 650W UAV	650	0.81	2.41	802.47	269.26	Included	Air
IE 800W UAV	800	0.93	2.74	860.22	291.97	Included	Air
IE 2.4kW UAV	2400	3.25	12.85	738.46	186.77	Included	Air
IE FCM-801	1200	10.00	42.08	120.00	28.52	Included	Air
IE FCM-802	2500	18.00	74.25	138.89	33.67	Included	Air
IE FCM-804	4000	20.00	74.25	200.00	53.87	Included	Air
Ballard FCAir - 600	600	1.80	2.13	333.33	281.69	Included	Air
Ballard FCAir - 1200	1200	4.00	7.08	300.00	169.49	Included	Air
Powercell MS-30	30000	145.00	174.00	206.90	172.41		Liquid
Powercell PS-5	5000	110.00	246.00	45.45	20.33		Liquid
Ballard FCVelocity-MD	30000	125.00	162.00	240.00	185.19		Liquid
Ballard HD60	60000	349.00	496.87	171.92	120.76		Liquid
Ballard HD85	85000	361.00	496.87	235.46	171.07		Liquid
Ballard HD100	100000	390.00	527.00	256.41	189.75		Liquid
Hydrogenics HD10-200	10000	33.00	27.52	303.03	363.37	Partial	Liquid
Hydrogenics HD15	16500	55.00	52.34	300.00	315.25	Partial	Liquid
Hydrogenics HD30	31000	75.00	76.18	413.33	406.93	Partial	Liquid

2.2.2 Fuel storage

Hydogen

Hydrogen can be stored in majorly three forms: pressurized gas, cryogenic liquid, and in solid state in metal hydrides. A comparison of theoretical storage density of various H_2 storage forms is presented in Figure 2.5 [23, 24]. $LiBH_4$ and liquid hydrogen are very promising in terms of energy density, surpassing the theoretical storage energy density of pressurized hydrogen. However as of date $LiBH_4$ storage tanks do not exist commercially and hence have not been explored in this study. Liquid hydrogen, due to high production and storage costs and high boil-off losses [25] has also not been explored in this study.

Table 2.2 compares the specifications of some commercially available pressurized storage tanks. The tank storage density (η_{Tank}) is defined as the amount of fuel stored per unit mass of empty container; the volumetric density (η_{Tank}^{Volume}) is the weight of empty tank per unity volume. These are calculated via

$$\eta_{Tank} = \frac{M_{fuel}}{M_{EmptyTank}} \qquad \eta_{Tank}^{Volume} = \frac{M_{EmptyTank}}{V_{Tank}} \tag{2.12}$$

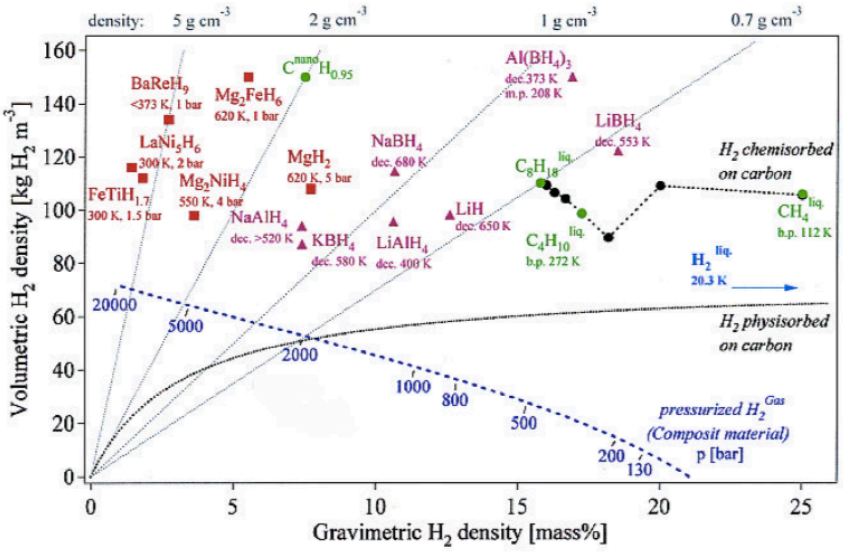

Figure 2.5: Storage density for various H_2 storage forms [23].

Where M_{fuel} is the mass of fuel stored, $M_{EmptyTank}$ is the mass of empty tank, and V_{Tank} is the outer volume of tank.

Table 2.2: Some of commercially available pressurised hydrogen storage options [16, 26, 27].

Tank	Storage pressure [bar]	Outer dimensions (dia x length) [mm]	Outer volume [L]	Inner volume [L]	Fuel capacity [kg]	Empty weight [kg]	η_{Tank} [-]	η_{Tank}^{Volume} [kg/L]
Mahytec A	60	840x1870	1035.79	850	3.95	215	0.018	0.208
Mahytec B	525	490x3070	578.63	300	8.23	260	0.032	0.449
Mahytec C	700	328x1160	97.97	52	1.677	53.6	0.031	0.547
HL A	200	315x1060	90.35	46	0.7	16	0.044	0.177
HL I	700	319x906	72.37	36	1.4	34	0.041	0.470
HL J	700	238x1600	71.14	39	1.6	29	0.055	0.408
HL K	700	420x845	117.01	64	2.4	43	0.056	0.367
HL L	700	440x1050	159.57	76	3.1	59	0.053	0.370
HES A12		196x532	16.04	12	0.377	3.5	0.108	0.218
HES A20		230x655	27.20	20	0.629	7	0.090	0.257

From Table 2.2, it is observed that the storage density varies significantly, with the best available tank (the HES A12) having a storage density of $\eta_{Tank} = 10.8\%$.

Propane

Propane is used as a fuel for SOFCs. Lightweight storage tanks for liquid propane are readily available commercially. Some of these tanks are listed in Table 2.3 [28].

Comparing the tank storage densities of pressurized H_2 and propane in Table 2.2 and Table 2.3 respectively, it can easily be noticed that storage density of propane tanks is an order of magnitude higher than that of hydrogen tanks.

Table 2.3: Some commercially available propane storage tanks [28].

Name	Outer dimensions (dia x length) [mm]	Outer volume [L]	Inner volume [L]	Fuel capacity [kg]	Empty weight [kg]	η_{Tank} [-]	η_{Tank}^{Volume} [kg/L]
Viking 11 lbs	304x383	27.79	12.47	5	4.08	1.23	0.147
Viking 17 lbs	304x465	33.73	18.33	7.64	4.54	1.68	0.135
Viking 22 lbs	304x571	41.42	24	10	5.44	1.84	0.131

2.2.3 Batteries

Lithium batteries are often used as power source in motive applications. In Table 2.4, the characteristics of three batteries are described. The A123 ANR26650m1b [29] is a high power density, low energy density cell, the SolidEnergy Hermes [3] is a low power density high energy density cell, and the Sony VTC6 [30] is a balanced cell, i.e. has both good power and energy density. These cells have been specifically selected to demonstrate the impact of power and energy density of cells on the optimal configuration and overall weight.

Table 2.4: Rated characteristics of battery cells used for system sizing [30, 3, 29].

	A123 ANR26650m1-b	Sony US18650VTC6	SolidEnergy Hermes
	"High power density"	"Balanced"	"High energy density"
Chemistry	LiFePO4	LiNMC	Li-Metal
Nominal voltage [V]	3.3	3.60	3.8
Max. voltage [V]	3.6	4.20	4.2
End of discharge voltage [V]	2	2.50	3
Rated capacity [mAh]	2.5	3.00	3.2
Max. cont. C-rate [-]	20	5.00	2
Max. cont. discharge power [W]	180	54.00	24.32
Weight / cell [kg]	0.076	0.0465	0.029
Volume / cell [L]	0.0345	0.0165	0.015
Specific energy density [Wh/kg]	108.55	232.26	419.31
Volumetric density [kg/L]	2.20	2.81	1.93
Power density [W/kg]	2368.42	1161.29	838.62
Typical cycle life	1000+	∼400	∼120

2.2.4 DC-DC converters

DCDC converters are commonly employed in fuel cell - battery hybrid powertrain designs to match the fuel cell voltage to bus-bar voltage, and to also maintain fuel cell output power. Such converters typically are 94-98% efficient at the rated loads [31, 32]. Tame-Power [33] provides air cooled DC-DC converters with power densities upto 1.36 kW/kg and upto 95% nominal efficiency. Zekalabs [34] provides liquid cooled DCDC converters with power density of upto 0.75 kW/kg and minimum efficiency of 94%.

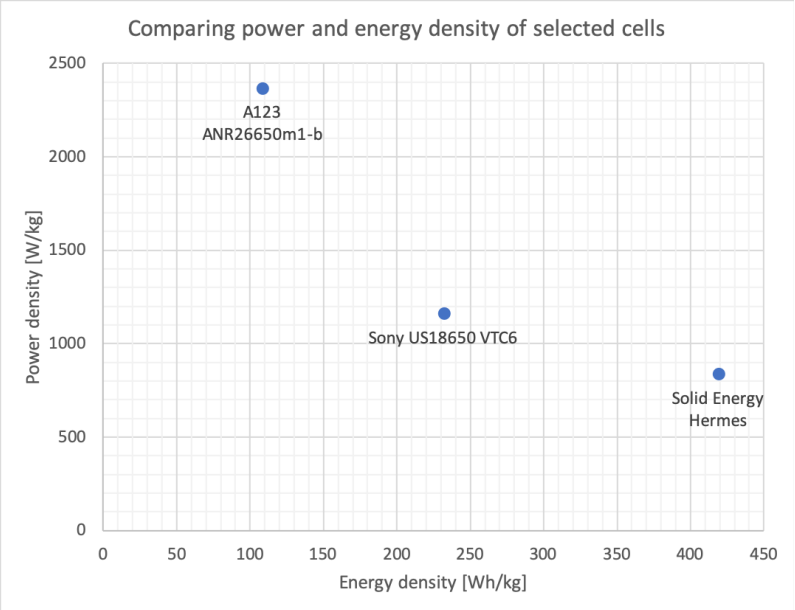

Figure 2.6: Comparing power and energy density of selected battery cells.

2.3 The Pipistrel Alpha Electro

2.3.1 Overview of Aircraft

The Pipistrel Alpha Electro (previously known as Pipistrel WattsUp) is a 2-seater aircraft from the Slovenian aircraft manufacturer Pipistrel [35]. The Alpha Electro is designed to be a trainer aircraft, and is optimized for traffic patterns operation. It is theoretically able to recuperate up to 13% energy during approach and descent.

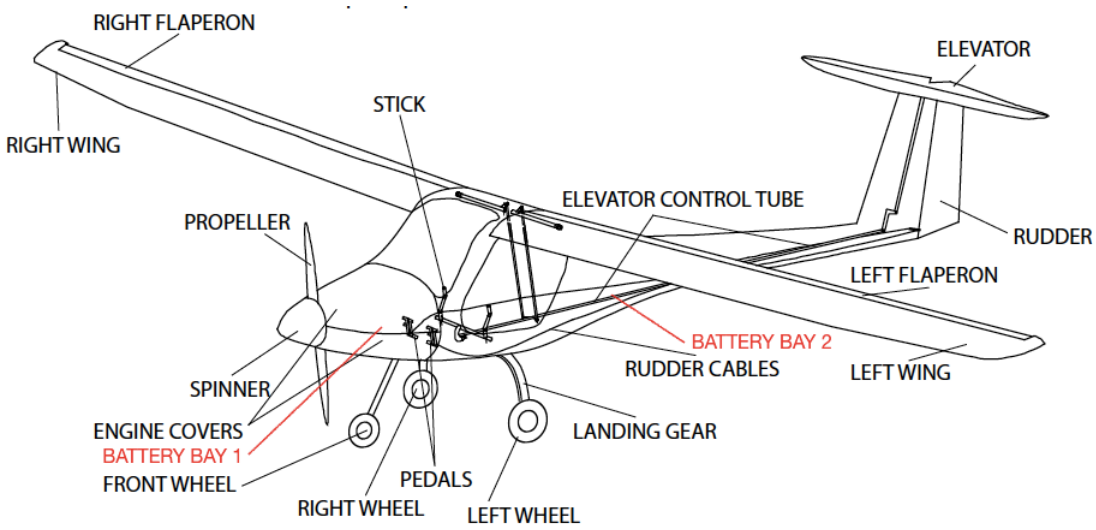

Figure 2.7: Pipistrel Alpha Electro [35]

2.3.2 Aircraft powertrain

Existing powertrain

The aircraft's existing powertrain design consists of two separate battery bays, one in front of the passenger cabin and one on the rear. Each battery bay has a volumetric capacity of 69.38L [35], and houses a battery of 10.5 kWh. Both the batteries along with the motor controller (inverter) connect to the junction box. A DC-DC converter converts the junction box voltage to 12V required for main computer operation. The motor is controlled via a digital throttle input given to the main computer. The main computer also receives data from each of the batteries and displays all information about the aircraft on the cockpit instruments. The charger for the batteries is not on-board, and thus cannot be carried along. The motor is liquid cooled 3 phase, controlled via the motor controller. These schematics are represented in Figure 2.8, and the dimensions of front the battery bay are represented in Figure 2.9.

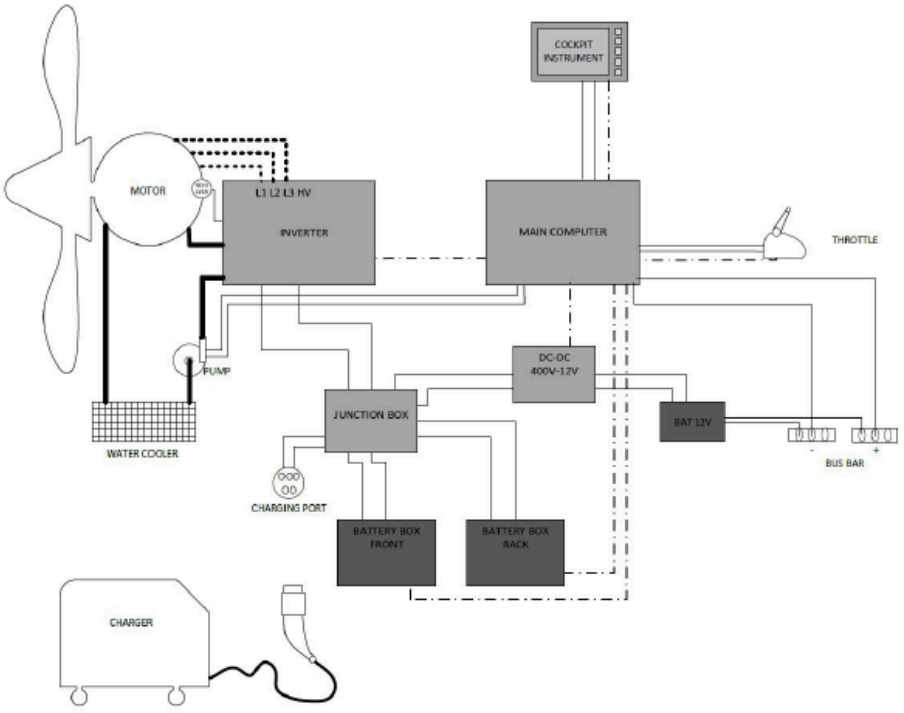

Figure 2.8: Electrical system schematics of Pipistrel Alpha Electro [35].

Flight course for powertrain design

The Pipistrel Alpha Electro is a trainer aircraft and is optimised for traffic patterns operation. Accurate information about power requirements and flight course was

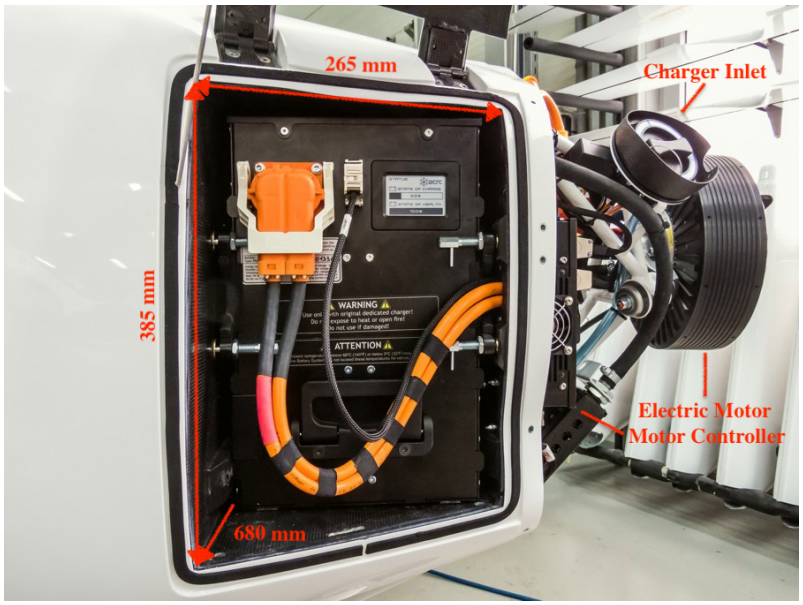

Figure 2.9: Front battery bay dimensions [35].

not available, and hence certain assumptions have been made. This flight course along with the assumptions is mentioned hereafter.
The cruise altitude is chosen for traffic patterns operation (1000 feet AGL) as per [36] specifications for traffic patterns operation. It is assumed that the flight starts at sea level and hence the cruise altitude is assumed to be 1000 feet (300m) MSL.

The flight starts with the ”takeoff” phase, where the power required by the aircraft is maximum, i.e. 65 kW [35]. This phase lasts for 1 minimum, and the aircraft enters the ”climb” phase when it altitude is more than 15m AGL [35, 37]. The ”climb” phase lasts for another 1 minimum until the aircraft climbs to its cruise altitude of 1000 feet AGL (300 m), after which it continues to cruise at 140 kmph, during which it consumes 18 kW. It is assumed that power consumption of the auxiliary components is included in the 18 kW cruise power consumption. Since the aircraft can recuperate energy while descent and landing, it is assumed that the aircraft does consume any power at that time, and the duration of descent is negligible as compared to cruise. The flight course is summarised in Table 2.5, and represented visually in Figure 2.10.

Design requirements for hybrid powertrain

The hybrid powertrain design explored in this work must be able to supply more than 18 kW continuously, and 65 kW for at least 2 minutes. The powerplant must weigh under 126 kg, and must occupy under 138.7 L. The junction box voltage at all times should be between 100V and 450V, and the nominal junction box voltage should be close to 345V. At the specified flight course, the powerplant

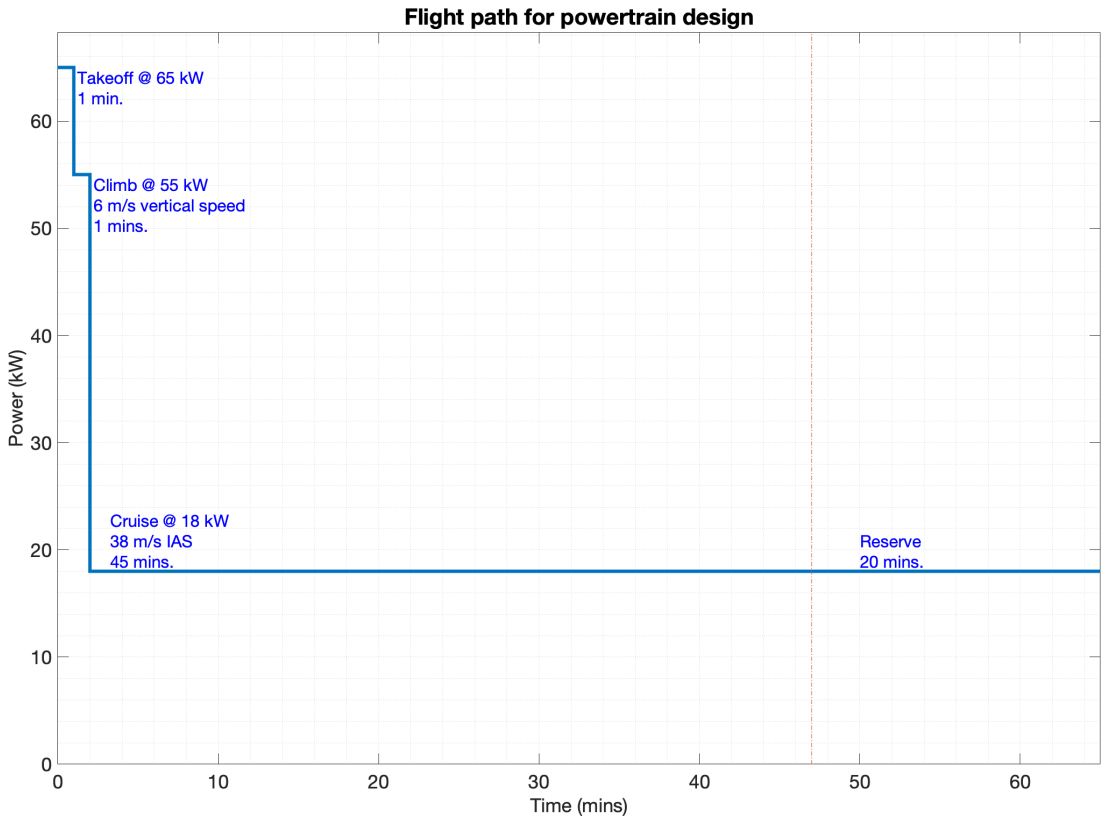

Figure 2.10: Selected flight path for powertrain design

must contain sufficient energy to last for at least 65 minutes cruise flight (inc. 20 minutes reserve). This translates to at least 21 kWh of energy available at the junction box. The flight course requirements are summarized in Table 2.5 and Figure 2.10. Effect of altitude on aircraft and fuel cell performance is not taken into account in this study.

2.4 Exergy-gravimetric analysis

Exergy is defined as the work that can be obtained from an amount of energy (converted in a well defined system), under ideal conditions (under a reversible process) using the environment as a reservoir of heat and matter [38]. Exergetic efficiency measures entropy production, and hence irreversibility losses associated with chemical and thermal processes [9]. Unlike energy, exergy can be, and is destroyed when transformed from one source to the other.

In fuel cells, exergy is destroyed due to each of the irreversibilities described in section 2.1.1, and lost due to processes like purging. BOP components also contribute towards exergy destruction. Electrical components like pumps, compressors and DC-DC converters contribute towards exergy destruction due to

their electrical and mechanical inefficiencies.

2.4.1 Efficiency calculations

Exergy efficiency can be defined in two ways: the universal exergy efficiency, given by Equation 2.13; and the functional exergy efficiency, given by Equation 2.14.

$$\eta_{Ex,univ} = \frac{Exergy_{out}}{Exergy_{in}} \tag{2.13}$$

$$\eta_{Ex,func} = \frac{Exergy_{recovered}}{Exergy_{expended}} \tag{2.14}$$

The universal exergy efficiency is defined as the ratio of the total sum of exergy leaving the system to the total sum of the exergy entering the system. It gives an intuitive measure of the system performance, but however since this efficiency measure includes *all* the exergy leaving the system, i.e. also exergy which is not used to provide useful work, this efficiency is not as useful. The functional exergy efficiency is defined as the ratio of total exergy recovered to the total exergy expended into the system. Thus the functional exergy efficiency gives more information about how the system performs in terms of the actual exergy expended and actual useful work produced. For a fuel cell, the exergy efficiencies are given by:

$$\eta_{Ex,Univ} = \frac{P_{el,out} + Ex_{out,cathode} + Ex_{out,anode} + Ex_{out,cooling}}{Ex_{in,fuel} + Ex_{in,cathode} + Ex_{in,cooling}} \tag{2.15}$$

$$\eta_{Ex,Func} = \frac{P_{el,out}}{(Ex_{in} - Ex_{out})_{fuel} + (Ex_{in} - Ex_{out})_{cathode} + (Ex_{in} - Ex_{out})_{cooling}} \tag{2.16}$$

The functional exergy efficiency is a very good parameter to understand the performance of a component in consideration. However, since by definition the functional exergy efficiency excludes the non-electrical exergy outflows from the anode, cathode and cooling channels, it is of little engineering value. From an engineering stand point, a useful exergy efficiency parameter would be the one which takes into account all the fuel provided to the system, and the useful work derived out of the system. This exergy efficiency is given by:

$$\eta_{Ex} = \frac{P_{el}}{\dot{m} * \Delta G^{\circ}} \tag{2.17}$$

Where $\dot{m}$ is the mass flow rate of the fuel (kg/s) and ΔG° is the standard state molar Gibbs free energy (kJ/mol).

For a battery, exergy losses are due to the battery heating during charge and discharge, and self discharge. Self discharge for a lithium-ion battery can be neglected [39]. The only measure of exergy stored in the battery is through the power supplied to the battery during charging. Since the power supplied to charge the battery is also purely electrical, the exergy efficiency of the battery is equal to its energy efficiency (Equation 2.18) [40].

$$\eta_{Ex,Func} = \frac{P_{el,out} * t}{StoredExergy} = \frac{P_{el,out}}{P_{el,in}} = \eta_{En} \tag{2.18}$$

However, the exergy efficiency for a hybrid system is not the same as the exergy efficiency of either the fuel cell system or the battery system alone. Thus the exergy efficiency of a hybrid system (during a certain flight phase) is calculated using:

$$\begin{aligned} \eta_{Ex,hybrid} &= \frac{P_{Flight}}{\frac{P_{FC}}{\eta_{Ex,FC}} + \frac{P_{BATT}}{\eta_{Ex,BATT}}} \\ P_{Flight} &= P_{FC} + P_{BATT} \end{aligned} \tag{2.19}$$

Where P_{Flight} is the combined power output of the power system during a given flight phase, η_{Ex} is the exergy efficiency, P_{FC} is the power output of the fuel cell, while P_{BATT} is the battery power output.

Exergy and energy efficiency of the fuel cell system play a major role in determining the rate of fuel consumption for the aircraft. This, along with the endurance requirements determine the total fuel weight (and fuel tank weight) to be carried. The energy and exergy efficiency of the fuel cell are influenced by factors like the operational voltage (as described in Equation 2.9), parasitic power consumption etc. An mass-minimized design at the powerplant level is also influenced by the battery selection, i.e. by the power and energy density of the battery, the endurance requirement, and power output by the fuel cell during cruise flight. Due to the large number of variables involved, a method has been developed to identify the most suitable system configuration. This method is explained in this section.

2.4.2 Exergy-gravimetric approach

This section highlights the method used to arrive at an exergy-gravimetrically analyzed powerplant configuration design for mass minimization. The steps followed are mentioned below. These steps are also shown in the flowchart in Figure 2.11.

1. The system design starts with identifying the most appropriate fuel cell. In this case, the fuel cell is selected based on highest specific power density.

2. Sources of exergy destruction are identified within the fuel cell system. These include polarization losses, BOP power consumption etc.

3. Feasibility of flexibility of the above identified variables is analyzed. In other words, it is analyzed if any alterations to the given system for the identified exergy destruction (or loss) sources are possible or not. For example, though the cooling system of a fuel cell contributes towards parasitic power consumption, it may not be possible to completely eliminate the cooling system.

4. The various fuel cell system configurations arising out of eliminating exergy destruction sources are modeled in **CycleTempo**, and energy and exergy efficiency of each configuration is calculated.

5. Design variables for the powerplant system design are identified. These include the parameters identified for fuel cell, and additional variables like choice of battery selection, endurance requirement.

6. Next, various systems are sized theoretically to determine the fuel cell and battery combinations for mass minimization. **MATLAB** is used to define and solve the optimization problem.

7. The expected weight and exergy efficiency difference with respect to base case are quantified.

8. Configurations with the lowest mass are identified for practical sizing.

9. Selected configurations are practically sized, such that they adhere to additional constraints such as volume budget, junction box voltage specifications, and include the integer effect[1].

10. These sized systems are simulated on **Simulink** to verify system performance.

Theoretical vs. practical system design

Systems are sized theoretically first to allow narrowing down the number of design choices. However, theoretical sizing ignores several factors which practical system sizing takes into account:

[1]The integer effect is explained in the next subsection.

- **Integer-nature of components (or, capacity limitation of components):** Due to the integral nature of components (fuel cells, batteries, fuel tanks), it may not always be possible to achieve the exact power / quantity required in the configuration yielding the lowest system mass. For example, consider a system requiring a fuel cell power of 2.5 kW. If this system were to be sized using a fuel cell with a rated power of 1 kW, 2.5 fuel cells would be required. Obviously this is not possible, and the system would consist of either two or three fuel cells. This affects the mass estimation arrived at in the theoretical system sizing, and may also shift the optimality equilibrium. The same is applicable to batteries and fuel tanks as well.

- **Voltage constraints:** Often, the motor and motor controller in a hybrid system specify the acceptable voltage limits. For high power systems like the one in consideration, high voltages are generally suitable since ohmic losses in cables, bus bars can be minimized. However these voltage requirements impose additional constraints on the system design. For example, consider a battery system requiring 10W power at 10.8V nominally. If a system is sized using a typical Li-Ion battery with nominal voltage 3.6V, the number of cells in series required to achieve the voltage is 3. Now to achieve required power output, only the cells in parallel can be varied.

- **DC-DC converter:** Due to the above two reasons mentioned, it sometimes is possible that the required voltage cannot be achieved with the desired system. In such cases, a DC-DC converter can be employed to convert the powerplant voltage to required voltage levels. If a DC-DC converter is used in a hybrid system, the system is called a **indirect hybrid system**, else it is called a **direct hybrid system**.

- **Battery voltage variation**: Battery nominal voltage depends on a number of factors, including the State of Health (SOH), State of Charge (SOC), output current per cell, operating temperature etc. Due to these factors, the output voltage of the battery is not constant. Depending on the type of hybridization (direct / indirect), this could affect the fuel cell performance.

The effect of the above factors on the system design will be explored in chapter 6.

Table 2.5: Chosen flight path for powertrain design

Flight Phase	Duration [mins]	Power at Junction Box [kW]	Conditions
Takeoff	1.00	65.00	Airspeed during takeoff: 28 m/s
Climb	1.00	55.00	Climb altitude: 300 m (1000 ft) AGL Vertical speed: 6 m/s
Cruise	45.00	18.00	Cruise altitude: 300m (1000 ft) AGL
Reserve	20.00	18.00	Cruise speed: 38 m/s (140 kmph)
Total flight time [mins.]		67	
Total energy [kWh]		21.5	

Table 2.6: Electrical powertrain specifications of the Pipistrel Alpha Electro [35].

Name	Specification
Motor	**Siemens PEM60MVLC**
Peak power (1 min)	80 kW
Continuous power	50 kW
Controller	**Emsiso H300A**
Nominal Power	60 kW
Output continuous current	300 A
Output max current (1 min)	450 A
Input DC voltage range	100V to 450 V
Output continuous power	135 kVA
Output peak power (1 min)	200 kVA
Battery	
Total capacity	21.0 kWh
Useful capacity	20 kWh
Peak voltage	399 V
Nominal voltage	345 V
Lowest voltage	288 V
Total weight	126 kg
Battery bay dimensions (each)	680 * 385 * 265 mm
Total available volume	138.8 L

Table 2.7: Pipistrel Alpha Electro: Aircraft Specifications [35, 41]

Pipistrel Alpha Electro			
Seating capacity (including pilot)	2	Stall speed (with flaps down) (calibrated) [m/s]	21.6
Power system	Electric	Stall speed (without flaps) (calibrated) [m/s]	23.15
Aircraft purpose	Trainer	Typical cruise speed [m/s]	43.73
		VNE (Indicated) [m/s]	90
Wingspan [m]	10.5	Max speed with flaps down (indicated) [m/s]	36
Height [m]	2.05	Maneuvering speed (indicated) [m/s]	44.2
Length [m]	6.5		
Aspect Ratio (AR)	11.3	Best climb speed [m/s]	33.4
Wing area [m^2]	9.51	Max climb rate [m/s]	6.12
Rudder area [m^2]	1.1	Best glide ratio speed [m/s]	32.9
Horizontal tail area [m^2]	1.08	Best glide ratio	01:15
Positive flaps	0, 15, 25		
		Take off run @ MTOW [m]	150
Center of Gravity (Mean Aerodynamic Chord) [%]	20 to 38	45°- 45°roll time [s]	2.6
Center of Gravity (aft of datum) [mm]	195 to 368		
		Endurance (incl. reserve) [mins]	65
Empty weight (with batteries) [kg]	350	Standard range at cruise [km]	120
Empty weight (inc. PRS) [kg]	379	Max load factor permitted	4g, 2g
Min pilot (payload) weight [kg]			
MTOW [kg]	550	Service ceiling [m]	3900
Payload [kg]	200	Max crosswind component [m/s]	9.26

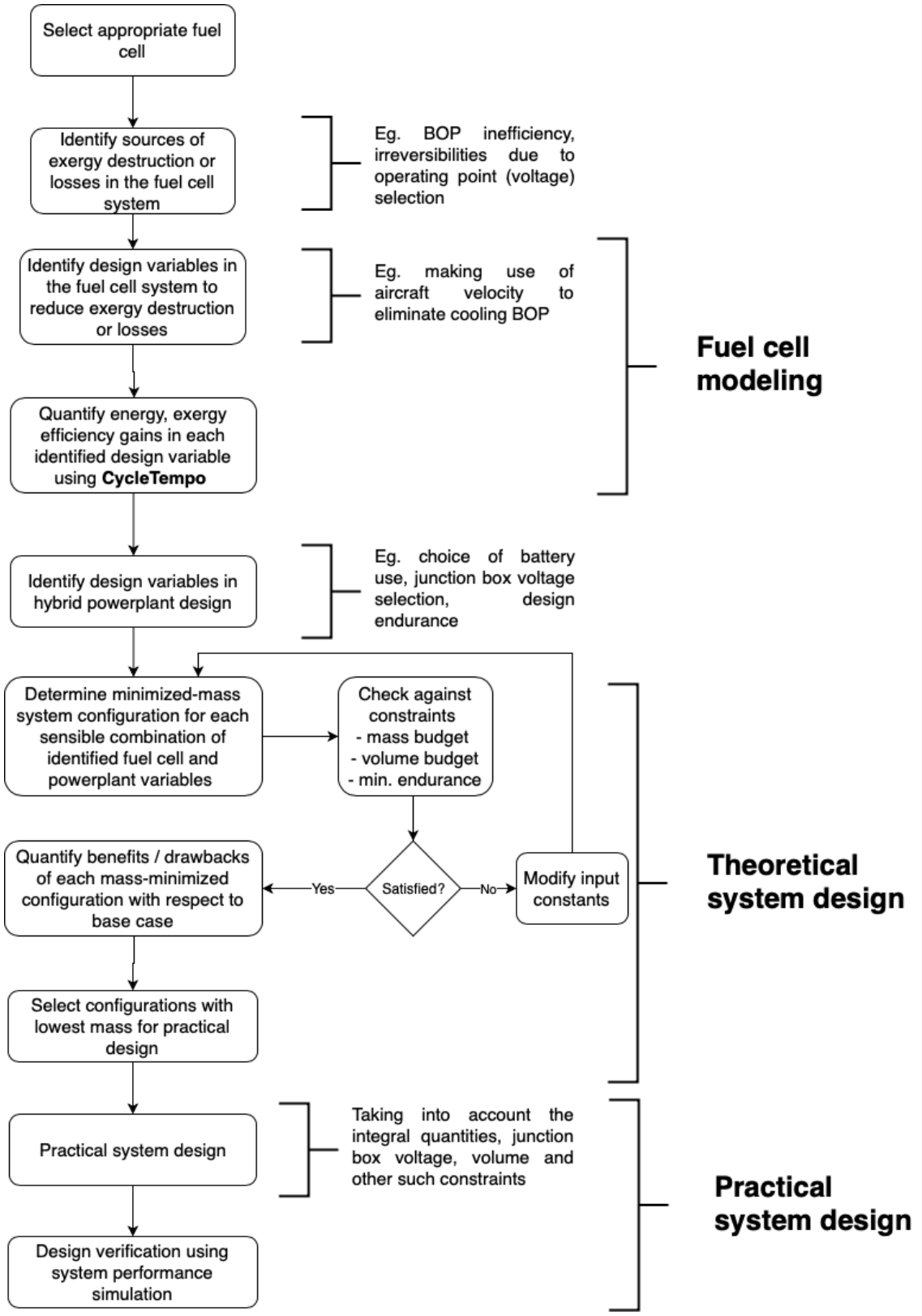

Figure 2.11: Exergy-gravimetric approach to select mass-minimized powerplant configuration

Chapter 3

Literature Review

In this chapter, previous work on exergy-gravimetric analysis, design of fuel cell-hybrid aircrafts, and analysis of previously flown aircrafts is summarized.

3.1 Exergy-gravimetric analysis

An exergy-gravimetric approach was suggested by Haynes et. Al. in [7] to design for an increased SOFC system density. In this study, the authors aimed at an exergy-aided weight reduction of the overall system, including fuel, based on the added insights provided by 2nd law analysis. The authors modeled and simulated a conceptual Solid Oxide Fuel Cell system for long duration unmanned aerial vehicle applications. Analysis included exergy analysis, and its impact on system weight. Two separate concepts are discussed in the publication. In the first concept, a coupled electrochemical-thermal SOFC transport phenomena are modeled and simulated in MATLAB, and in spatio-temporal manner. Exergy destruction was calculated along the flow channels, and "dead fuel" assessment is carried out using 1^{st} law and 2^{nd} law. The second concept was a systems level approach to determine the exergy and size relevant metrics in an overall attempt to increase the compactness of a power dense SOFC concept. "High efficiency" and "High power" systems were conceptualized and impact on overall system weight was demonstrated for the specific mission. Similarly, a "small cell" and a "big cell" were compared to understand the impact of cell size on system weight. It was found that a "big cell" design was lighter than the "small cell" design at the system level. In the study, it is unclear how the approach towards an exergy-gravimetric design is developed and applied to an overall minimized system weight. It is also not clear how various operating parameters of SOFC like inlet air temperature, and power density have been determined for system design. The impact of design variables on exergy-gravimetrics has also not been demonstrated.

3.2 Hybrid aircraft designs

A fuel cell sizing methodology is presented by Guida et. Al. in [42] based on an optimization procedure concerning the size and efficiency of each power system component in order to achieve the max. specific energy (higher than 500 Wh/kg). This paper presents equations used for determining the optimal system size, i.e. number of fuel cell stacks, air blowers, batteries and fuel tanks to achieve a system level energy density of more than 500 Wh/kg. The system is designed around the HES A1000 fuel cell stack (which during 2017 was supplied as stack-only without integrated fan). The number of stacks was varied to analyze its impact on the specific energy density at the system level. It was demonstrated that PEM fuel cell power plants can guarantee higher system level specific energy density. Further, an optimal configuration for the project requirements was determined. However, no exergy analysis has been presented.

Romeo et. Al. in a series of publications have suggested design methodologies for a Hydrogen powered 2-seat aircraft propulsion system. In [32], an aircraft selection methodology is published where the aircraft is selected based on comparing multiple parameters like the power vs. velocity curves, wing loading etc. Next, based on aircraft selection, a preliminary set of requirements for the aircraft powertrain is outlined, specifying the power and energy requirements. The powerplant is parametrically sized considering the specific and volumetric energy and power density of batteries, fuel cells, and fuel tanks. The impact of fuel cell power density on powerplant volume and payload capacity are analyzed. In [43], it is mentioned that one of the most critical aspect of a PEM fuel cell powered flight is the temperature control of the stack, specially at high altitudes. In [44], the power system is described. The fuel cell system is sized to supply 20 kW output power, sufficient to power the aircraft for cruise flight. A final flight endurance of 40 minutes was achieved, with the limitation being water consumption of the fuel cell and not the fuel quantity on-board. The optimization method used in this research considers the fuel cell operating only at its rated output power, and minimizing exergy losses by operating the fuel cell at lower power density is not considered. Moreover, this research sizes the powerplant for a fully fuel cell powered flight only, and an optimal powerplant configuration where battery and fuel cell, both provide power during cruise flight is not provided.

The Antares DLR-H2 project served as the flying test-bed for testing fuel cell powerplants for aircraft applications. This aircraft's powerplant was designed completely with using fuel cells, and batteries were used only for smaller transients.

In [45, 46], the aircraft Antares 20E was modified to include two additional payload nacelles on the bottom of the wings. These nacelles provided an additional payload capacity of about 100kg each to provide additional payload capacity and volume for the fuel cell system. The fuel cell system is capable of providing 30 kW continuous power, while the cruise power of the aircraft is 14-16 kW. The fuel tank has a capacity of 4.9 kg H_2. The fuel cells are mounted within one nacelle, while the fuel tank is contained in the other. Fuel cells are hybridized with batteries using "direct hybridization" scheme. This aircraft demonstrated an endurance of 5 hours, consuming about 1 kg H_2/hr. on a level flight.

The Stalker XE is an Unmanned Aerial System (UAS) designed for reconnaissance missions. This long endurance developed by Lockheed Martin is powered by SOFCs, and provides a flight time of more than 8 hrs. The UAS weighs only 24 lbs (10.9 kg), with a payload capacity of up to 5.5 lbs (2.5 kg). Further information about system is unavailable.

3.3 Hybridization schemes

Planes et. Al. in [47, 48, 49] analyzed two different architectures for a hybrid power source comprising a PEM fuel cell and a Li-Ion battery, for the first fuel cell powered aircraft, the Boeing FCD. The objective is to analyze the two power system architectures for this hybrid power source, the regulated and the unregulated. For this aircraft flight course, both batteries and fuel cells supply power during takeoff and climb, while only fuel cells provide power during cruise. Battery is not recharged during cruise. In the unregulated architecture, the fuel cells and battery are connected together to the junction box by OR'ing diodes. In the second architecture, regulation is achieved by means of a series boost converter. The fuel cell system was sized to supply a continuous 24 kW out of the 40 kW requirement. For a regulated system, the battery weight savings amounted to about 6 kg (assuming an energy density of 70 Wh/kg, in 2008). For the technology available in 2008, it was concluded that although the unregulated system is less complex, more reliable, has higher efficiency, and lower cooling requirements, the regulated system weighs less due to potential battery savings, and is more robust in controlling the power distribution between battery and fuel cell.

In [50], Nishizawa et. al. have presented a battery sizing method for fuel cell hybrid system design, based on numerical modeling and theoretical experiments, including recharging experiments using the same hybrid system setup. The following steps are suggested for sizing an appropriate battery system for a direct

hybrid fuel cell powerplant:

1. Define the max. power output from the fuel cell.
2. Select the number of fuel cells required to achieve the maximum power.
3. Define the maximum acceptable voltage, V_{FC0} for the selected fuel cell.
4. Define the voltage V_{FC1} at maximum power output from the fuel cell system. This is found using the IV curve of the fuel cell.
5. Select the number of cells in series for the battery such that the OCV of the battery, V_{BATT0} is in the range $V_{FC1} < V_{BATT0} < V_{FC0}$, and the minimum voltage at the max. current, V_{BATT1} is close as possible to V_{FC1}.

$$\begin{aligned} V_{FC1} < V_{BATT0} < V_{FC0} \\ V_{BATT1} \approx V_{FC1} \end{aligned} \tag{3.1}$$

For the specific design, the impact of number of batteries in series is shown in Figure 3.1 below.

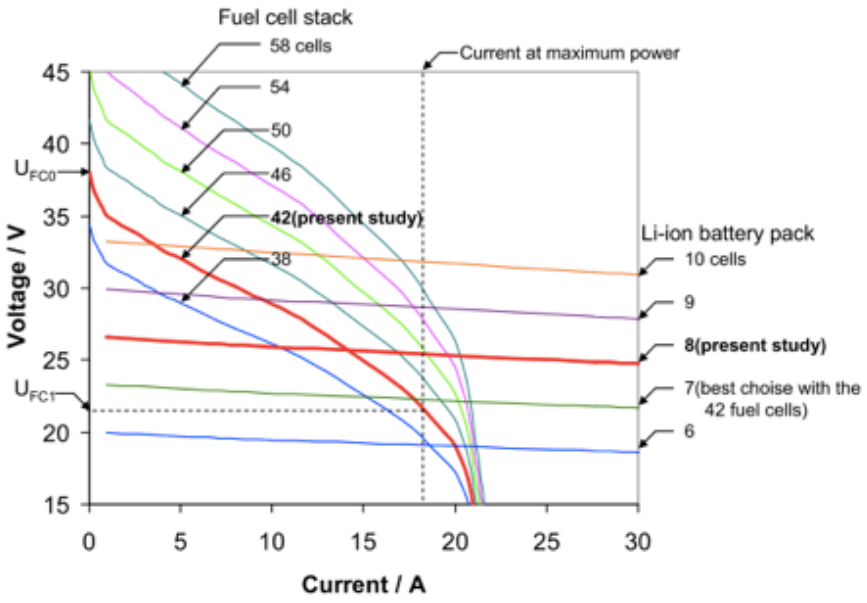

Figure 3.1: Combination map of the number of fuel cell stacks and Li-Ion battery packs in the hybrid system.

The Figure 3.1 shows the IV curves of fuel cell system with different number of cells connected in series, along with different number of battery cells in series. Similar approach has been suggested and tested [51, 52, 53] for selecting the number of cells in series for a direct hybrid powerplant. This approach is also used in this thesis work to select the number of battery cells.

Chapter 4

Fuel cell modeling

4.1 Introduction

Exergy-gravimetric analysis for powerplant system sizing requires exergy and energy efficiency analysis. This analysis requires modeling of the fuel cell system, which is explained in this chapter.

CycleTempo [54], a powerful software developed within TU Delft for thermodynamic analysis, was used for exergy and energy efficiency analysis of the fuel cell system. Although much of the information required for CycleTempo modeling was available, some data was still not available with complete ambiguity. To overcome this, a curve-fit MATLAB model was developed to approximate these parameters from available data and literature.

This chapter starts with explaining the modeling methodology, followed by fuel cell selection for modeling. Next, the MATLAB and CycleTempo models for the fuel cell are explained. Results, analysis and conclusion is presented towards the end.

4.2 Modeling methodology

This section describes the steps followed to model the fuel cell system on MATLAB and CycleTempo to compute the energy and exergy efficiency of identified exergy-gravimetric cases. The first part of this section explains the MATLAB modeling method, and the second part explains the CycleTempo modeling method.

4.2.1 MATLAB modeling

Once the fuel cell is selected, all available data about the fuel cell is gathered. For MATLAB modeling, the required information is:

- Number of cells per stack.
- IV curve of the fuel cell per cell. If per-stack is available instead of per-cell, the per-cell IV curve can be calculated by dividing the voltage by number of cells.
- Anode, cathode inlet pressure (or range).
- Fuel cell operating temperature (or range).

Next, a 1-dimension electro-chemical model is developed on MATLAB using the fuel cell polarization equations (Equation 2.9).
An IV curve is generated using available information, and *guesses* for parameters for which accurate information is unavailable (eg. anode pressure, operating temperature). This IV curve is compared against the IV curve provided by the manufacturer, and SSE (Sum of Squared Error) is calculated. This is repeated until sufficiently small SSE is attained. Once these iterations are complete, the outcome is fuel cell parameters, henceforth called ”characteristic values” to avoid ambiguity (eg. exchange current density, limiting current density). Since the exact value of these parameters is unknown, these values are validated against literature. This process of user-provided *guesses* is repeated until the parameters are within range specified in literature. After validation, the *guesses* are used as input data for CycleTempo modeling, as well as to generate current and voltage data at the simulation points for CycleTempo. This methodology is explained in Figure 4.1.

4.2.2 CycleTempo modeling

CycleTempo is a very powerful modeling software in which fuel cell systems including BOP components can be modeled. It also calculates energy and exergy efficiencies for individual components, and for a system as a whole. Thus, CycleTempo was used for the exergy efficiency computations. The first step is fuel cell system schematics identification. This requires information about fuel cell cooling method, membrane humidification method, and fuel characteristics. Using this information, data generated in MATLAB, and certain assumptions, a ”scheme” is developed. This scheme is run at ”rated output” of the fuel cell, and results are run through sanity checks to validate model. If sanity checks fail, either scheme or

assumptions (or both) are modified. This is repeated until the model is validated. These sanity checks include checking for negative exergy flow, abnormal fluid flow rates, and outlet humidity of the cathode (which should be between 80% to 100% [8])

After scheme validation, various exergy-gravimetric cases identified are simulated to obtain energy and exergy efficiencies. This data is then used to theoretically size minimized-mass systems, as explained in the next chapter. This modeling methodology is presented in Figure 4.2.

4.3 Fuel cell selection

Commercially available PEM fuel cell systems are explored in this study. A list of most promising fuel cell systems (in terms of specific power density at system level) are presented in Figure 4.3. These systems are compared against each other on the basis of specific power density and volumetric power density at their rated power output. The figure also presents a segregation between air-cooled and liquid-cooled PEM fuel cells.
Figure 4.3 compares the specific and volumetric power density of some commercial fuel cell systems. Note that these densities do not include the weight of fuel and fuel storage. From Figure 4.3, it is evident that air cooled systems have comparatively higher specific power density than liquid cooled systems. However the volumetric power density of liquid cooled systems is higher. It should be noted that although air cooled fuel cells have higher specific power density than their liquid cooled counterparts, they are available in lower power levels ($\leq$ 2 kW), and thus need to be stacked together to reach required power levels.

4.3.1 Selection criteria

Specific power density of the fuel cell and energy efficiency are important for this thesis work since the presented work aims to obtain minimized-mass configurations for a fuel cell-hybrid powerplant for an aircraft. Hence, the selection criteria is to select the fuel cell with the highest specific power density. BOP components not only add parasitic weight, but also inefficiencies to the system. This results in lower power density. This is also evident from Figure 4.3 where liquid cooled systems, which have considerably higher BOP components, have much lesser specific power density compared to their air-cooled counterparts.
This way, the air cooled fuel cell ”UAV 800W” from Intelligent Energy [15],

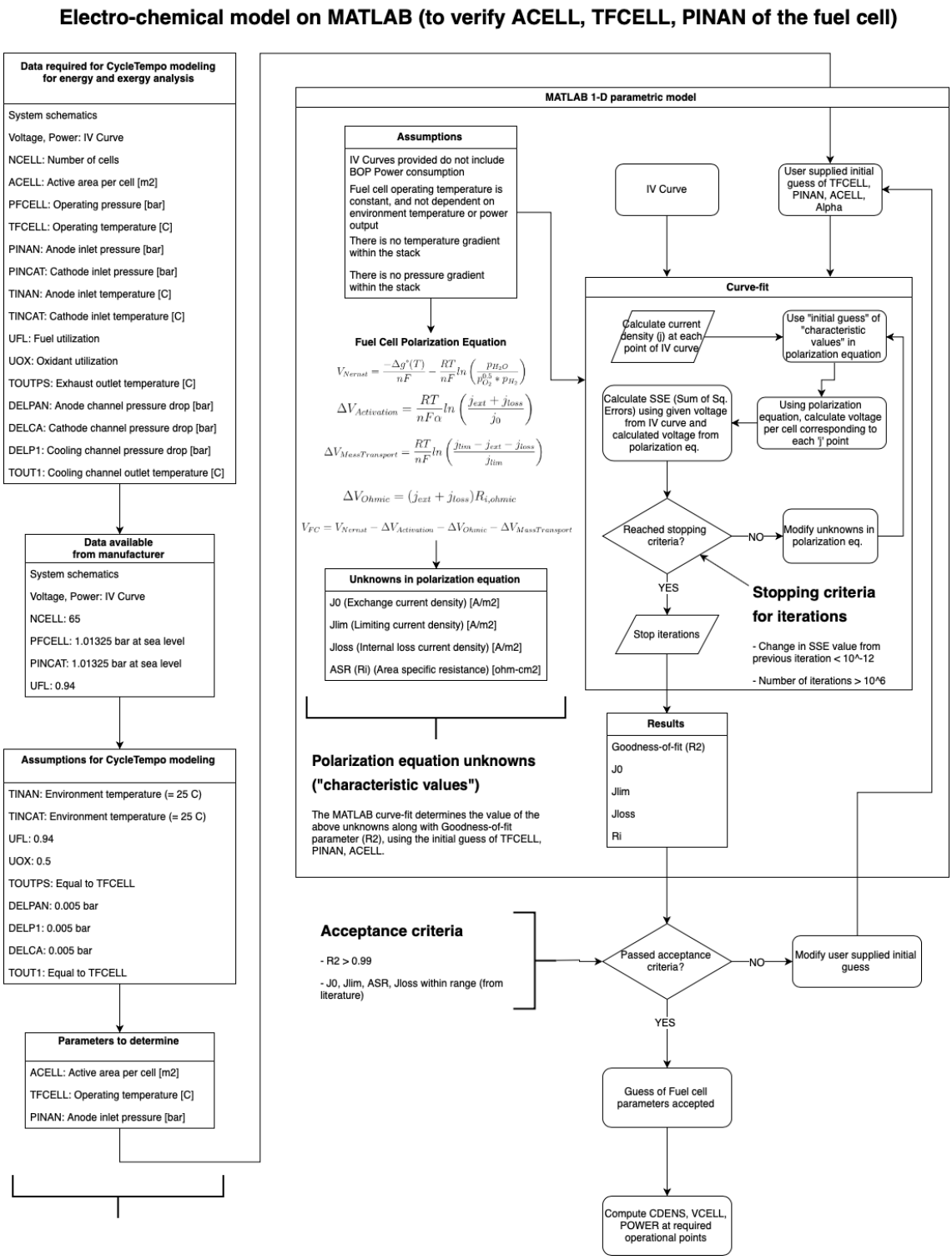

Figure 4.1: Modeling methodology on MATLAB

with a specific power density of up to $860.2W/kg$ outclasses all other fuel cells available commercially. However, sufficient information required for MATLAB and CycleTempo modeling is not available from the manufacturer. Hence the next-best fuel cell system (in terms of specific power density), the "HES A1000-65" with a specific power density of about $555W/kg$ [16] is selected. This fuel cell

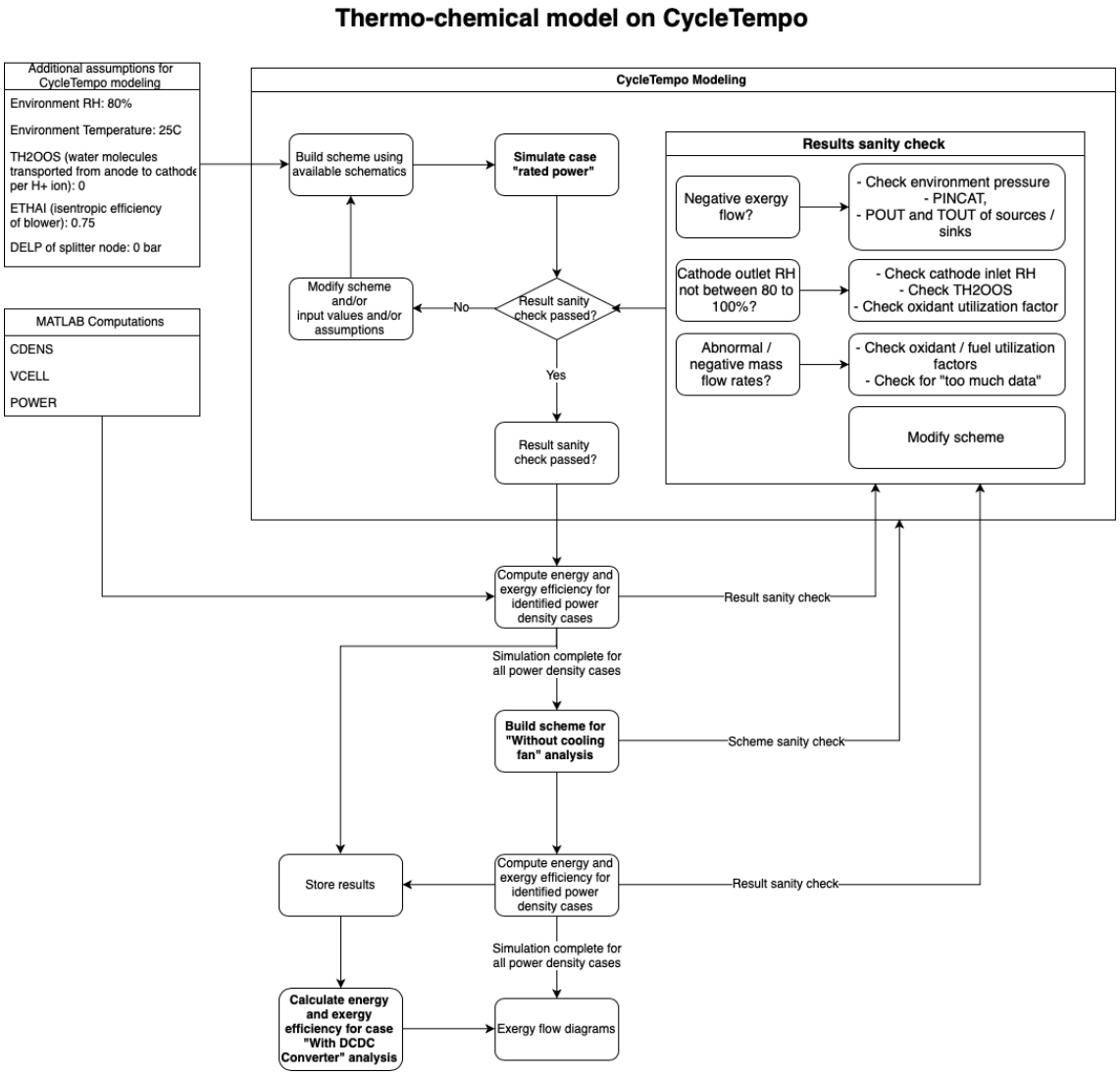

Figure 4.2: Modeling methodology on CycleTempo

will be used for all modeling, simulations, and system sizing.

4.3.2 Information about selected fuel cell

The HES AeroStak A1000-65 is a PEM air cooled fuel cell system designed specifically for aerial vehicles. The A1000-65 delivers a rated continuous output power of 1000W, and has 65 cells connected in series [16].

Summary

A summary of all the information available about the fuel cell is tabulated in Table 4.1. The manufacturer provided IV curve is shown in Figure 4.4. The information required for CycleTempo modeling is tabulated in Table 4.2 [16]. Accurate information about certain parameters, like fuel cell stack IV curve, num-

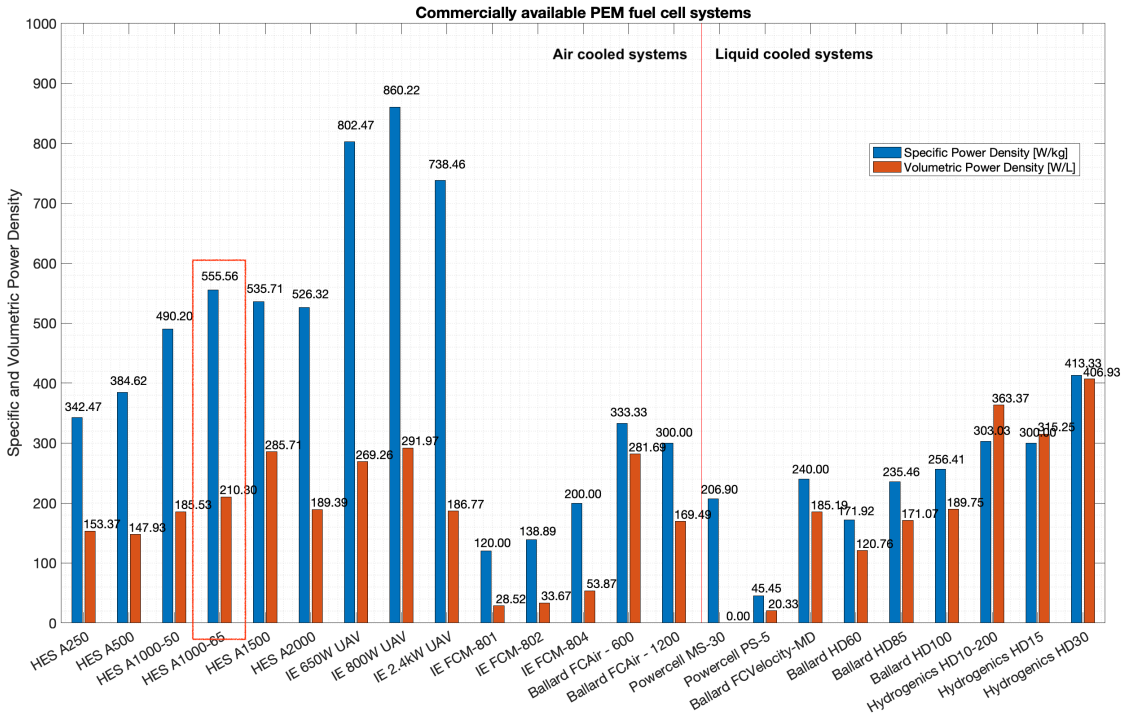

Figure 4.3: Commercially available PEM fuel cells

ber of cells, and cathode inlet pressure is available from the manufacturer. The fuel utilization factor (UFL) accounts for fuel lost due to purging. However the values marked in *red* in the Table 4.2 are ambiguous, i.e. exact values are not known / available. These parameters and the ambiguity is explained next.

Active area per cell (ACELL): The manufacturer specifies the MEA (membrane-electrode assembly) dimensions as 180 * 34 mm (= 61.2 cm^2 max.), however also mentions that the active area is less due to glue at the edges [16]. Thus the active area could be anything up to the maximum.

Fuel cell operating temperature (TFCELL): The max. operating temperature of the fuel cell is specified as 70 °C. This means that the actual operating temperature could be any value less than 70 °C. Practically, the operating temperature would depend on a number of variables, such as ambient temperature and fuel cell output power. However modeling the effect of these parameters on the fuel cell is beyond the scope of this work, and hence a single temperature value is required for modeling and simulations.

Anode inlet pressure (PINAN): The anode inlet pressure specified by manufacturer is 0.6 to 0.8 bar. It is not clear however if this is absolute pressure or gauge pressure. Moreover, since the fuel cell is also purged, it is not clear how it can be purged if the anode pressure is less than ambient pressure.

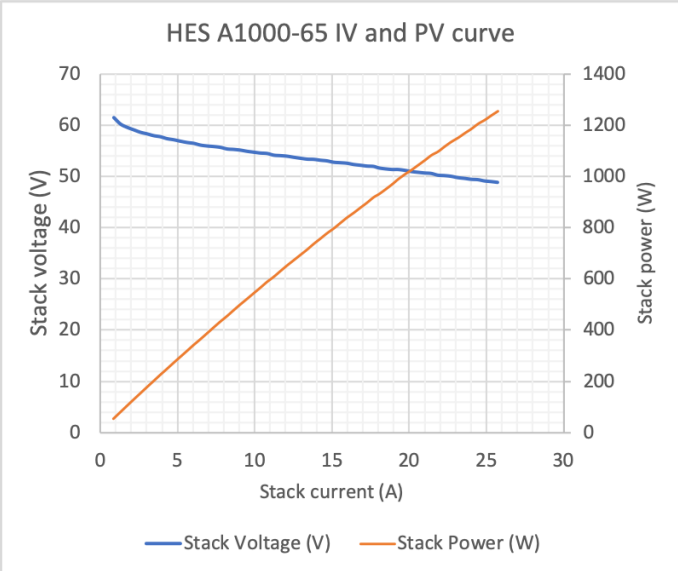

Figure 4.4: IV curve of the HES A1000-65, reproduced from the IV curve image provided by the manufacturer [16].

Since these values are ambiguous, the MATLAB model developed is used to verify the guesses for the above mentioned parameters. As observed in Figure 4.4, the IV curve provided by the manufacturer does not provide voltage values corresponding to current less than 1A. Simulink model of the system in Chapter 6 requires fuel cell voltage at 0V and 1V, which are also calculated using the developed model.

System schematics

Exact system schematic was not available from the manufacturer and hence it was reconstructed using the information already provided by them. Due to self humidification, the fuel cell stack does not require an external humidifier. The manufacturer also states that cathode fan is also used to cool the fuel cell, and hence only a single fan is needed. The air inlet pressure is also specified as "ambient" by the manufacturer. On-board electronics on the stack do not include a DC-DC converter [16]. The cooling channel and cathode channel are separate, but exhaust via the same fan placed downstream.
Using this information, the reconstructed system schematic is presented in Figure 4.5.
The cooling unit (fan/blower) can either be placed upstream or downstream. Since it is given that the cathode inlet pressure is ambient pressure, an upstream unit would mean that inlet pressure at cathode is higher than ambient, which contradicts the information available. Hence, the cooling fan is placed downstream. Note that although the fan is represented as a separate unit in the schematics, it is already integrated into the fuel cell system.

Table 4.1: Summary of available information about HES AeroStak A1000-65 [16].

HES Aerostak A1000-65	
Number of cells	65.00
Nominal power [W]	1,000.00
Peak power [W]	1,300.00
Anode input pressure [bar]	0.6-0.8
Cathode pressure [bar]	Open air cathode, ambient pressure
Humidification method	Self humidified
Stack voltage range [V]	39 - 61.8
Stack current range [A]	0 - 35
Total weight per stack [kg]	1.80
FC system dimensions [mm]	194*127*193
H_2 purity [%]	>99.99
Max H2. consumption [L/min]	<15.2
Power de-rating per 1000m [%]	1.50
Max. system temperature [°C]	70.00
Cooling mechanism	Cathode air fan also cools the cells
Fuel utilization	∼0.94
MEA dimensions [mm]	180*34

Table 4.2: Summary of input data required for CycleTempo model of the HES AeroStak A1000-65. The value of some parameters is not available, and these are assumed, as explained in section 4.4.

Data for CycleTempo simulations			
Parameter	**Unit**	**Description**	**Value**
Power	W	Stack power	From IV curve
VCELL	V	Cell voltage	From IV curve
NCELL	-	Number of cells	65
ACELL	cm^2	Active area per cell	max. 61.2
PFCELL	bar	Operating pressure	
TFCELL	°C	Operating temperature	max. 70
PINAN	bar	Anode inlet pressure	0.6 to 0.8
PINCAT	bar	Cathode inlet pressure	Ambient
TINAN	°C	Anode inlet temperature	
TINCAT	°C	Cathode inlet temperature	Ambient
UFL	-	Fuel utilization	0.94
OUX	-	Oxidant utilization	
TOUTPS	°C	Exhaust outlet temperature	
DELPAN	bar	Anode channel pressure drop	
DELCA	bar	Cathode channel pressure drop	
DELP1	bar	Cooling channel pressure drop	
TOUT1	°C	Cooling channel outlet temperature	

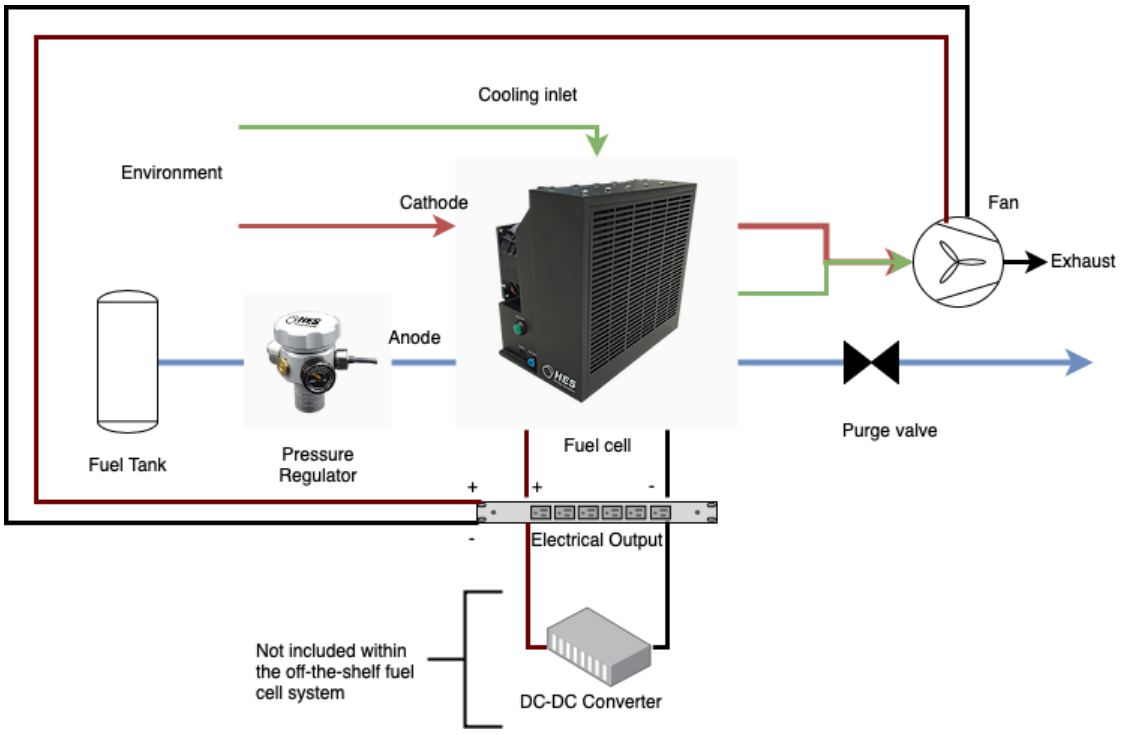

Figure 4.5: System Schematics of HES-A1000-65

Exergy-gravimetric cases

The electrical efficiency of a fuel cell is directly a function of its voltage, which is a function of current density j_{ext} (Equation 2.9), and thus, the fuel cell efficiency is a function of its operational power density. Therefore, one of the cases identified for exergy-gravimetric analysis is the operational power density (as % of the rated power density of the fuel cell).
The fuel cell schematics in Figure 4.5 show that the system does not have many BOP components, except the fan and DC-DC converter. Hence these components are identified as the other cases for exergy-gravimetric analysis. These cases and their values are summarized in Table 4.3.

Table 4.3: Identified exergy-gravimetric cases for HES A1000-65 fuel cell

Operational power density		Use of DC-DC converter	Use of cathode fan
% of rated	Specific power density [W/kg]		
25	138.75	No	No
50	277.5	Yes	Yes
75	416.25		
100	555		
125	693.75		

A note on use of DC-DC converters

For weight estimation purposes, the power density of DC-DC converters is taken as 1.36 kW/kg from literature [33]. DC-DC converters are used to match the fuel cell voltage to bus-bar voltage, and to also maintain fuel cell output power. In some cases when matching the fuel cell system voltage to the required junction box voltage is possible without the use of DC-DC, their use can be avoided by passive-hybrid system design, explained in chapter 6.

A note on use of cathode fan

The fan ensures sufficient air flow rate is maintained across cathode and cooling channels. It is demonstrated [55] that if proper airflow is not maintained in cooling channels, it can lead to temperature gradients of about 5 °C, even up to 8 °C in the fuel cell stack (depending on the shape and size of the stack and flow channels), which is also known to degrade stack performance and lifetime [56, 57, 58, 59, 60, 61, 62, 63, 64, 65]. This increase in stack temperature leads to faster water evaporation causing the membrane to dry out. If sufficient humidity is not maintained, the ionic conductivity of Nafion decreases (and ohmic resistance increases) [66, 12, 67]. Acceptable temperature gradients up to 2 degree across the flow channels have been reported in literature [68, 69].

4.4 Fuel cell modeling

For simulating various exergy-gravimetric cases identified in Table 4.3, the current density and voltage values are approximated using the MATLAB model, which are then used in the CycleTempo model. Effect of the use of cathode fan is also simulated using CycleTempo. Since DC-DC converter is a pure electrical device, its effect on energy and exergy efficiency is calculated after calculating efficiencies of all other cases, by directly multiplying its efficiency with the results. Fuel cell models developed on MATLAB and CycleTempo are explained in this section, along with assumptions, validation criteria and results.

4.4.1 MATLAB model

As explained in subsection 4.3.2, parameters ACELL, PINAN, and TFCELL required for CycleTempo model are ambiguously known. This section explains the MATLAB model developed to guess these parameters, the validation criteria, and results.

Assumptions

Modeling a 1-D model of PEM fuel cell required certain assumptions to simplify calculations:

1. The IV curve provided by the manufacturer is for the stack-only, and does not include the parasitic power consumption of balance-of-plant components, i.e. in this case, the cooling fan. As will be seen in the CycleTempo results later, the cooling fan consumes less than 1.5% power produced by the fuel cell operating at its peak power, and thus the power consumption of the cooling fan is insignificant.

2. Operating temperature of the fuel cell is maintained constant, and is not dependant on the ambient temperature or operating power. This assumption is often used in literature for modeling a fuel cell parametrically [12, 9, 8, 70, 71]. It is also assumed that the temperature within the stack is uniform, i.e. there are no temperature gradients within the stack.

3. The reaction pressure at the anode is the average pressure across the flow channel. Same is assumed for cathode. The pressure across flow channels drops due to fuel and oxidant consumption. As with the previous point, single pressure values are often used in literature [12, 9, 8, 70, 71].

4. *Characteristic values*: limiting current density (j_{lim}), loss current density (j_{loss}), charge transfer coefficient (α), and area-specific resistance (R_i) and exchange current density (j_0) used in fuel cell polarization equation are constants and independent of operating temperature or pressure. These values are generally modeled as constants in simplified 1-D models such as the one used in this work [12, 9].

5. Inlet fuel is of high purity ($> 99.99\%$) [16].

6. Oxygen concentration in ambient inlet air is 21%.

7. Charge transfer coefficient (α) is assumed to be 0.5 [12, 9].

Since the range of possible values for ACELL, TFCELL and PINAN is very large, some additional assumptions were made to reduce the number of iteration runs.

1. **Active Area per Cell (ACELL)**: The manufacturer specifies the MEA dimensions as 180 mm * 34 mm per cell, which gives an area of 61.2 cm^2 [16], however they also specify that the active area per cell is lower because of the glue on the perimeter of the MEA. The glue on MEA perimeter is assumed to be either 1mm, or 2mm on each edge. This results in ACELL to be either 52.8 cm^2 or 56.9 cm^2.

2. **Anode Inlet Pressure (PINAN)**: As per the manufacturer, the anode pressure is 0.6 to 0.8 bar. However as mentioned earlier, it is not clear if this is gauge pressure of absolute pressure. Moreover, if this pressure is absolute pressure, it is not sure how purging can be achieved. Hence, it is assumed that anode inlet pressure specified by manufacturer is absolute pressure. Furthermore, it is assumed that the inlet pressure is the average of the manufacturer specified range, hence 1.7 bar absolute pressure.

3. **Fuel cell temperature (TFCELL)**: Since the max. operating temperature of the fuel cell is 70 °C, the nominal would be lesser, and 70 °C is excluded from input parameter iterations. The iterations are thus run for 60, 62, 64, 66, 68 $^{\circ}C$.

Using the above mentioned assumptions, a list of parameters (with their possible different values) is mentioned in Table 4.4.

Table 4.4: Different operation condition combinations

PINAN [bar]	**TFCELL [C]**	**ACELL [cm^2]**
1.7	60	52.8
	62	56.96
	64	
	66	
	68	

The next part describes how the most suitable combination is selected out of all the above combinations.

Modeling method

The IV curve of the fuel cell as provided by the manufacturer are in an image. This image is fed into an image-processing open-source software [72] to extract the data points in a .csv format. Voltage values in the data are divided by the number of cells in the stack (65) to obtain IV curve per cell. This per-cell IV data is used for all further calculations.

Fuel cell polarization equation (Equation 2.9) is used model the IV curve of the fuel cell on MATLAB. Optimizer function *fmincon* is used in MATLAB to evaluate cost function and iterate variables to arrive at the most feasible solution.

Objective function

The objective function used for curve-fitting is given in the equation below.

$$min.SSE = \sum_{I=0}^{endvalue} (V_I - f(I, TFCELL, PINAN, ACELL))^2 \tag{4.1}$$

Where V_I is the voltage from the provided IV curve, and $f(...)$ is the voltage value obtained using the fuel cell polarization equation. The objective of this function is to minimize the sum-of-squared-errors (SSE) between the provided IV curve and the IV curve generated using the user-provided input constants and the polarization equation Equation 2.9 at each current value.

Variables

Variables are the *characteristic values* of the fuel cell, which are determined using curve-fitting. These variables are:

1. Exchange current density (j_0) [A/m^2].
2. Loss current density (j_{loss}) [A/m^2].
3. Limiting current density (j_{lim}) [A/m^2].
4. Area-specific resistance (R_i) [$\Omega - cm^2$].

fmincon returns the values of these variables such that the value of the objective function is minimum at the resultant values of these variables.

Stopping criteria

The number of iterations performed in MATLAB *fmincon* and *GolbalSearch* [73] depend on the stopping criteria. Iterations terminate when these tolerances are hit. Following tolerances were defined for optimization runs:

- FunctionTolerance: 10^{-12}
- StepTolerance: 10^{-12}
- MaxIterations: 10^6

Definitions of the above tolerances can be found in [73]. Loose tolerances mean that the system converges quickly, and so the result may be a local optimum but not global optimum. Tight (strict) tolerances however might lead to non-convergence. These tolerance values were arrived at after numerous iterations with varying values. The *GlobalSearch* function in MATLAB runs iterations with different starting points to arrive at the global optimum.

Input constants

The curve-fit function requires values of operational parameters of the fuel cell, which are used in the fuel cell polarization equation (Equation 2.9). These values are:

1. Fuel cell operating temperature (TFCELL) [°C].
2. Active area per cell (ACELL) [cm^2].
3. Anode inlet pressure (PINAN) [bar].
4. Cathode inlet pressure (PINCAT) [bar].
5. Fuel concentration.
6. Oxidant concentration.

Value of fuel and oxidant concentration are assumed (as mentioned in assumptions earlier). PINCAT is taken to be ambient atmospheric pressure. The value of remaining constants (ACELL, TFCELL, PINCAT) need to be verified, and are manually entered for all combinations as per Table 4.4. The input combinations for these variables is already known from Table 4.2.

Validation criteria

Values suggested in literature have been used to validate the results obtained via curve-fit. Since its not possible to determine precise values, the obtained results are accepted if they fall in the same range as reported in literature. Table 4.5

Table 4.5: Literature suggested range for characteristic values.

Characteristic value	**Values suggested in literature**	**Notes / references**
j_0 [A/cm^2]	10^{-9} to 10^{-5}	[74, 75, 76, 77, 8, 78]
j_{lim} [A/cm^2]	0.9, 1.6	[12, 8, 79]
j_{loss} [A/cm^2]	10^{-4} to 10^{-2}	[12, 8]
R_i [ohm-cm^2]	0.15 to 0.41	[12, 75, 8, 76]

Apart from these values, the R^2 value (Goodness-of-Fit) is also calculated. The results are accepted if $R^2 > 0.99$ [80].

Results and analysis

Calculations were run for all the input combinations mentioned in Table 4.4. The selected results are listed in Table 4.6. For the selected values, the Goodness-of-fit (R^2) was calculated to be 0.99743, higher than the acceptance criteria.

Table 4.6: Resultant parameters after curve-fitting

Parameter	Value	Characteristic value	Value
TFCELL [°C]	62	j_0 [A/cm^2]	$9.293 * 10^{-7}$
PFCELL [bar]	1.7	j_{lim} [A/cm^2]	2
ACELL [cm^2]	52.8	j_{loss} [A/cm^2]	10^{-4}
		R_i [ohm-cm^2]	0.1997

The corresponding IV curve generated using the above set of values is shown in Figure 4.6. The vertical lines in the plot represent the different power settings identified for exergy-gravimetric cases in Table 4.3, along with cell voltage at each point. These current density and cell voltage values at various operating points is mentioned in Table 4.7, and will be used for CycleTempo simulations in the next section.

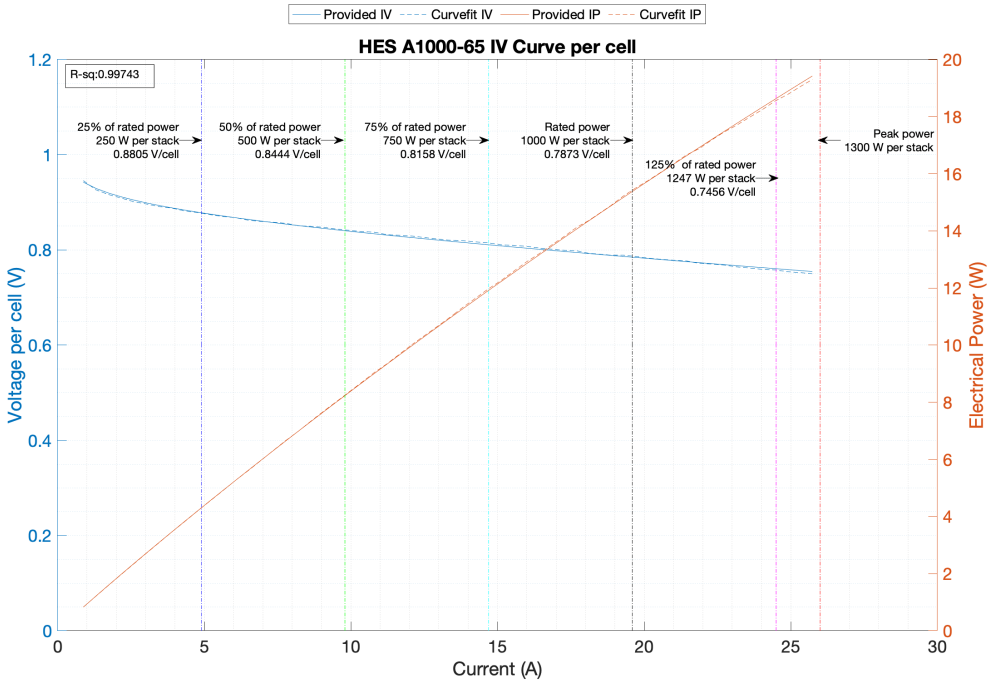

Figure 4.6: Actual IV curve of HES A1000 plotted against its curve-fit.

4.4.2 CycleTempo model

The air-cooled self humidified HES A1000-65 fuel cell was modeled in CycleTempo for energy and exergy flow analysis. This section explains the assumptions used to develop the CycleTempo model, the system scheme, and finally the energy and exergy efficiency results.

Table 4.7: Current density and cell voltage values at various power density settings.

% of Rated Power	25	50	75	100	125
Current [A]	4.3708	9.1101	14.1434	19.6000	25.7300
Current density [A/m2]	827.80	1725.39	2678.67	3712.12	4873.10
Voltage per cell[V]	0.8805	0.8444	0.8158	0.7873	0.7456
Power per cell [W]	3.84	7.69	11.53	15.43	19.18
Power per stack [W]	250.15	500.01	749.98	1003.02	1246.97
Operating temperature [C]	62	62	62	62	62
Cathode pressure [bar]	1.01325	1.01325	1.01325	1.01325	1.01325
Anode pressure [bar]	1.7	1.7	1.7	1.7	1.7

Two CycleTempo schemes were developed: one for the system with the fan, and another model for one without the fan. For both these schemes, simulations were run for all the different power density cases identified in Table 4.3 to calculate energy and exergy efficiencies.

System scheme

The scheme for *as-is* system, i.e. with fan is shown in Figure 4.7. The *blue* stream represents the fuel flow channels, while the *red* represent cathode air, and *green* represent the cooling air flows. Apparatus 100 is the SPFC (PEM) fuel cell. Apparatus 101 is the fuel tank. Apparatus 111 and 121 represent ambient atmosphere. Figure 4.8 shows the scheme for exergy-gravimetric case *without fan*.

The additional assumptions made to develop and simulate the schemes are described in the next subsection.

Assumptions

The below set of assumptions are made for the *as-is* scheme (with fan) represented in Figure 4.7.

1. Losses due to pressure regulator value and purge value are neglected. It is assumed that the fuel inlet to the fuel cell is directly at 1.7 bar absolute pressure in pipe 101.
2. Since the PEM fuel cell is air-breathing, it is assumed that the air flow in pipes 111 and 121 is at ambient pressure and temperature [16].
3. It is assumed that the fuel tank is in thermal equilibrium with the environment, and hence the flow through pipe 101 is at ambient temperature, 25°C.

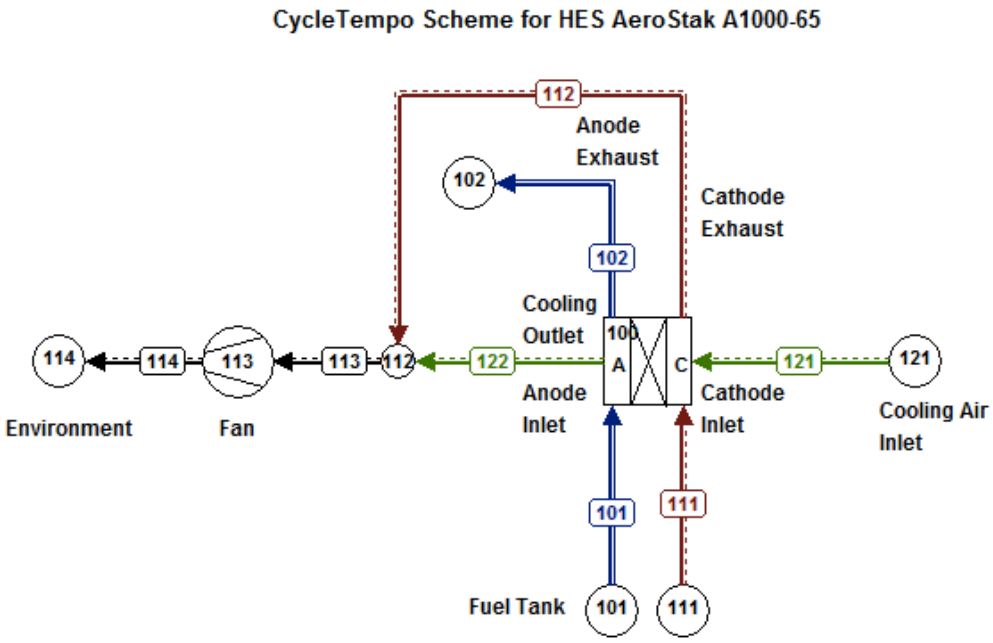

Figure 4.7: CycleTempo scheme of HES A1000-65 with cathode and cooling fan.

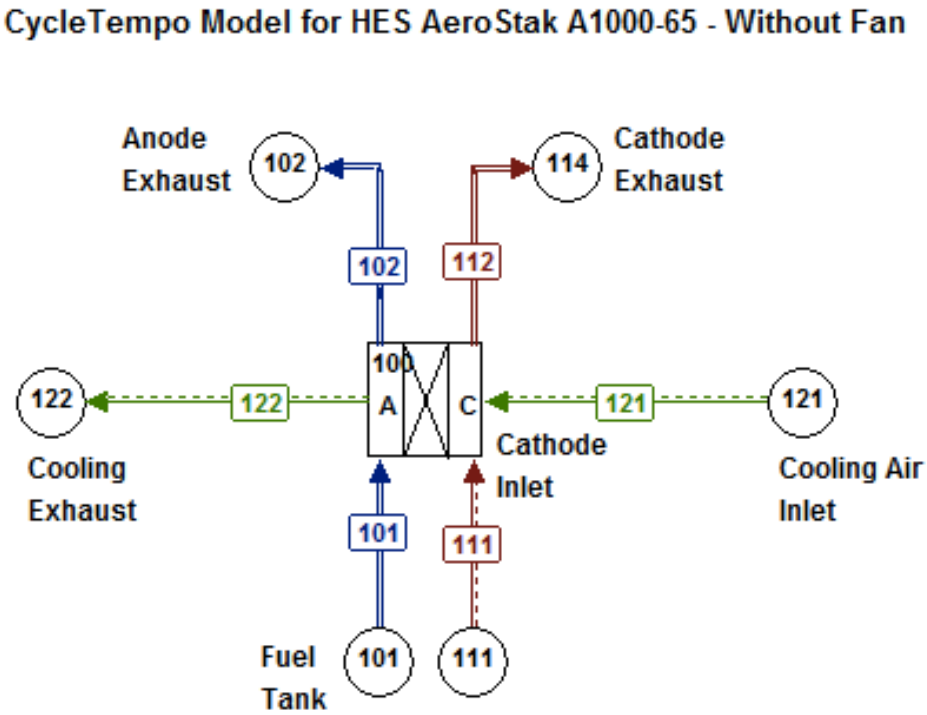

Figure 4.8: CycleTempo scheme of HES A1000-65 without fan.

4. The fuel lost due to purging is accounted for via the fuel utilization factor (*UFL*) in the fuel cell (apparatus 100).

5. Node 112, where the cathode and cooling exhaust pipes combine, is assumed to be ideal and has no pressure drop.

6. Outlet from fan (apparatus 113) is at the ambient pressure [16].

7. The effect of pressure at the flight altitude (i.e. at 300m) on fuel cell performance is assumed to be negligible. The manufacturer specifies a power de-rating of 1.5% per 1000m from sea level [16]. Since the flight altitude is even lower, the power de-rating is neglected.

For the case *without fan* represented in Figure 4.8, it is assumed that sufficient air flow and pressure to the cathode and cooling inlet can be maintained somehow.

Additional assumptions are made to make up for the unavailable physical values of the fuel cell. These assumptions are valid for both schemes.

1. Outlet temperature of all exhaust streams (pipe 102, 112, 122 in Figure 4.7, and pipe 102, 114, 122 in Figure 4.8) (TOUTPS) are at fuel cell operating temperature TFCELL.

2. Pressure drop in flow channels for fuel cell (apparatus 100) of anode (DELPAN), cathode (DELPCA) and cooling channel (DELP1) is constant 0.005 bar, and is not dependant on fuel cell power output. The pressure drop in flow channels is highly dependant on the flow field pattern [81] and thus needs to be measured experimentally. Moreover, the air cooling fan used in the fuel cell system also compensates for this pressure drop. Drawing a parallel between cooling fans used for computer cooling purposes, the best available cooling fans in the market with adequate air flow rate required for the fuel cell can exert a pressure of up to 0.001 mbar [82]. In that sense, if similar air cooling fans are used in the fuel cell system, it is unlikely that the pressure drop across flow channels would be any higher than the capacity of the fan.

3. The oxidant utilization (*UOX*) for the fuel cell (apparatus 100) is 50%. This implies an air stoichiometry of 2, which is commonly used in literature [83, 84, 85].

4. Isentropic efficiency (ETHAI) of fan (apparatus 113) is assumed to be 75% [83, 86] .

5. Net number of water molecules transported per H^+ ion movement from anode to cathode (TH2OOS) is assumed to be 0. Values of 0.07 to -0.2 mol H_20/H^+ have been reported in literature [87, 88].

6. Efficiency of DC-DC converter is assumed to be constant 95% [33, 34], and not dependant on output power.

Environment definition The environment is taken at the standard state, i.e. temperature is 25 °C and pressure is 1.01325 bar.

Efficiency calculation

The energy efficiency of a fuel cell can be given either with respect to HHV of fuel or LHV of fuel. When the fuel cell operating temperature is under 100°C, liquid water is produced and hence it makes sense to define efficiency in terms of HHV. For a fuel cell providing P_{el} output power, the electrical efficiency of the fuel cell is given by

$$\eta_{En,el} = \frac{P_{el}}{\dot{m} * \Delta H^{\circ}{}_{HHV}} = \frac{I * V(I)}{\dot{m} * \Delta H^{\circ}{}_{HHV}} \tag{4.2}$$

Where $\dot{m}$ is the mass flow rate of the fuel (kg/s), I is the fuel cell output current (amps), and $V(I)$ is the fuel cell terminal voltage (V) at current I as given by Equation 2.9. The energy efficiency in CycleTempo is computed using LHV of water. Since the fuel cell is operating at 62°C and liquid water is produced, the following equation is used to calculate *HHV* energy efficiency from *LHV* energy efficiency:

$$\eta_{En,el,HHV} = \left(\frac{\Delta H^{\circ f}{}_{H_2O,LHV}}{\Delta H^{\circ f}{}_{H_2O,HHV}} \right) \eta_{En,el,LHV} \tag{4.3}$$

Efficiency for case "With DC-DC converter": Since the DC-DC converter is an electrical device and converts input power from one voltage level to the other, the efficiency of DC-DC converter is directly multiplied by the results to obtain overall energy and exergy efficiency due to the use of DC-DC converters.

$$\eta_{withDC-DC} = \eta_{withoutDC-DC} * \eta_{DC-DC} \tag{4.4}$$

4.4.3 Results and analysis

Base case used for comparing energy and exergy efficiency is taken to be *with fan, with DC-DC converter*. The efficiency difference between cases (*with DC-DC and without DC-DC converter*) is computed via:

$$\begin{aligned} \Delta\eta_{Energy} &= \eta_{Energy,WithoutDC-DC} - \eta_{Energy,WithDC-DC} \\ \Delta\eta_{Exergy} &= \eta_{Exergy,WithoutDC-DC} - \eta_{Exergy,WithDC-DC} \end{aligned} \tag{4.5}$$

The efficiency difference between cases (with fan and without fan) is computed via:

$$\begin{aligned} \Delta\eta_{Energy} &= \eta_{Energy,WithoutFan} - \eta_{Energy,WithFan} \\ \Delta\eta_{Exergy} &= \eta_{Exergy,WithoutFan} - \eta_{Exergy,WithFan} \end{aligned} \tag{4.6}$$

Results of energy and exergy efficiency for all cases identified in Table 4.3 are presented in Figure 4.10 and Figure 4.11 respectively. Operational power density is varied along the x-axis. The orange bar graphs show the energy and exergy efficiency respectively in the base case: use of both, fan and DC-DC converter. The text in *blue* shows the efficiency difference between the base case and comparison case.

In part (a) of both figures, the energy and exergy efficiency of the fuel cell system is compared in two cases: with fan, with DC-DC; and without fan, with DC-DC. Similarly in part (b), energy and exergy efficiency is compared for the two cases: *without DC-DC, with fan* with *with DC-DC, with fan*. In the third plot (part (c)), the efficiencies for the following cases are compared: *without DC-DC without fan* with *with DC-DC with fan*.

- Energy and exergy efficiency of the systems strongly depends on the operational power density. The difference is more than 8% in all the cases, when comparing efficiency at 25% power density with efficiency at 125% power density.
- For the assumption of flow channel pressure drop in this study (0.005 bar), not using the cooling fan only marginally increases the energy efficiency, and the gains are less than 1% in all cases.
- Energy efficiency benefits of not using a cooling fan increase as the power density increases from 25% to 125%, but the the increase is again only marginal, under 0.1%.
- As expected, the energy efficiency benefits of not using a DC-DC converter are significant, more than 2%, while the exergy efficiency benefits are even higher, over 3% in some cases.
- The energy and exergy benefits of not using the DC-DC converter decrease as the power density increases, the energy efficiency difference between case 25% power density and 125% power density being still marginal, about 0.44% while the exergy efficiency difference being about 0.5%. The Equation 4.4 gives the efficiency calculation when DC-DC converters are used. Since the efficiency of the DC-DC converter itself is assumed to be constant, the variation in efficiency with respect to operational power density in cases where DC-DC is used is only dependant on the efficiency variation due to operational power density variation.

- Figure 4.9 shows the exergy flow diagram of the fuel cell system operating at 100% rated power. Although the inlet air at cathode and cooling channels has the same pressure and temperature as environment, a small exergy flow can be observed since the environment is at 100% relative humidity while the cathode and cooling inlets are at 80% relative humidity.
- For this operating condition, it can be observed that out of the 1660 W exergy input in the fuel cell, the irreversibilities due to ohmic losses, activation losses and mass transport losses contribute to more than 538 W, i.e. $> 32\%$ exergy destruction. Purging losses are comparatively lower at 6%. The next most significant losses are due to DC-DC converter at almost 3%, followed by cooling fan, which is $< 1\%$.

The exergy flow diagrams for other operating power densities can be found in Appendix A.

4.5 Chapter conclusion

In this section, the effect of varying operational power density, the effect of using DC-DC converters, and the use of cooling fan on the overall energy and exergy efficiency of the fuel cell system has been analysed. The effect of the use of these components, and system efficiency on the weight of the hybrid powerplant will be analysed in the next chapter.

Effect of operational power density

The energy and exergy difference is most profound as operational power density is varied from 25% of rated power to 125% of rated power, showing an $\eta_{En,el}$ difference of up to 8.6%. The η_{Ex} difference of over 10% between 25% and 125% operational power density for the case (*with fan, without DC-DC*). From a purely energy and exergy efficiency perspective, it is most beneficial to operate the fuel cell at the lowest possible power density. However, this may not be suitable for an aircraft application due to the increase in weight of the fuel cell itself when operating at lower power densities. The effect of varying operational power density on the powerplant weight is analyzed in the next chapter.

Effect of use of DC-DC converter

Results show significant gain in energy efficiency if DC-DC converter is not used, of up to 2.7%. Exergy efficiency gains stand higher, up to 3.2%. The option of

not using DC-DC converter and its effects on overall system weight will thus be explored in the next chapter.

Effect of use of cooling fan

In the energy and exergy efficiency analysis using CycleTempo given in Table 4.9, the difference between with and without using a fan is $\approx 0.6\%$. For a fuel cell system supplying 1 kW for 1 hour, this corresponds to less than 1 gram H_2 weight, which is insignificant. Moreover according to the drawbacks of improper cooling mentioned earlier, further research is needed to ascertain if proper cooling of fuel cells can be achieved without the integrated cooling fan. This most likely would involve changes to the aircraft air-frame to direct air flow towards the fuel cell bay. Besides, the possibility of increase in ohmic resistance due to membrane drying could potentially negate the energy savings of not using a cooling fan. Since the potential mass benefit of not using a cooling fan is not significant and have the possibility of even increased losses due to increase in ohmic resistance [8, 89], theoretical systems will not be sized for the case: *without fan*.

In conclusion, the following cases will be explored in the next chapter to understand their impact on the minimized system weight:

- *Varying power density - with fan - without DC-DC converter*
- *Varying power density - with fan - with DC-DC converter*

The mass flow rate calculations from CycleTempo are tabulated in Table 4.8, while efficiency results are tabulated in Table 4.9 and will be used to theoretically and practically size the powerplant for the aircraft, in the next two chapters.

Table 4.8: Mass flow rates for anode, cathode and cooling inlets.

	Flow rate (with fan) at inlet [g/s]			**Flow rate (without fan) at inlet [g/s]**		
Power density [%]	**Anode**	**Cathode**	**Cooling**	**Anode**	**Cathode**	**Cooling**
25	0.003	0.207	2.589	0.003	0.207	2.573
50	0.007	0.431	5.97	0.007	0.431	5.97
75	0.01	0.669	9.971	0.01	0.669	9.908
100	0.014	0.927	14.786	0.014	0.927	14.692
125	0.019	1.217	21.272	0.019	1.217	21.137

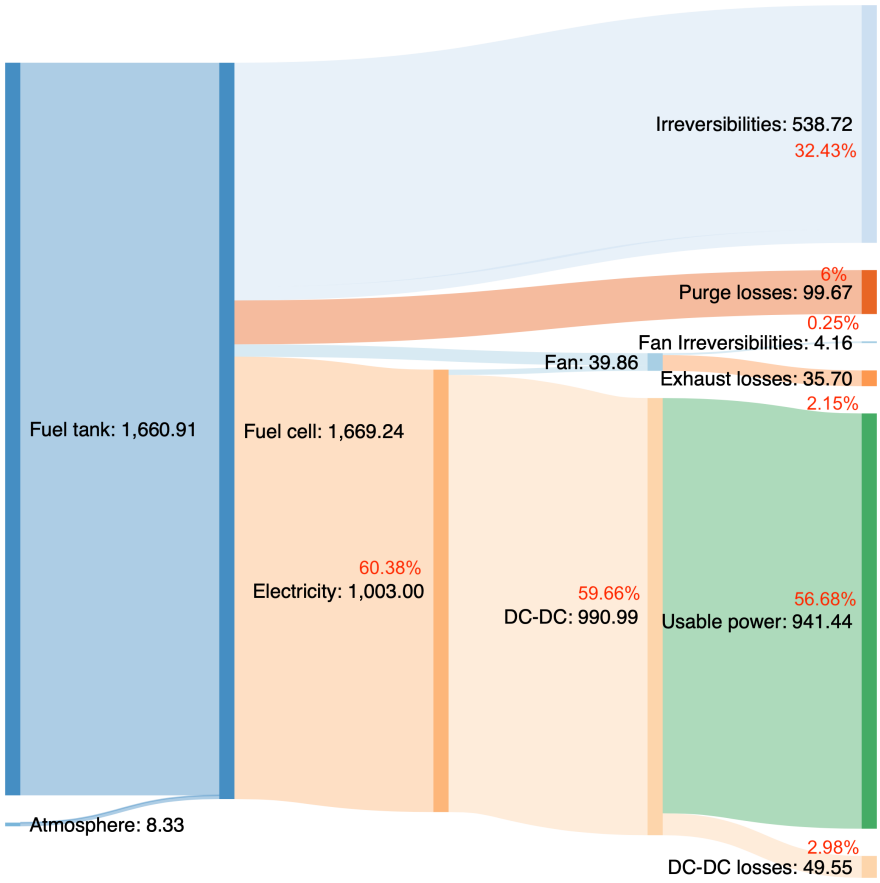

Figure 4.9: Exergy flow diagram for fuel cell operating at 100% rated power.

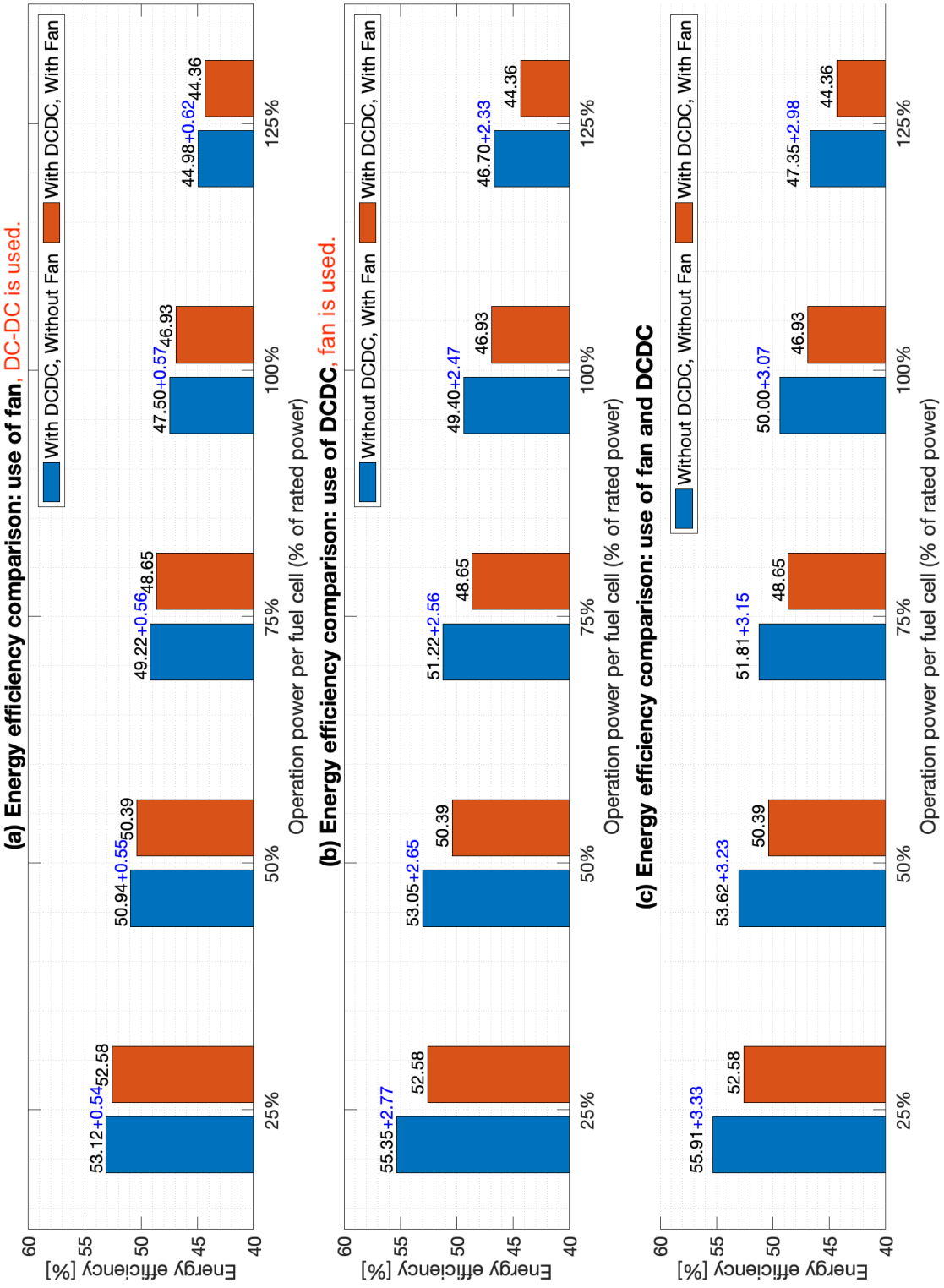

Figure 4.10: Comparing energy efficiency of the use of fan and DC-DC, and variable operational power %.

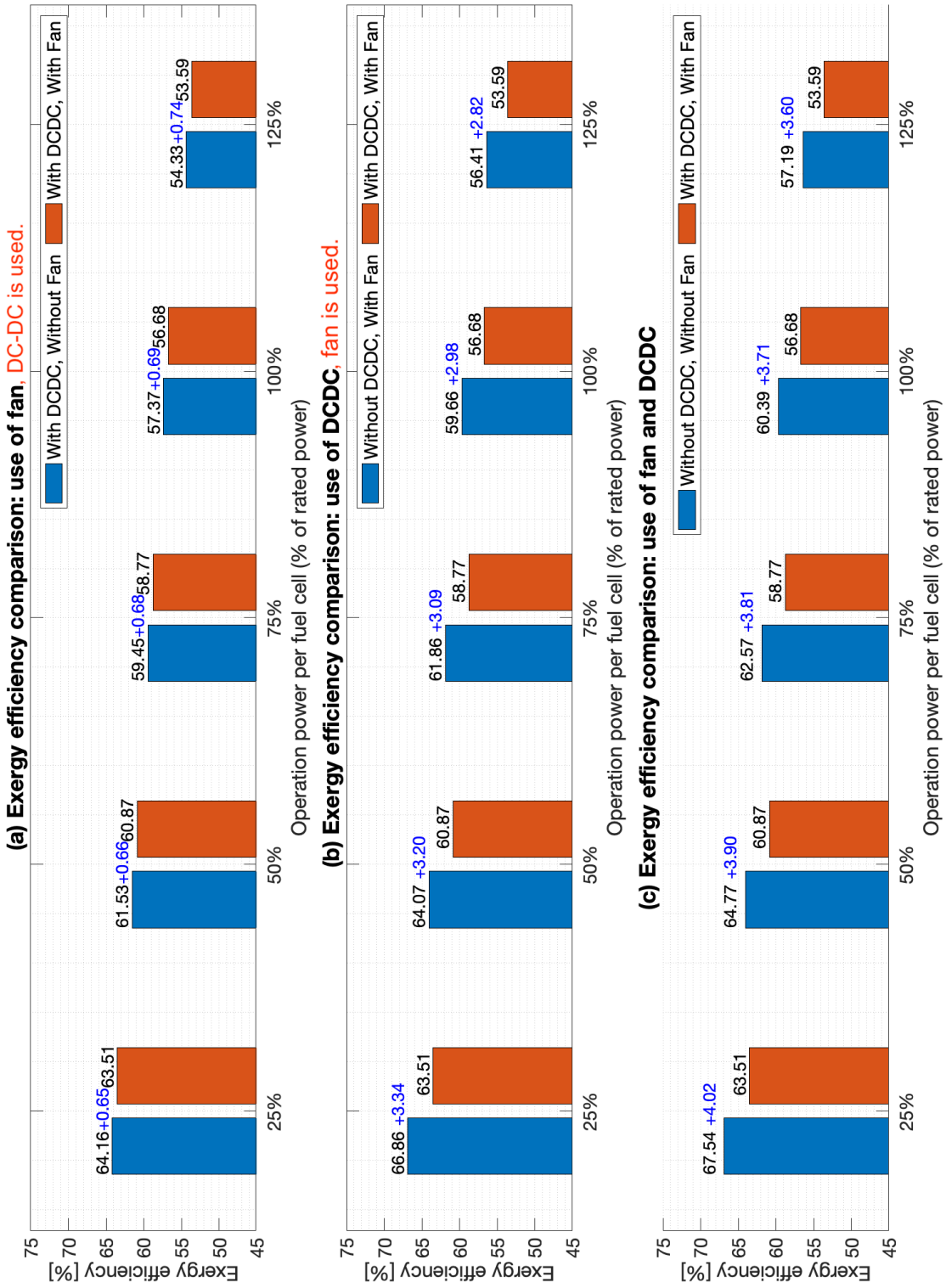

Figure 4.11: Comparing exergy efficiency of the use of fan and DC-DC, and variable operational power %.

Table 4.9: CycleTempo simulation results for different settings. Highlighted cells are for the base case: *With fan, with DC-DC converter*.

	Power Setting			Net energy efficiency [%]		Net exergy efficiency [%]		Difference: Without DCDC - With DCDC	
Fan	% of rated power	Nominal output power per stack [W]	Power Density [W/kg]	With DC-DC	Without DC-DC	With DC-DC	Without DC-DC	ΔEnergy efficiency [%]	ΔExergy efficiency [%]
With fan	25	250	138.75	52.58%	55.35%	63.51%	66.86%	2.77%	3.34%
	50	500	277.5	50.39%	53.05%	60.87%	64.07%	2.65%	3.20%
	75	750	416.25	48.65%	51.22%	58.77%	61.86%	2.56%	3.09%
	100	1000	555	46.93%	49.40%	56.68%	59.67%	2.47%	2.98%
	125	1247	693.75	44.36%	46.70%	53.59%	56.41%	2.33%	2.82%
Without fan	25	250	138.75	53.12%	55.91%	64.16%	67.54%	2.80%	3.38%
	50	500	277.5	50.94%	53.62%	61.53%	64.77%	2.68%	3.24%
	75	750	416.25	49.22%	51.81%	59.45%	62.57%	2.59%	3.13%
	100	1000	555	47.50%	50.00%	57.37%	60.39%	2.50%	3.02%
	125	1247	693.75	44.98%	47.35%	54.33%	57.19%	2.37%	2.86%
Difference: Without fan - With fan	25	250	138.75	0.54%	0.57%	0.65%	0.68%		
	50	500	277.5	0.55%	0.58%	0.66%	0.70%		
	75	750	416.25	0.56%	0.59%	0.68%	0.71%		
	100	1000	555	0.57%	0.60%	0.69%	0.72%		
	125	1247	693.75	0.62%	0.65%	0.74%	0.78%		

Chapter 5

Theoretical system design

In the previous chapter, energy and exergy efficiency were calculated for different exergy-gravimetric cases identified. Out of all the cases, it was concluded that not using cooling fan had insignificant efficiency gain ($\approx 0.6\%$), and thus will not be considered for system sizing.

Besides the operational power density of the fuel cell and the use of DC-DC converter, the mass of a hybrid powerplant also depends on the power and energy density of the batteries, and the mission endurance requirement. Hence the total mass of the powertrain is influenced by several factors: peak power and its duration, nominal power and duration, power and energy densities of batteries and fuel cells, specific energy density of fuel, storage efficiency (mass of stored fuel / mass of empty tank), and system efficiency. Apart from this, available volume is another factor which limits options.

As per component research in section 2.2, the fuel storage density (mass of fuel stored per unit empty tank mass) of compressed hydrogen is very low, $< 10\%$. However, commercially available storage tanks for liquid Propane are available with storage densities $> 150\%$, i.e. these tanks can store more liquid fuel than their own mass. Besides, liquid storage tanks are also smaller in volume. Hence, Propane powered SOFCs present an interesting case for a hybrid powerplant. In this chapter, multiple PEM-hybrid and SOFC-hybrid mass-minimized systems will be sized, and the impact of each variable on the overall system sizing will be analyzed.

This chapter starts with explaining the design methodology, followed by results of systems sized with PEM and SOFCs, and finally the analysis of results and the conclusion.

5.1 System Optimization Method

5.1.1 Coding scheme for design optimization

Due to the large number of variables involved in the system design, a coding scheme has been developed to identify each combination. This coding scheme is presented in Table 5.1 and will be used throughout this and next chapter to identify system combinations.

Table 5.1: Coding scheme for optimization conditions

Optimization conditions coding scheme				
Variable	**Code**	**Options**	**Units**	**Notes**
Endurance	E	65, 110, 155	mins.	Including reserve
Fuel Cell	FC	PEM, SOFC		
Fan	BL	0, 1		Does not apply to SOFC
DC-DC	DC	0, 1		
Power Density	PD	138.75, 277.5, 416.25, 555, 693.75	W/kg	25, 50, 75, 100, 125
Battery	BT	VTC6, SE, A123	Selection	Commercially available batteries
Condition	C	OPT, FCCRUISE		Fuel cell power during cruise

Example: E65-FCPEM-BL1-DC0-PD555-BTVTC6-COPT would mean the following:

- E*65*: 65 mins. cruise endurance (including 20 mins. reserve).
- FC*PEM*: HES AeroStak A1000-65 fuel cell.
- BL*1*: Air fan is used.
- DC*0*: DC-DC converter is not used.
- PD*555*: Operational specific power density of fuel cell is 555 W/kg.
- BT*VTC6*: Sony VTC6 cells are used for sizing battery pack.
- C*OPT*: Optimal configuration for reducing system mass.

The next section presents the methodology followed to size the mass-minimized systems.

5.1.2 Mass-minimization methodology

Designing a mass-minimized system for an electric aircraft, using a hybrid powerplant is a complex system-level problem. Optimally solving this problem involves including the impact of each variable on the system mass and efficiency. In this section, it is explained how all such constraints and bounds and variables are formulated into an optimization problem, which is solved with the objective to determine the lowest system mass.

Method

The flight is split into multiple phases: Takeoff, climb, and cruise. Constraints are defined for each flight phase. The minimization function aims to minimize the overall system mass while adhering to all constraints, to determine the value of all variables. These optimization variables, cost function, and constraints are explained next.

Variables

The number of optimization variables depend on the number of flight phases. The following optimization variables are added for each flight phase. These variables apply to only the specific flight phase.

- Power delivered by fuel cell P_{FC}.
- Power delivered by battery P_{BATT}.

The following optimization variables are used as global variables, i.e. the same variables apply during all flight phases.

- Mass of fuel M_{Fuel}.
- Mass of battery M_{BATT}.

For a flight consisting of three flight phases, i.e. *takeoff*, *climb*, and *cruise*, following 9 are the optimization variables: $P_{BATT,takeoff}$, $P_{FC,takeoff}$, $P_{BATT,climb}$, $P_{FC,climb}$, $P_{BATT,cruise}$, $P_{FC,cruise}$, M_{Fuel}, and M_{BATT}.
To arrive at an optimal theoretical powertrain design as a start point, the integer nature of system as described above was ignored. It is assumed that a system of exact specifications can be designed and manufactured to meet all the constraints. This is to understand the theoretical limit to which the system can be optimized. Hence, all variables are treated as continuous.

Constants

The optimizer function needs the following inputs from the user:

1. Flight course: power and duration of each flight phase
2. Fuel cell specific power density ($PDENS_{FC}$) [W/kg]
3. Fuel energy density ($EDENS_{FC}$) [Wh/kg]
4. Fuel cell nominal operating efficiency (η_{FC}) [%]
5. Fuel tank storage density (η_{Tank}) [kg/kg]
6. Battery power density ($PDENS_{BATT}$) [W/kg]
7. Battery energy density ($EDENS_{BATT}$) [Wh/kg]
8. Battery discharge efficiency (η_{BATT}) [%]
9. Specific power density of DC-DC converters $PDENS_{DC-DC}$ [W/kg]

Besides the above constants, mass of components like mass of bus bars and cell holders for battery are directly dependant on the sizing of respective systems. To account for the mass of such components, another variable called *BOP Weight Factor* is introduced in the optimizer. This factor is independently configurable for Fuel cells and Batteries. The BOP weight factor is defined as:

$$BOPWeightFactor(\beta) = 1 + \frac{WeightOfPassiveComponents}{UnitWeightOfActiveComponents} \tag{5.1}$$

where *active components* imply battery and fuel cells, and *passive components* are all other components essential for system operation but are not a source of power or energy. Note that this factor only includes the mass of passive components which scale with the size of the active components. Weight of one-time components such as switches is not included in BOP weight factor.
For the batteries, this includes mass of bus bars, enclosures, cell holders, misc. sensing cables, cell fuses etc. For fuel cells, this includes mass of fuel hoses, pressure reducers etc.
Example: for a battery system, a *BOP Weight Factor* of 1.15 implies that an additional 15% mass than the cell-only mass is required for other battery BOP components.

Cost function

Similar to exergy economics where *cost* is the *cost of energy*, the cost function here considers the cost as the total system mass, which is a function of battery mass, fuel cell mass, fuel mass, fuel tank mass, and mass of BOP.

$$M_{System}(kg) = [M_{FC} * \beta_{FC}] + M_{Fuel} + [M_{BATT} * \beta_{BATT}] + \frac{M_{Fuel}}{\eta_{Tank}} + M_{DC-DC} \quad (5.2)$$

$$Objective \rightarrow minimize \;\; M_{System}$$

Where β_{FC} and β_{BATT} is the BOP weight factor of fuel cell and battery respectively. M_{FC} and M_{BATT} are given by:

$$\begin{aligned} M_{FC} &= \frac{max.(P_{FC})}{PDENS_{FC}}, \qquad M_{DC-DC} = \frac{max.(P_{FC})}{PDENS_{DC-DC}} \\ M_{BATT} &= max.\left(\frac{max.(P_{BATT})}{PDENS_{BATT}}, \frac{E_{BATT}}{EDENS_{BATT}}\right) \end{aligned} \quad (5.3)$$

As mentioned previously, the optimizer computes the power output by battery and fuel cell for each flight phase individually. In Equation 5.3, the maximum power output from the fuel cell is used to calculate the mass of the fuel cell, and the DC-DC converter. For battery, the mass is dependent on both, its specific power density and specific energy density. This relation is explained later. The objective of this mass-minimization cost function is to minimize the system mass M_{System}, which is a function of the masses of fuel cell, fuel tank, fuel, and batteries. The mass of fuel tank is a function of the mass of fuel.

Constraints

Power balance: Each flight phase has its power balance equation. This constraint ensures that sufficient power is delivered by each source for all flight phases.

$$P_{BATT,i} + P_{FuelCell,i} = P_{Phase,i} \quad (5.4)$$

where i corresponds to each individual flight phase. This constraint simply implies that the total power output from the battery and fuel cell during every individual flight phase must be equal to the power required by the aircraft during that flight phase.

Fuel mass to be carried: The next constraint is for the amount of fuel to be carried. This constraint is very important since this takes into account the opera-

tional efficiency of the fuel cell system during each flight phase.

$$M_{Fuel} = \left(\frac{1}{EDENS_{FC}}\right) \sum_{i=FirstFlightPhase}^{LastFlightPhase} \int_{T_{Phase,start}}^{T_{Phase,end}} \frac{P_{FC,i}}{\eta_{FC,i} * UFL} \tag{5.5}$$

First, the power input to the fuel cell, required to provide output power P_{FC} is calculated by using the fuel cell efficiency η_{FC} calculated using CycleTempo. This is integrated over the entire flight phase, and summed for all flight phases, which gives the total input energy. The fuel mass is simply calculated by dividing this input energy by energy density of fuel.

Battery mass, power density, energy density: Since a battery is both a source of power and energy, it is modeled using two variables: battery power for each flight phase ($P_{BATT,i}$), and total battery mass (M_{BATT}). The below two constraints ensure that the mass of the battery is in accordance with its power density and its energy density.

$$max\left(P_{BATT}\right) \leq \left(M_{BATT} * \eta_{BATT} * PDENS_{BATT}\right) \tag{5.6}$$

$$\sum_{i=FirstFlightPhase}^{LastFlightPhase} \int_{t=PhaseStartTime}^{PhaseEndTime} P_{FC,i} t_i \leq \left(M_{BATT} * EDENS_{BATT} * \eta_{BATT}\right) \tag{5.7}$$

The first equation (Equation 5.6) constraints the maximum power output from the battery. This constraint ensures that the maximum power output from the battery is less than the rated continuous output from the battery. Drawing more power than rated leads to battery over-heating, and may cause thermal runaway. The second equation is to ensure that the total energy supplied by the battery is less than the total energy the battery holds.

Variable bounds

All the optimization variables are bounded such that optimization provides realistic results. The upper bounds of all variables is set to $+\infty$. There are two cases for lower bounds:

1. Fuel cell acts as range extender: lower bound of fuel cell power P_{FC} is set to 0 for all flight phases.
2. Fuel cell fully powers cruise flight: lower bound of fuel cell power during cruise flight P_{FC} is set to the power required by aircraft during cruise flight P_{Cruise}, and is set to 0 for all other flight phases.

Algorithm and Tolerances

A number of optimization solvers are available in MATLAB [73]. Out of these, *fmincon* solver was selected since it has the ability to work with nonlinear constraints, non-linear objective functions, and variable bounds. The *sqp* algorithm within *fmincon* is selected since it is best suited for small and medium sized problem [73]. Furthermore, to ensure that the solver converges on global minima, the *fmincon* is invoked using *GlobalSearch* function, which scans all the local minima to converge at the global minima [73].
Tolerances on solvers define the threshold on the change in iteration result, which if crossed, halts the solver [73]. *StepTolerance* and *FunctionTolerance* as defined in MATLAB, were set to 10^{-12} each. This means that the solver stops iterations when the change in M_{System} is less than 10^{-12} kg.

Assumptions

Certain assumptions are made to simplify the mass-minimization problem. These assumptions apply generally to both PEM and SOFC system sizing cases for all combinations. These are stated below:

1. Fuel cell operates at constant power output during all flight phases, and hence its efficiency remains constant throughout the flight.
2. Fuel cell performance is not affected by environment variables (temperature, pressure) at the flight altitude.
3. Variables: *Fuel cell power density ($PDENS_{FC}$)*, *Fuel energy density ($EDENS_{FC}$)*, *Battery power density ($PDENS_{BATT}$)* and *Battery energy density ($EDENS_{FC}$)* are treated as continuous variables. The effect of treating them as discrete variables on the system mass is explored in the next chapter. This also implies that design constraints: bus bar voltage and current limitations are ignored in this chapter.
4. The efficiency of DC-DC converters (η_{DC-DC}) as a function of power output remains constant in the region of heavy duty operation [90, 91], and is assumed to be 95%.
5. The mass of DC-DC converters scales linearly as a function of its output power.
6. The contribution of components such as signal cables, connectors, exhaust hose etc. is excluded from BOP weight factors. Components such as *contactors* and switches, whose quantity required is not dependant on the optimal solution are also not included.

5.1.3 Mass-minimization cases

The number of cases for which mass-minimized systems are sized are broadly categorized into two categories: PEM powered, and SOFC powered. Within these two categories, different degrees of hybridization and specific power density are used as variables for sizing mass minimized systems. Different exergy-gravimetric cases identified (fuel cell operational power density and use of DC-DC converters) are used for PEM systems. Below is a summary of the cases.

1. Fuel cell used for sizing

   FC*PEM*: System sizing for HES AeroStak A1000-65 PEM fuel cell.

   FC*SOFC*: System sizing for theoretical SOFCs.

2. Degree of hybridization

   C*FCCruise*: Entire cruise flight powered only by fuel cells.

   C*OPT*: Both, fuel cells and batteries provide power during cruise flight.

Using the above variables, mass-minimized systems are sized for three different endurance cases:

1. E*65*: 45 mins. + 20 mins. cruise time.
2. E*110*: 90 mins. + 20 mins. cruise time.
3. E*155*: 135 mins. + 20 mins. cruise time.

For all cases of condition *COPT*, *Degree of Hybridization* (DOH) will also be compared. The degree of hybridization is defined as:

$$DOH = \frac{P_{FC}}{P_{Cruise}} \tag{5.8}$$

The DOH is basically a measure of the contribution of fuel cell power output during cruise flight to the total power required during cruise flight. Higher DOH is desirable. DOH close to 1 would mean that most of the power required during cruise is provided by the fuel cell, and hence simply more fuel can be carried to increase endurance.

5.2 System sizing: FC*PEM*

This section explains the methodology followed for sizing the PEM powered systems, followed by the results and analysis of system sizing.

5.2.1 Assumptions

Apart from the general assumptions stated in the previous section, some specific assumptions were made to size the PEM-hybrid system:

1. A safety factor of 1.2 is used on the battery energy density, and 1.25 on the battery power density. This implies that the power density of batteries used for system sizing is 20% less than rated power density, and 25% less than rated energy density.
2. No safety factors are applied to estimated volume calculation.
3. Cycle-life and degradation of batteries and fuel cells is not taken into account.
4. A BOP weight factor β_{BATT} of 1.15 is used. This implies that mass of BOP components of the battery is assumed to weigh 15% the mass of the cells. This factor is found to vary greatly depending on end application of the battery pack. For aerospace applications (from experience), it could be as low as 15%, while for automotive applications, it could as high as 40% [92].
5. Round-trip efficiency of all the battery cells used for theoretical sizing is assumed to be constant 95% [93].
6. The additional mass of fuel hoses, mounting etc. is accounted for in BOP weight factor ($\beta_{FC} = 1.1$).
7. Power density of DC-DC converters ($PDENS_{DC-DC}$) is assumed to be 1.36 kW/kg [33].

5.2.2 Input summary

A list of all parameters required for mass-minimization on MATLAB is given in the table Table 5.2.

5.2.3 Results and analysis

Results from system sizing using the selected PEM fuel cells, and their analysis is presented in this section. The following cases have been evaluated:
Set 1: 65 mins. cruise endurance (45 mins. + 20 mins. reserve):

1. E65-FCPEM-BL01-DC00-PD(Variable)-BT(Variable)-FCCruise
2. E65-FCPEM-BL01-DC00-PD(Variable)-BT(Variable)

Table 5.2: Input summary of values used for mass-minimization for PEM.

Component	Symbol	Parameter	Value	Notes
Fuel cell	$PDENS_{FC}$	Power density [W/kg]	Variable	Table 4.1
	η_{FC}	Efficiency [%]	Variable	Table 4.9
		Volumetric density [kg/L]	0.378	
	β_{FC}	BOP Weight Factor	1.1	
	$PDENS_{DC-DC}$	DC-DC power density [W/kg]	1.36E+03	[33]
Fuel	$EDENS_{FC}$	Energy density [Wh/kg]	39,410.00	HHV of H_2 @ 25 °C
Fuel tank	η_{Tank}	Fuel storage density [-]	0.08	HESA20 cylinder
		Volumetric density [kg/L]	0.218	exc. fuel mass
Battery	β_{BATT}	BOP Weight Factor	1.15	
	η_{BATT}	Efficiency [%]	95	
A123	$PDENS_{BATT}$	Power density [W/kg]	1776	
	$EDENS_{BATT}$	Energy density [Wh/kg]	86	
		Volumetric density [kg/L]	2.157	
VTC6	$PDENS_{BATT}$	Power density [W/kg]	900	
	$EDENS_{BATT}$	Energy density [Wh/kg]	192	
		Volumetric density [kg/L]	2.73	
SE	$PDENS_{BATT}$	Power density [W/kg]	629	
	$EDENS_{BATT}$	Energy density [Wh/kg]	335	
		Volumetric density [kg/L]	1.93	

3. E65-FCPEM-BL01-DC01-PD(Variable)-BT(Variable)

Set 2: Cruise endurance doubled: 110 mins. (2x45 mins. + 20 mins. reserve).

4. E110-FCPEM-BL01-DC00-PD(Variable)-BT(Variable)

5. E110-FCPEM-BL01-DC01-PD(Variable)-BT(Variable)

Set 3: Cruise endurance tripled: 155 mins. (3x45 mins. + 20 mins. reserve).

6. E155-FCPEM-BL01-DC00-PD(Variable)-BT(Variable)

7. E155-FCPEM-BL01-DC01-PD(Variable)-BT(Variable)

To compare the relative benefits of the systems sized with the base system, % change in total system mass, % change in exergy efficiency, and degree of hybridization have been plotted. For the lowest 6 combinations, mass and volume distribution has been plotted. A point to note is that the volume estimations do not include any volume required for air flow, mounting, clearances, and enclosures. The actual volumes will only be higher than those estimated. These volume calculations are for indicative purposes only.
Another point to note is that the total energy content could be different in each of the cases due to different energy densities of the batteries in each case. However the impact of energy content on mass and endurance is compared by comparing different endurance cases.

Endurance: 65 mins. cruise (*E65)*

Results for mass-minimized system sizing for case E65-FCPEM-BL01-DC(Variable)-PD(Variable)-BT(Variable)-CFCCruise are presented in Figure 5.1.

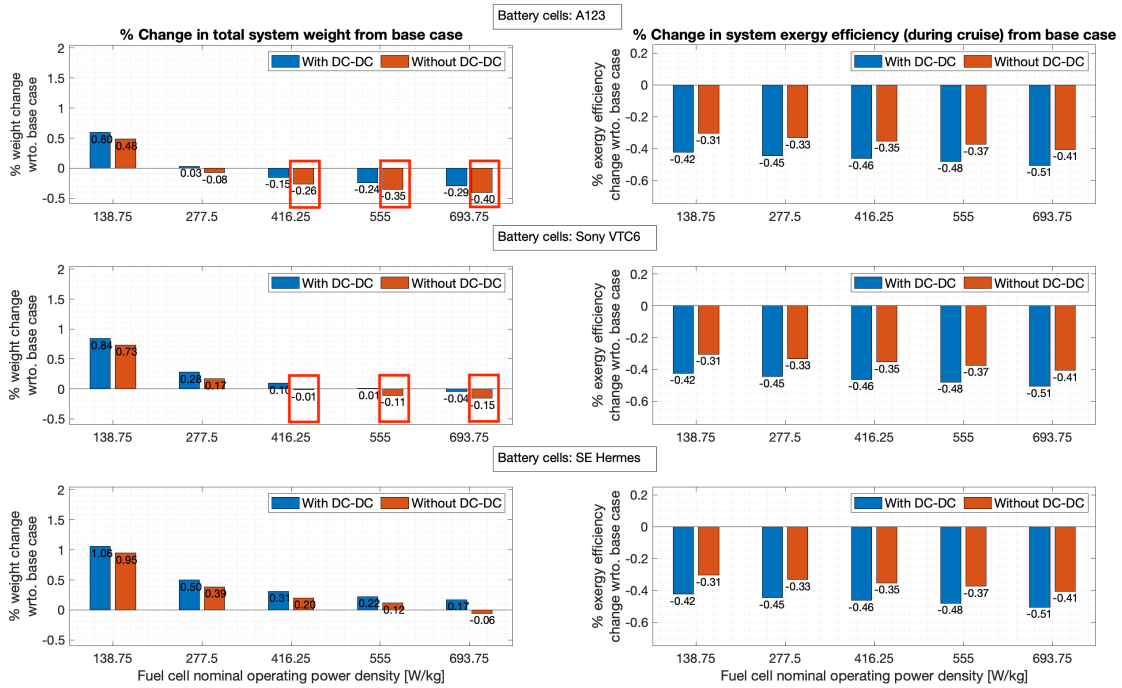

Figure 5.1: Weight and exergy efficiency comparison against base case for E65-FCPEM-BL01-DC(Variable)-PD(Variable)-BT(Variable)-CFCCruise. Mass and volume distribution for marked configurations is shown in Figure 5.2.

From the plots for case E65-FCPEM-BL01-DC(Variable)-PD(Variable)-CFCCruise (Figure 5.1) following are the observations:

- The negative exergy efficiency change indicates that hybridization will always have higher losses than pure battery systems. This is expected since fuel cells have lower exergy efficiency than batteries.
- For this endurance case, hybridization yields no mass benefits if the system level power density of fuel cells is less than 277.5 W/kg.
- Exergy destruction is higher when DC-DC converters are used. As expected, exergy destruction also increases with increase in operational power density of the fuel cell.
- The total system mass however decreases with increase in operational power density. This implies that the benefit of increased power density of the fuel cell is higher than the loss due to higher fuel mass required. This trend is observable in case of all batteries.

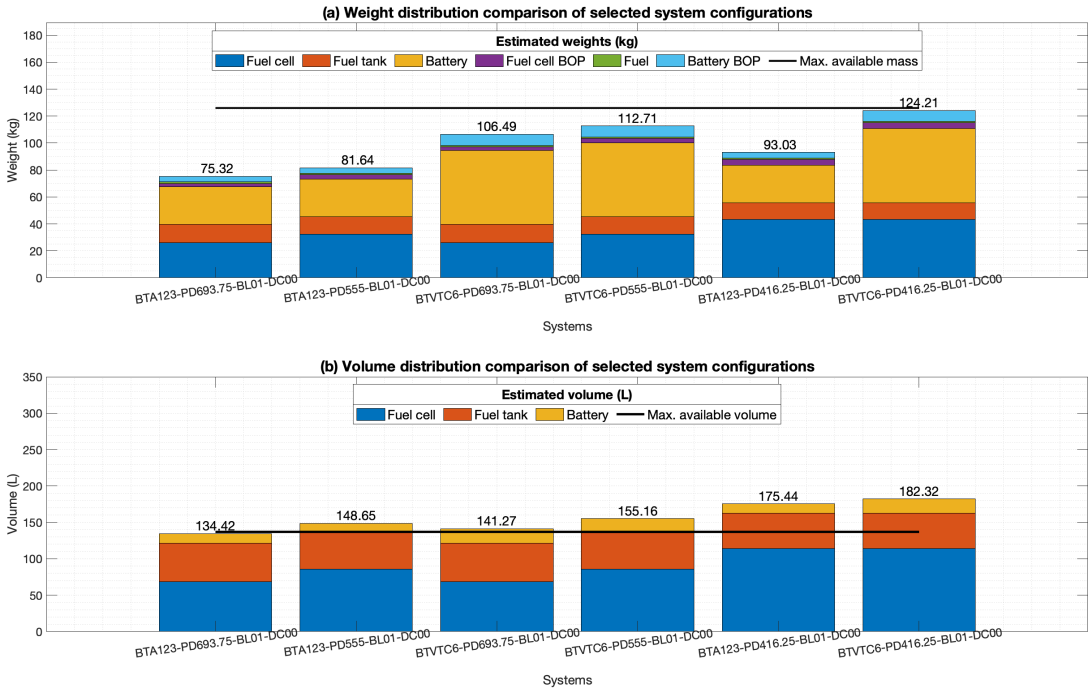

Figure 5.2: Weight and volume distribution of the six lowest mass combinations for the case:
E65-FCPEM-BL01-DC(Variable)-PD(Variable)-BT(Variable)-CFCCruise

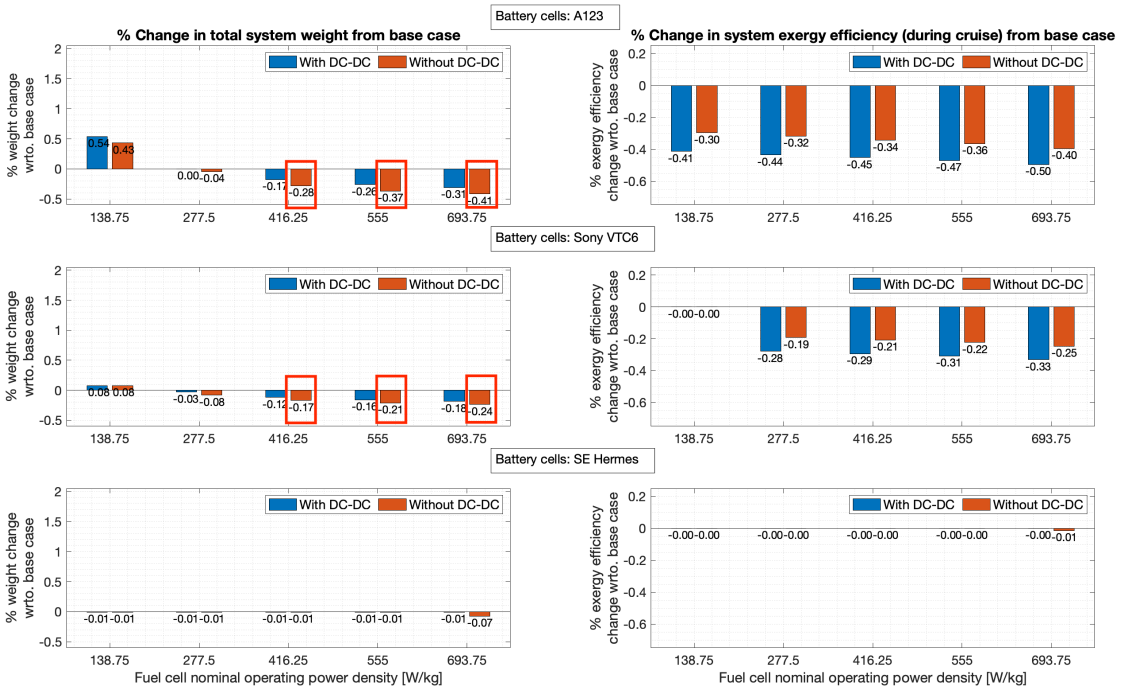

Figure 5.3: Weight and exergy efficiency comparison against base case for E65-FCPEM-BL01-DC(Variable)-PD(Variable)-BT(Variable)-COPT. Mass and volume distribution for marked configurations is shown in Figure 5.5.

- High energy density batteries (Solid Energy Hermes) are not suitable for hybridization, and all combinations except one (PD693.75-BTSE-BL1-DC0)

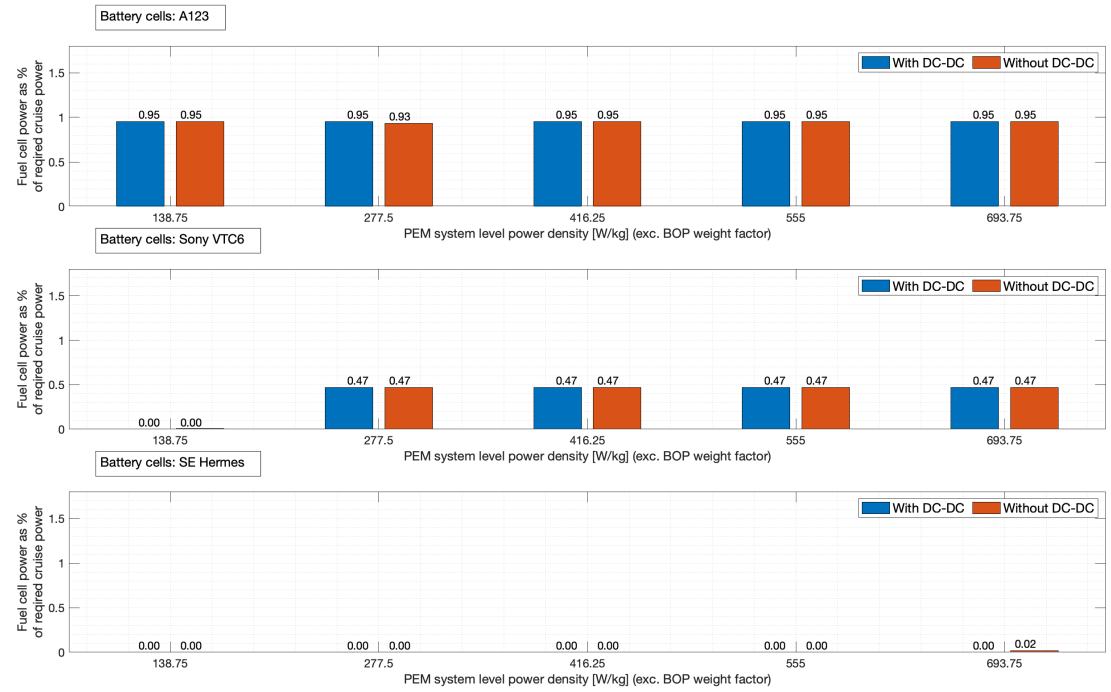

Figure 5.4: Comparison of degree of hybridization for all the sized systems for case: E65-FCPEM-BL01-DC(Variable)-PD(Variable)-BT(Variable)-COPT.

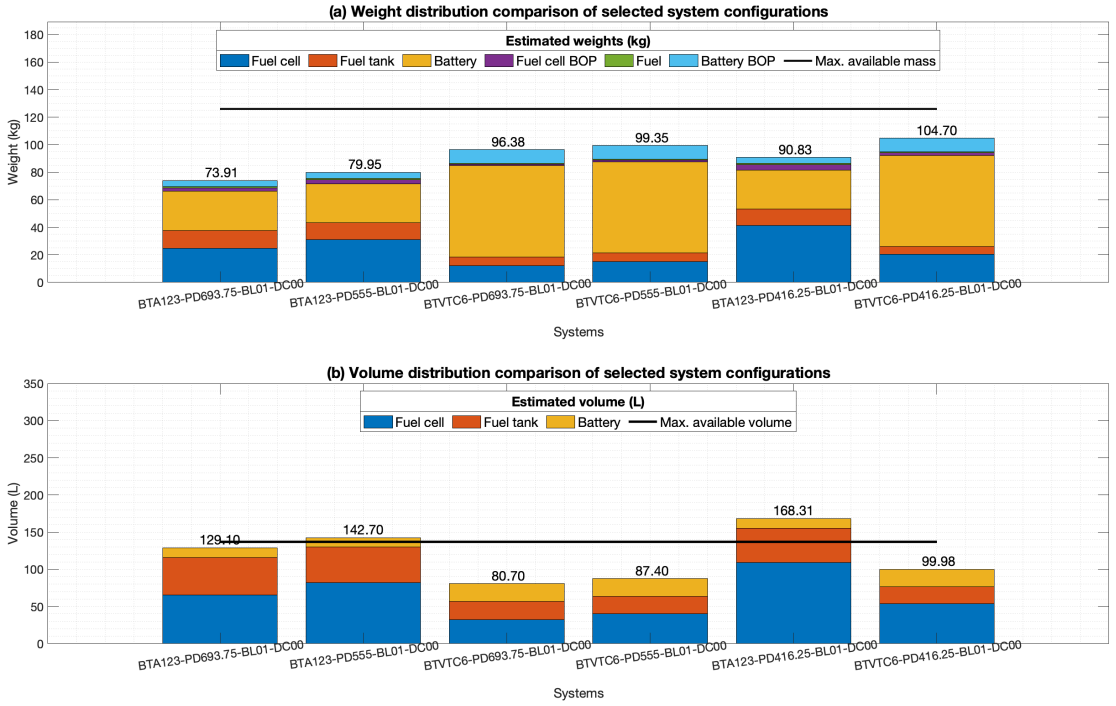

Figure 5.5: Weight and volume distribution of the six lowest mass combinations for the case: E65-FCPEM-BL01-DC(Variable)-PD(Variable)-BT(Variable)-COPT.

result in higher than base case mass. This can be inferred from Figure 5.4c, where the degree of hybridization is 0 for all cases (except PD693.75-BTSE-

BL1-DC0).

- Use of DC-DC converters results in higher exergy loses and higher mass, and hence should be avoided as much as possible.
- The most suitable cells for hybrid powerplant are those with the highest power density. Hence A123 cells in the present study are the most suitable.

Figure 5.2 compares the mass and est. volume distribution for the 6 lowest mass configurations (which do not include DC-Dc converters). These configurations are marked with red boxes in the figures. It can be noted that most configurations provide a mass-benefit with respect to the base case, but volume is questionable. In Figure 5.2b, the graph shows that volume of all configurations is beyond the volume budget (marked with the red line). Majority of this volume is occupied by fuel cell, followed by fuel tank.
At this result, it can be concluded that a fully hydrogen powered cruise is possible within the mass budget, but not within the given volume budget.

Figure 5.3 compares the mass and exergy efficiency difference from the base case. Following are the observations:

- The optimal case (COPT) only yields marginal benefits in terms of % change in total system mass ($\approx 1\%$) from the case CFCCruise in the best case.
- If current state-of-the-art batteries (Solid Energy Hermes) is used for the aircraft, there is no benefit of a hybrid system. This can be observed from the exergy efficiency difference, which shows no difference. This can also be inferred from Figure 5.4, where the degree of hybridization is 0% (i.e. no fuel cells are required to meet all the constraints) when Solid Energy Hermes cells are used.
- The degree of hybridization is highest when high power density cells (A123) are used, up to 95%, even in the optimal sizing case. This decreases as the energy density of batteries gets higher. The hybrid system with VTC6 cells yields 47% degree of hybridization, while systems with Solid Energy Hermes cells yields 0%.
- The degree of hybridization remains constant with operational power density (and hence efficiency) of fuel cells, in all battery options. Hence no significant correlation is found between the optimal power output from fuel cell vs. power density of fuel cells. However there is strong correlation between degree of hybridization and battery power and energy density.

- From Figure 5.5, it can be observed that for the 6 systems with lowest mass (excluding DC-DC converter), the systems with A123 cells have high volume, and may not fit within the given volume budget. Hence the high power density of these cells does result in lowest mass configurations, but volume is high.
- Only the systems sized with VTC6 cells fit within the volume budget. Comparing these with results in Figure 5.2, the volume of optimal systems is considerably lower, up to 40 % lower than for the case CFCCruise.

Endurance: 110 mins. cruise (*E110)* and 155 mins. cruise (*E155*)

The results for theoretical sizing of these endurance cases are presented in Appendix Appendix B. From the plots, following are the observations:

- A number of configurations exist for systems sized for E110-CFCCruise, E155-CFCCruise, E110-COPT and E155-COPT which have a mass lower than the base case. Similar to case *E65*, hybrid systems with "high power density" cells (A123) resulted in the lowest system mass.
- In Figure B.3, Figure B.8, Figure B.1 and Figure B.6, the system configurations with the lowest mass estimate are plotted for their mass and volume distribution graphs in Figure B.5, Figure B.10, Figure B.2 and Figure B.7. It can be observed that the estimated volume for all these systems is higher than the volume budget, where majority volume is taken up by fuel cell and fuel tank.
- When sizing optimal cases, degree of hybridization remains constant with fuel cell power density (and also fuel cell efficiency), but depends strongly on the battery selection. The degree of hybridization also strongly depends on endurance: higher the endurance requirement, higher the degree of hybridization.
- Optimal hybrid systems sized with the state-of-the-art batteries (Solid Energy Hermes) yield 0% degree of hybridization with E110, but as the endurance requirement is tripled, i.e. to 155 minutes, hybridization is more favorable.

5.3 System sizing: FC*SOFC*

Commercially available SOFC systems, specially for aircraft applications are limited. However, to understand if SOFCs present a case against PEMs for an

aircraft application, theoretical systems are sized at different power densities, and efficiencies [94]. These power densities and efficiency assumptions, along with other assumptions are listed below.

5.3.1 Assumptions

The following assumptions were made while sizing an SOFC-hybrid powerplant:

- SOFCs are available at system level power densities of 138.75, 277.5, 416.25, 555, 293.75. These values correspond to the power density of PEM used in the previous section, at 25%, 50%, 75%, 100%, 125% of rated power density respectively [94]. Assuming these power densities allows for direct comparison with PEM systems. Stack level power densities of up to 1 kW/kg have been reported in literature [95, 96].
- The mass of insulation, heat exchangers and fans / blowers is included in the power density of the fuel cells; i.e. The power densities in the previous point are at a fuel cell system level.
- A fuel utilization factor, i.e. the ratio of rate of reacted fuel over the rate of inlet fuel is assumed to be 80% [83].
- Since accurate data regarding SOFC system efficiencies are not available for the above power densities, multiple operational electrical efficiency cases (based on the LHV of propane, 12.9 kWh/kg) were sized for. These are: 40%, 50%, and 60% [94].
- Storage density of propane tanks (η_{Tank} = fuel capacity/mass of empty tank) is assumed to be 1.5 [28] (Table 2.3). It is also assumed that the storage ratio remains constant with fuel capacity.
- A BOP weight factor ($\beta_{FC} = 1.1$) is used for the fuel cell system. This is kept to be same as that for PEM system such that the systems can be compared directly.
- A safety factor of 1.2 is used on the battery energy density, and 1.25 on the battery power density. This implies that the power density of batteries used for system sizing is 20% less than rated power density, and 25% less than rated energy density.
- Cycle-life and degradation of batteries and fuel cells is not taken into account.

- A BOP weight factor β_{BATT} of 1.15 is used. This implies that mass of BOP components of the battery is assumed to weigh 15% the mass of the cells.
- Coulombic efficiency of all the battery cells used for theoretical sizing is assumed to be constant 95% [93].
- Since stack level voltages are unknown, it is assumed that SOFC systems are available at the required output voltage, and hence DC-DC converter is not required, and therefore the case is not sized.

5.3.2 Input summary

The Table 5.3 summarizes all the options possible for the system level mass minimization.

Table 5.3: Input summary of values used for mass-minimization for SOFC

Component	Symbol	Parameter	Value	Notes
Fuel cell	$PDENS_{FC}$	Power density [W/kg]	138.75, 277.5, 416.25, 555, 693.75	[94]
	η_{FC}	Efficiency [%]	40, 50, 60	Table 4.9
	β_{FC}	BOP Weight Factor	1.1	
Fuel	$EDENS_{FC}$	Energy density [Wh/kg]	12,900.00	Propane LHV @ 25 °C [83]
Fuel tank	η_{Tank}	Fuel storage density [-]	1.5	Table 2.3 [28]
Battery	β_{BATT}	BOP Weight Factor	1.15	
	η_{BATT}	Efficiency [%]	95	
A123	$PDENS_{BATT}$	Power density [W/kg]	1776	
	$EDENS_{BATT}$	Energy density [Wh/kg]	86	
		Volumetric density [kg/L]	2.157	
VTC6	$PDENS_{BATT}$	Power density [W/kg]	900	
	$EDENS_{BATT}$	Energy density [Wh/kg]	192	
		Volumetric density [kg/L]	2.73	
SE	$PDENS_{BATT}$	Power density [W/kg]	629	
	$EDENS_{BATT}$	Energy density [Wh/kg]	335	
		Volumetric density [kg/L]	1.93	

5.3.3 Results and analysis

Results for mass-minimized system sizing using theoretically assumed power density and efficiency of SOFCs, and their analysis is presented in this section. The following cases have been analyzed:
Set 1: 65 mins. cruise endurance (45 mins. + 20 mins. reserve)

1. E65-FCSOFC-PD(Variable)-CFCCruise
2. E65-FCSOFC-PD(Variable)-COPT

Set 2: 110 mins. cruise endurance (45x2 mins. + 20 mins. reserve)

1. E110-FCSOFC-PD(Variable)-CFCCruise

2. E110-FCSOFC-PD(Variable)-COPT

Set 3: 155 mins. cruise endurance (45x3 mins. + 20 mins. reserve)

1. E155-FCSOFC-PD(Variable)-CFCCruise
2. E155-FCSOFC-PD(Variable)-COPT

Endurance: 65 mins. cruise (*E65*)

Results for cases E65-FCSOFC-PD(Variable)-CFCCruise and E65-FCSOFC-PD(Variable)-COPT are presented in Figure 5.6 and Figure 5.7 respectively.

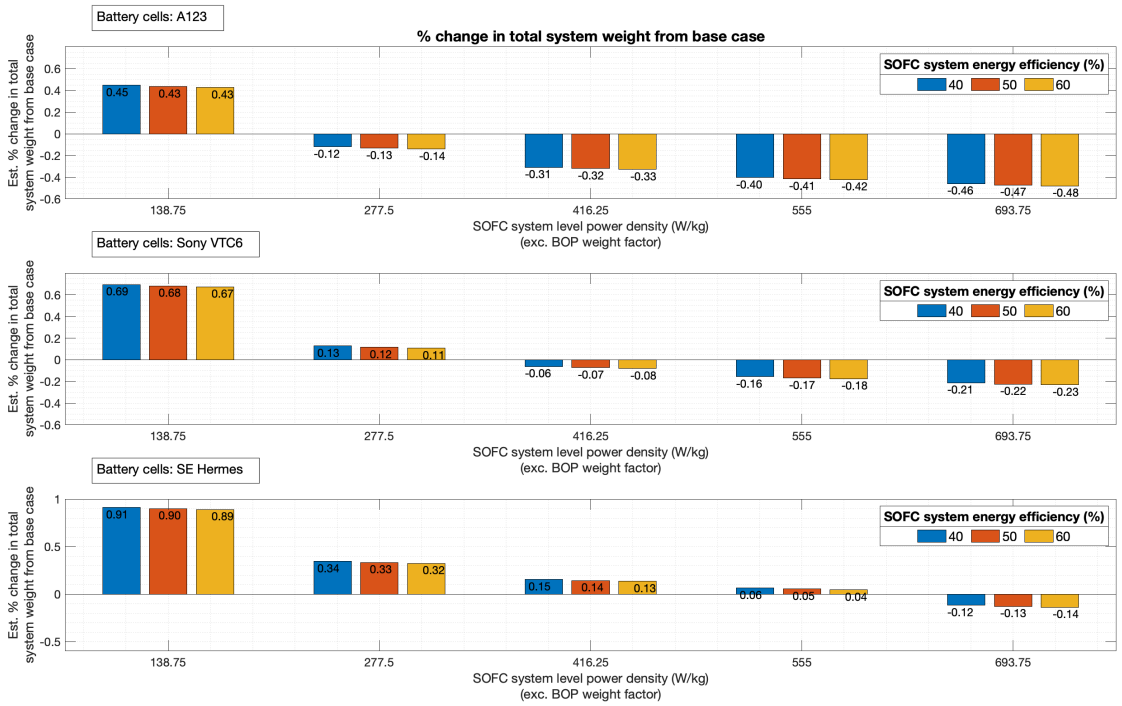

Figure 5.6: Mass comparison against base case for E65-FCSOFC-BT(Variable)-CFCCruise

Following are the observations:

- From Figure 5.6, it can be seen that a fully fuel cell powered cruise flight is not favorable if the system level specific power density of the fuel cell is below 277.5 W/kg.
- As was the case with PEM fuel cells, the most suitable battery for hybridization in the present study is A123, the ”high power density” cells.
- For this particular system design case, fuel cell efficiency was found to have a less stronger correlation with the total system mass than the fuel cell power density.

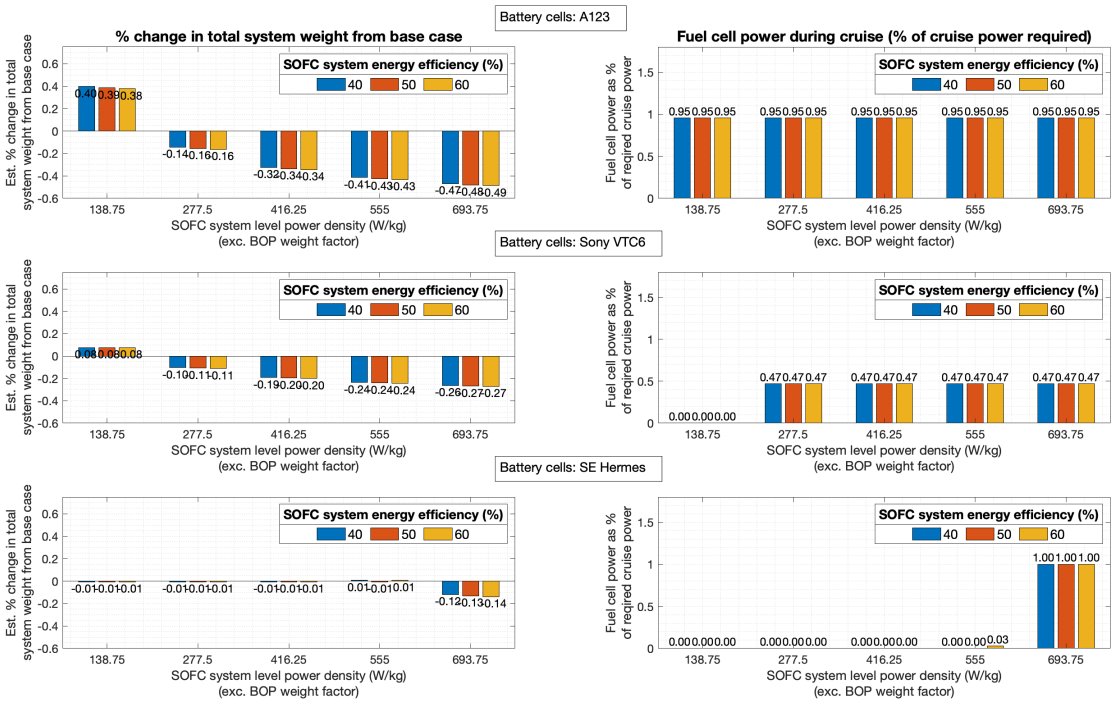

Figure 5.7: Mass comparison and degree of hybridization for E65-FCSOFC-BT(Variable)-COPT

- For the same power density as PEM, SOFC systems sized for CFCCruise could weigh upto 8% less than equivalent power density PEM fuel cells in the best case (i.e. operational electrical efficiency of SOFCs is 60%). Even with lower electrical operational efficiency of 40%, SOFC hybrid systems are lighter than similar PEM hybrid systems by up to 6%. This can be inferred from Figure 5.6 and Figure 5.1.

- For optimally sized systems (FCSOFC-COPT), slight positive correlation was found between fuel cell operating efficiency and minimized system mass. This correlation was found to be much stronger with operational power density.

- For higher power density batteries (BTVTC6), Almost negligible correlation was found between fuel cell efficiency and minimized system mass, the difference in mass being less than 1%.

- When a hybrid system is designed using Solid Energy Hermes, the degree of hybridization was found to be 0% for all cases except when the power density of fuel cell system is 693.75 W/kg. This can be explained by the fact that this power density of fuel cells is higher than the power density of the battery (=629W/kg).

- As was observed with PEM fuel cells, the degree of hybridization has a strong

correlation with the choice of battery. In the optimally sized system, the degree of hybridization is found to be as high as 95% for A123 cells, and 0% for Solid Energy Hermes cells.

The effect of endurance on minimized system mass is explored in the next section.

Endurance: 110 mins. cruise (*E110*) and 155 mins. cruise (*E155*)

System sizing results for E110 and E155 endurance conditions are presented in Appendix Appendix B. The observations from these plots is summarized below:

- From figures Figure B.11 and Figure B.13, it can be observed that doubling the endurance costs only about 2% mass. This correlation seems to hold true for all fuel cell power densities, all efficiencies, and all batteries.
- For tripling range, optimally sized SOFC hybrid systems are more favorable than pure battery systems, even if using state-of-the-art commercially available cells (Solid Energy Hermes [3]). This is inferred from Figure B.14.
- Systems sized with "High power density" cells (A123) resulted in the lowest total system mass in all of sized cases. They also resulted in highest degree of hybridization.
- The correlation of fuel cell efficiency with minimized system mass was found to be between 2% and 3% lower system mass for every 10% increase in system efficiency.

5.4 Discussion and summary

In this chapter, the method of arriving at an optimal system configuration was explained. This method was then used to size the mass-minimized system configuration for various combinations. These results helped narrow down the search region for a practical system sizing.

1. It is possible to double the range of the aircraft using current state-of-the-art batteries available commercially (Solid Energy Hermes). No hybrid system will be required if these batteries are used.
2. From a mass budget perspective, it is possible to triple the range of the current aircraft using optimally sized hybrid systems using commercially available technologies, with the configuration FCPEM-BTA123-PD693.75-DC00 and FCPEM-BTA123-PD555-DC00 weighing as much as 25% and

20% lower than the existing powertrain. However, volume of both these systems is estimated to be more than the available volume (of 138L).

3. "High power density" cells A123 were found to be the best candidate for hybridization. Optimal systems designed using these cells yielded more than 90% degree of hybridization for all endurance and power density cases.

4. Fuel cell power density has a much stronger correlation with total system mass than fuel mass. This is true even for higher endurance cases.

5. From a mass and exergy efficiency perspective, it is never beneficial to use a DC-DC converter. Hence, it should only be used if it is required for practical reasons.

6. It is observed that while doubling range with a PEM hybrid system costs about 7% mass, it costs only about 2% for propane fuelled SOFCs. It can be concluded that for high endurance systems, SOFCs have a significantly higher mass benefit over compressed hydrogen systems for similar system level power densities.

7. For *E65-FCCruise* condition, an SOFC-hybrid powerplant is more viable than battery-only system if specific power density of more than 277.5 W/kg can be achieved at a fuel cell system level, and results in a system mass about 12% - 14% lower than the existing aircraft. If a COPT system is sized for the same endurance requirement and fuel cell specific power density, the mass of the optimized powertrain design could be 14% to 16% lower than the existing aircraft.

8. For similar system-level power density, the SOFC-hybrid systems have the potential to be lighter than the PEM-hybrid systems. This correlation only increases as the endurance requirements increase.

9. SOFC-hybrid systems also have higher degree of hybridization for all sized cases, compared to PEM-hybrid systems. Hence it is much easier to increase range of the SOFC-hybrid systems, which would require only adding more fuel.

5.5 Chapter conclusion

For practical system sizing, following three combinations have been identified based on minimized mass and estimated volume. These were the only three

combinations which yielded an estimated volume within the volume budget. The specifications of these systems is presented in Table 5.4.

1. E65-FCPEM-BTVTC6-PD416.25-BL01-DC00-COPT
2. E65-FCPEM-BTVTC6-PD555-BL01-DC00-COPT
3. E65-FCPEM-BTVTC6-PD693.75-BL01-DC00-COPT

These combinations will be explored further in the next chapter for practical system sizing. No SOFC cases will be explored for practical sizing since no commercial SOFCs exist yet with the power densities used in this report.

Table 5.4: Results of mass minimization for the configurations selected for practical sizing.

Mass-minimized system	**PD416.75**	**PD555**	**PD693.75**
Weight [kg]	104.70	99.35	96.38
Fuel cell	20.30	15.23	12.17
Fuel cell BOP	2.03	1.52	1.21
Fuel	0.47	0.48	0.51
Fuel tank	5.84	6.05	6.41
Battery	66.14	66.14	66.14
Battery BOP	9.92	9.92	9.92
Energy [kWh]			
Stored H2	18.42	19.10	20.21
Battery	12.69	12.69	12.69
Total	13.23	31.79	32.90
Total usable	21.49	21.49	21.49
Nominal power [kW]			
Fuel cell	8.45	8.45	8.45
Battery	56.50	56.50	56.50
Volume [L]	99.96	87.10	80.68
Fuel cell	53.70	40.00	32.22
Fuel tank	22.73	23.57	24.93
Battery	23.53	23.53	23.53

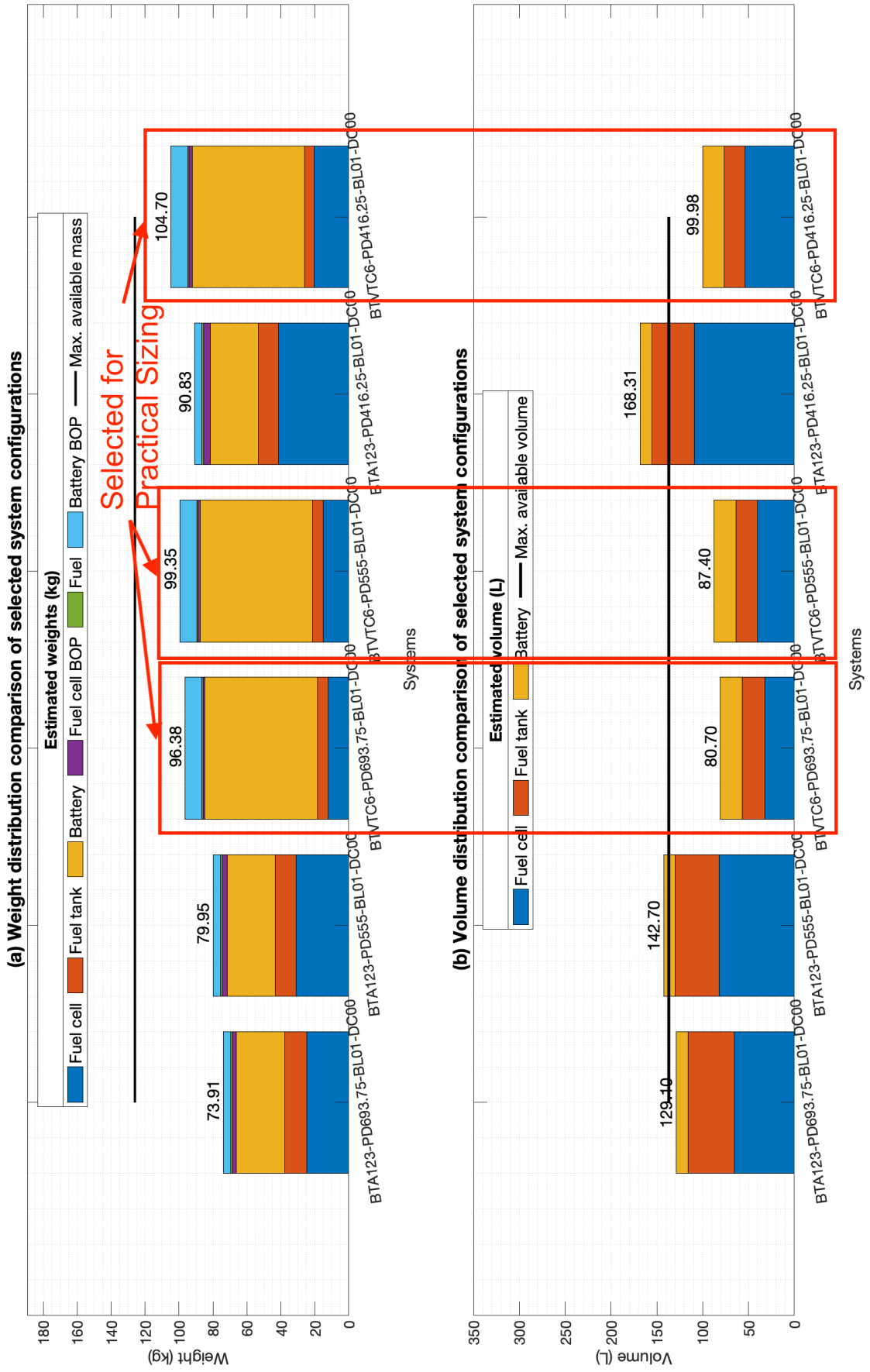

Figure 5.8: Systems selected for practical sizing.

Chapter 6

Practical system design

In the previous chapter, multiple cases were sized theoretically to understand the impact of variables such as operating power density, use of DC-DC converters, choice of batteries, type of fuel cell, and endurance on the minimized system weight. It was shown that the use of DC-DC converters resulted in higher exergy losses and added system weight. It was concluded that a fuel cell hybrid system is capable of doubling, even tripling the cruise range of Pipistrel Alpha-H_2 in the given weight budget. However, volume constraint proved to be more governing, and only three systems were estimated to fit within the given volume budget.

In this chapter, the systems selected in the previous chapter will be explored further, taking into account the differences between theoretical and practical system mentioned in section 2.4.2 (integer-nature or capacity limitation of components, junction box voltage requirement and battery voltage variation with SOC). Simulations are run on a drivetrain model developed on Simulink to verify the claims of system sizing. This chapter also

This chapter starts by explaining the approach for practically sizing the system, followed by explaining the Simulink model. Results, analysis and conclusions are presented towards the end of the chapter.

6.1 Approach and Methodology

6.1.1 Method of hybridization

Since all systems selected exclude the use of DC-DC converters, indirect hybridization scheme is used. The hybrid schematics are presented in Figure 6.1. Instead of DC-DC converters, two diodes are used to connect the fuel cell and battery. When the system is connected via the diodes, the bus bar voltage decides the

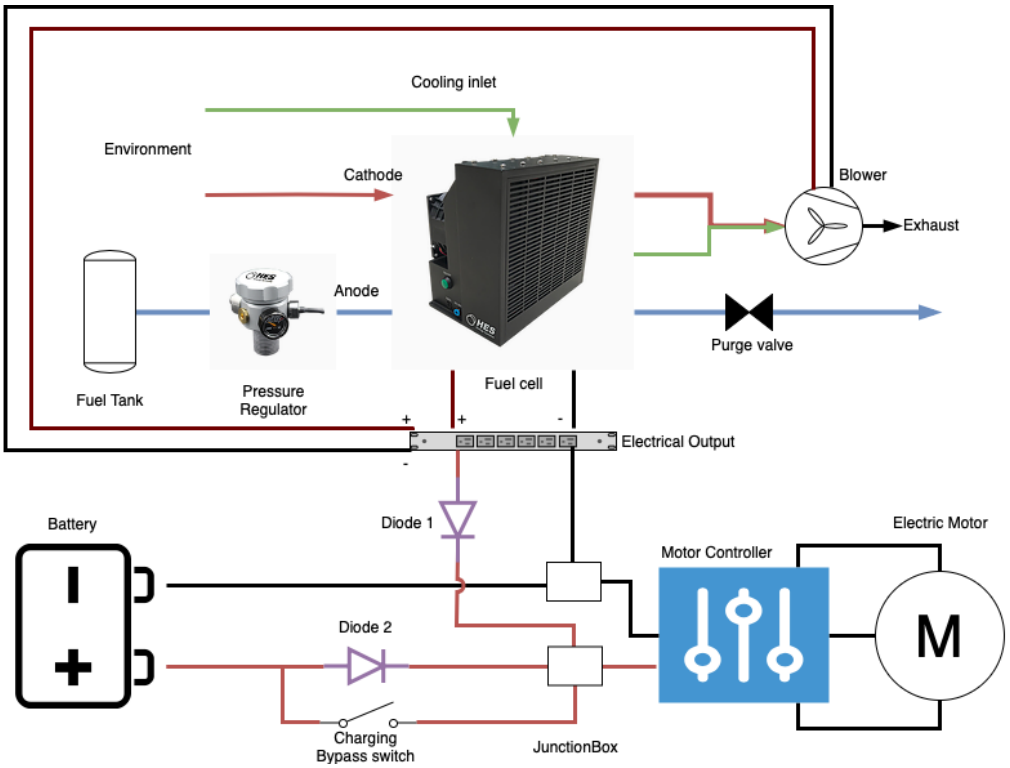

Figure 6.1: Hybridization scheme

power distribution between the fuel cell and the battery.
Consider the case when fuel cell voltage is higher than the battery voltage. In this case, the diode connected to the fuel cell is forward biased since the fuel cell is at a higher voltage than the battery. This way, the diode connected to battery is reverse biased due to same reason and effectively acts as an ”open switch”. As the power demand from the fuel cell increases, the voltage of the fuel cell decreases, and at a certain output power, the voltage goes below the battery voltage. When this happens, the diode connected to battery also gets forward biased, and the battery also starts supplying current. Thus, the power supplied by each of battery and fuel cell depends on the voltage of the component with the lower voltages. The downside of this method of hybridization is that the power output from the fuel cell can no more be controlled, and depends on the junction box voltage.

The method of sizing battery and fuel cell to match their voltages is explained in the next sections.

6.1.2 Fuel cell and battery sizing

Commercially available fuel cells and batteries have their rated voltage and power outputs. This section explains how the fuel cells and batteries are configured to match the designed system voltage and power with those of the system

requirements.

Fuel tank

Following information is required to size the fuel tank:

- System requirements

  M_{Fuel} (kg): Fuel mass required.

- Fuel tank specifications

  M_{Tank}^{Fuel} (kg): Fuel mass storage capacity of commercially available tank, having capacity closest to M_{Fuel}.

  M_{Tank} (kg): Mass of commercially available tank.

Number of fuel tanks required is found simply by

$$\lambda_{Tanks} = roundup\left(\frac{M_{Fuel}}{M_{Tank}^{Fuel}}\right) \tag{6.1}$$

Fuel cell

Following information is required for sizing the fuel cell system:

- System requirements

  $P_{FC}^{Required}$ (W): Nominal output power required from fuel cell system.

  $V_{Controller}^{Peak}$ (V): Max. allowed motor controller input voltage.

  $V_{Controller}^{Nominal}$ (V): Nominal motor controller input voltage.

- Stack specifications

  V_{FC}^{OCV} (V): Open circuit voltage per stack.

  V_{Cell}^{Op} (V): Operating voltage per cell in the fuel cell system.

  P_{FC}^{Rated} (W): Rated power per the fuel cell stack.

  n_{FC}^{Cells} (-): Number of cells per fuel cell.

- Stack operating condition specifications

  OPD (%): Operational power as % of rated power.

Number of fuel cells in series and parallel can be found in two ways:

Method 1: in this method, the motor controller max. input voltage is used to select the number of stacks in series. The number of stacks in parallel is calculated by using the number of stacks in series and total stacks required.

$$\lambda_{FC}^{Series} = rounddown\left(\frac{V_{Controller}^{Peak}}{V_{FC}^{OCV}}\right) \tag{6.2}$$

$$\lambda_{FC}^{Parallel} = roundup\left(\frac{\lambda_{FC}^{Total}}{\lambda_{FC}^{Series}}\right) \tag{6.3}$$

where,

$$\lambda_{FC}^{Total} = roundup\left(\frac{P_{Required}}{P_{FC}}\right) \tag{6.4}$$

$$P_{FC} = P_{FC}^{rated} * OPD \tag{6.5}$$

Where λ_{FC}^{Series} is the number of fuel cell stacks in series, and $\lambda_{FC}^{Parallel}$ is the number of fuel cell stacks in parallel. In some conditions, this might not yield optimal results. For example, if $\lambda_{FC}^{Total} = 10$ and $\lambda_{FC}^{Series} = 7$, then $\lambda_{FC}^{Parallel} = 2$ using the above method, and the actual total number of stacks would shoot to 14. In such conditions, DC-DC converters might result in a lower weight. In other words, if more fuel cells are required in series only to reach the required junction box voltage levels, it might be better to instead use less fuel cells and a DC-DC converter.

Method 2: However, if the voltage constraint is ignored, the combination yielding the least number of required fuel cells can be calculated directly.

$$\lambda_{FC}^{Total} = \lambda_{FC}^{Series} * \lambda_{FC}^{Parallel} \tag{6.6}$$

For the previous example, $\lambda_{FC}^{Series} = 5$ and $\lambda_{FC}^{Parallel} = 2$ would ensure that number of stacks is as close to the minimum required, while also keeping the voltage high enough.

υ_{FCS} is the fuel cell system voltage at which the system, in the configuration derived above, produces P_{FC}.

$$\upsilon_{FCS} = n_{FC}^{Cells} * \lambda_{FC}^{Series} * V_{Cell}^{Op} \tag{6.7}$$

υ_{FCS} will be used to size the battery system.
The max. number of fuel cells in series is subject to the constraint:

$$\lambda_{FC}^{Series} * V0_{Stack} \leq V_{Controller}^{Peak} \tag{6.8}$$

Where $V0_{Stack}$ is the open-circuit voltage per fuel cell stack. This constraint implies that the open-circuit voltage of the fuel cell system must not exceed the max. input voltage to the motor controller.

Battery

For sizing a battery system, following information is required about the system, fuel cell, and the battery cells:

- System requirements

  P_{BATT} (W): Nominal power output required from the battery system.

  υ_{FCS} (V): Nominal system voltage (fuel cell system voltage at required output power).

  $V_{Controller}^{Peak}$ (V): Max. allowed motor controller input voltage.

  E_{BATT} (Wh): Required energy of the battery pack.

  η_{BATT} (%): Battery efficiency.

- Cell specifications

  OCV (V): Max. voltage per cell.

  $V_{Cell}^{Nominal}$ (V): Nominal voltage per cell.

  V_{Cell}^{SOLR} (V): Cell voltage at the start of linear region at the max current.

  V_{Cell}^{EOLR} (V): Cell voltage at the end of linear region at the max current.

  $C_{Cell}^{Nominal}$ (Ah): Nominal capacity per cell.

  $CR_{Cell}^{Cont.}$ (-): Max. continuous discharge C-rate per cell.

Using the above information and the approach suggested in literature [50] the number of cells in series and parallel can be calculated

$$\upsilon_{FCS} \leq (OCV * \lambda_{BATT}^{Series}) \leq (V0_{Stack} * \lambda_{FC}^{Series}) \tag{6.9}$$

$$\lambda_{Batt}^{Parallel} = roundup\left(\frac{P_{BATT}}{\lambda_{Batt}^{Series} * C_{Cell}^{Nominal} * CR_{Cell}^{Cont.} * V_{Cell}^{Nominal} * \eta_{BATT}}\right) \tag{6.10}$$

Subject to constraints

$$(\lambda_{Batt}^{Series} * V_{Cell}^{Max}) \leq V_{Controller}^{Peak} \tag{6.11}$$

$$(\lambda_{Batt}^{Series} * V_{Cell}^{Nominal}) * (\lambda_{Batt}^{Parallel} * C_{Cell}^{Nominal}) * \eta_{BATT} \geq E_{BATT} \tag{6.12}$$

Equation 6.11 puts a constraint on the max. number of cells in series. It implies that the max. open-circuit voltage of the battery system must not exceed the peak input voltage of the DC-DC controller. However it must be noted that if Equation 6.8 and Equation 6.9 are satisfied, Equation 6.11 is automatically satisfied.
Equation 6.12 implies that the total energy content in the battery must be more than the total energy required, taking into account the battery discharge efficiency.

From Equation 6.9, it follows that there is a range within which the number of battery cells in series can fall. There is no upper limit for number of cells in parallel, but having cells more than required would only increase system weight.

6.1.3 Battery volume estimation

The volume of cells-only is different from the volume of the battery pack. This is because the volume of the battery pack needs to take into account the arrangement of cells in the battery pack, the cooling and air flow requirements, and the volume of the enclosure and mounting. Precise volume calculations would require CAD modeling, which is out of scope of this project. However, an estimation of battery pack volume can be made. *Cell packing density* is defined as the volume density of battery cells in the whole battery pack. Figure 6.2 shows the relation between cell arrangement and packing density [97].
Using Figure 6.2, it is assumed that the battery pack has a packing density of 0.8. Furthermore, it is assumed that additional 10% volume is required for enclosures and battery pack mounting. Thus the actual battery pack volume is estimated to be 1.375 times the volume of cells-only.

6.2 Simulink modeling

A Simulink model was developed with the aim to

- Verify the hybridization scheme, i.e. if the method of connecting fuel cell and battery together via diodes works.
- Verify if the power output of the fuel cell is as required by the theoretical sizing output.

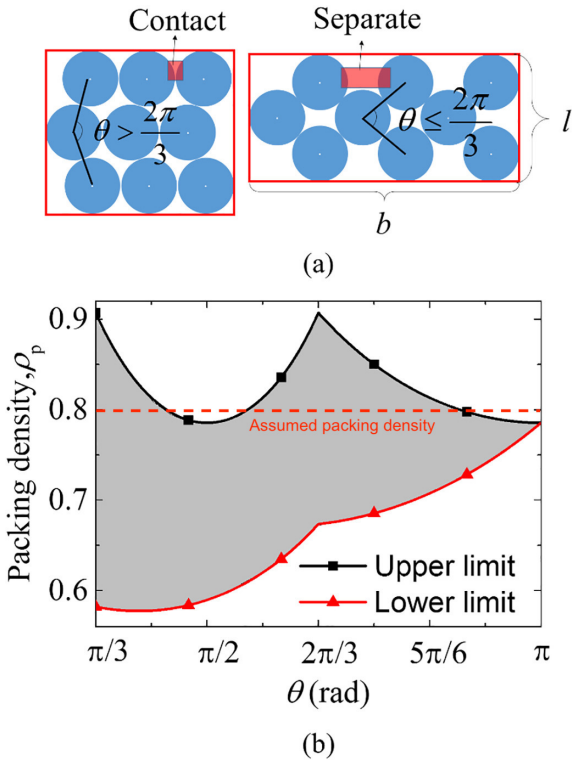

Figure 6.2: (a) Cell packing modes and pack sized defined by b, l, and θ.
(b) The upper and lower bounds of packing density against θ when l = b = 2 [97].

- Understand the power distribution between the battery and the fuel cell, specially towards low battery SOCs (State-of-Charge).

Model description

The hybrid scheme presented in Figure 6.1 is simulated on Simulink. The battery and the fuel cell models have been taken directly from the Simulink library. The electric motor and motor controller are considered a single system, and are simulated using the block ”DC Machine” in Simulink. The Simulink model is shown in Figure 6.3. The hybridization scheme used has been taken from [50]. Battery and the fuel cell are connected in parallel via forward biased diodes, and meet at the junction box. The motor is also connected to the junction box. All the blocks in the shaded areas are for measurements.

Assumptions

Certain assumptions were used to simulate the model on Simulink.

- The selected battery behaves in the same way as modeled by the Simulink battery model [73]. This is because the battery model on Simulink accepts battery parameters like the rated capacity, nominal voltage, peak voltage

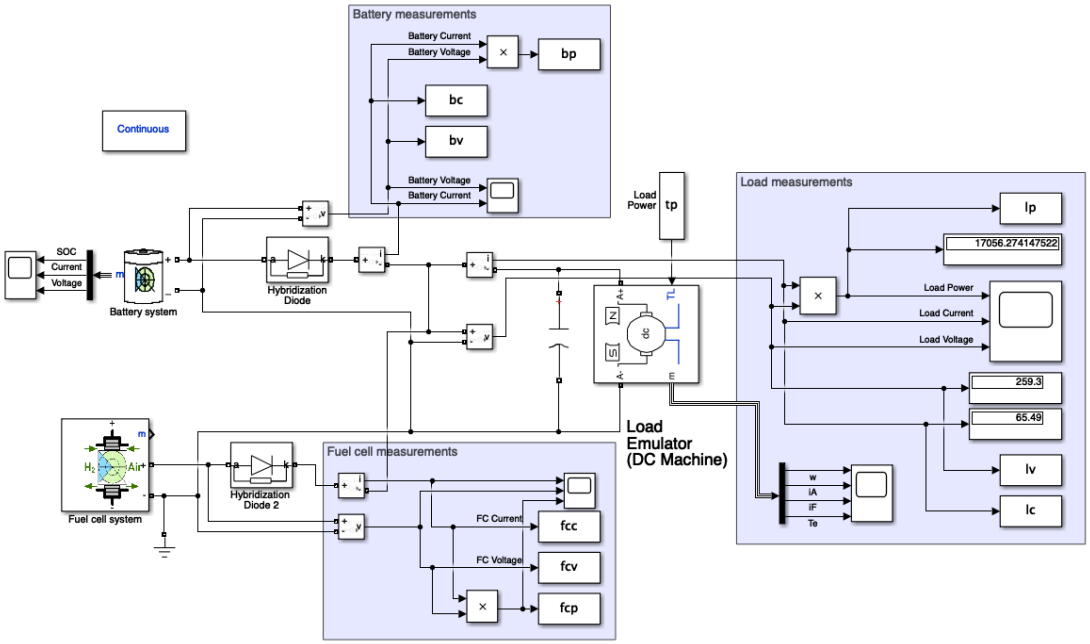

Figure 6.3: Simulink model for the hybridization scheme

etc. to simulate the battery. More about the battery model and its input parameters is mentioned in the battery model section.

- Effect of temperature on battery performance is not considered in this study.
- Dynamic behavior of the battery, fuel cell, and load is not a part of this study, and hence are not taken into account. Transients are ignored.
- The fuel cell model traces the IV curve of the selected fuel cell. This is because the fuel cell model in Simulink accepts fuel cell parameters like open-circuit voltage, nominal operating voltage and current, number of cells in series etc. to simulate the fuel cell's IV curve. Since only IV curve of the fuel cell are required for this simulation, the other calculations performed by the fuel cell model are not considered.
- Diodes are not ideal, and have their associated forward voltage drop of 0.7V each.
- Power demand by the aircraft during cruise flight remains constant. In other words, the aircraft cruise is assumed to be a steady level flight.
- The motor controller and the motor and modelled within the same "DC Machine" block in Simulink. This machine accurately simulates the motor used in the aircraft.

- Cruise endurance is directly governed by the available energy. Endurance for sized systems is estimated using the following equation:

$$Endurance_{Hybrid} = Endurance_{Base} * \frac{E_{Hybrid}}{E_{Base}}$$
$$E_{Hybrid} = (EDENS_{FC} * M_{Fuel} * \eta_{FC}) + (E_{BATT} * \eta_{BATT}) \tag{6.13}$$

  Where $EDENS_{FC}$ is the HHV of H_2 at 25 °C and 1 atm, and E_{BATT} is the energy content in the battery. This equation assumes that the endurance scales linearly with available energy.

Input parameters for model

Battery The input parameters required by the battery model, and corresponding description is mentioned in Table 6.1. The voltage values used in the model are shown on the discharge curve of the selected cell (Sony VTC6) in Figure 6.4a. Note that these values are per cell. The method to convert these values to battery pack level values is taken from the Simulink model guidelines, and corresponding equations are mentioned in Table 6.1. In the Figure 6.4a, ”SOLR” indicates the ”Start of Linear Region”, ”EOLR” indicates the ”End of Linear Region” and ”EODV” indicates the ”End-of-Discharge-Voltage”. While in general notion, the battery nominal voltage is indicated at is average voltage (which is about 3.6V/cell for Li-Ion), the Simulink model recognizes the ”EOLR” as the nominal voltage.

Table 6.1: Sony VTC6 battery parameters required by the Simulink block, and their corresponding values [30].

Battery model parameters	Symbol	Value / cell	Value for battery
Nominal Voltage (V)	EOLR	3.07	$EOLR * \lambda_{BATT}^{Series}$
Rated Capacity (Ah)	Crat	3	$Crat * \lambda_{BATT}^{Parallel}$
Initial state-of-charge (%)		100	
Maximum capacity (Ah)	Cmax	3.13	$Cmax * \lambda_{BATT}^{Parallel}$
Cut-off voltage (V)	EODV	2	$EODV * \lambda_{BATT}^{Series}$
Fully-charged voltage (V)	OCV	4.2	$OCV * \lambda_{BATT}^{Series}$
Nominal discharge current (A)	Inom	10	$Inom * \lambda_{BATT}^{Parallel}$
Internal resistance (ohms)	Ri	1.20E-02	$Ri * \lambda_{BATT}^{Series} / \lambda_{BATT}^{Parallel}$
Capacity at nominal voltage (Ah)	Cnom	2.5	$Cnom * \lambda_{BATT}^{Parallel}$
Exponential zone voltage (V)	SOLR	3.8	$SOLR * \lambda_{BATT}^{Series}$
Exponential zone capacity (Ah)	Cexp	0.1	$Cexp * \lambda_{BATT}^{Parallel}$

Fuel cell: The fuel cell model in Simulink requires certain parameters about the fuel cell to simulate the discharge characteristics of the modeled fuel cell. These parameters include the voltages at 0A, 1A output, at nominal operating output

current, and at rated maximum output current. Apart from these, the model also requires the number of cells as input, along with anode and cathode pressures and the fuel cell operating temperature. Using these values, the fuel cell model in Simulink simulates the fuel cell IV curve. The model uses fuel cell polarization equations mentioned in [98]. The values of all these input parameters to the Simulink fuel cell model are mentioned in Table 6.2, and illustrated in Figure 6.4b. These values have been derived from the MATLAB fuel cell model developed and explained in Chapter 4.

Table 6.2: Fuel cell parameters required by the Simulink block, and their respective values

Fuel cell model parameters	**Symbol**	**Value/cell**	**Value for system**
Voltage at 0 A (V)	V0	1.01	$V0 * \lambda_{FC}^{Series}$
Voltage at 1 A (V)	V1	0.94	$V1 * \lambda_{FC}^{Series}$
Nominal operating point current (A)	Inom		$Inom * \lambda_{FC}^{Parallel}$
Nominal operating point voltage (V)	Vnom		$Vnom * \lambda_{FC}^{Series}$
Max. operating point current (A)	Imax	28.1	$Imax * \lambda_{FC}^{Parallel}$
Max. operating point voltage (V)	Vmax	0.71	$Vmax * \lambda_{FC}^{Series}$
Number of cells (-)			$65 * \lambda_{FC}^{Series}$
Nominal stack efficiency (%)	η_{FC}		From Table 4.9
Operating temperature (C)	TFCELL	62	62
Nominal air flow rate (lpm)			200
Air supply pressure (bar)	PINCAT		1.01325
Fuel supply pressure (bar)	PINAN		1.7

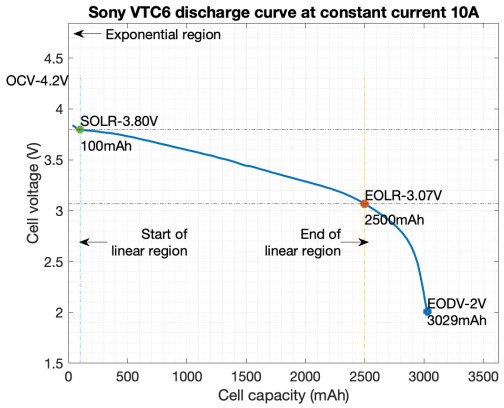

(a) Sony VTC6 (per cell) [30]

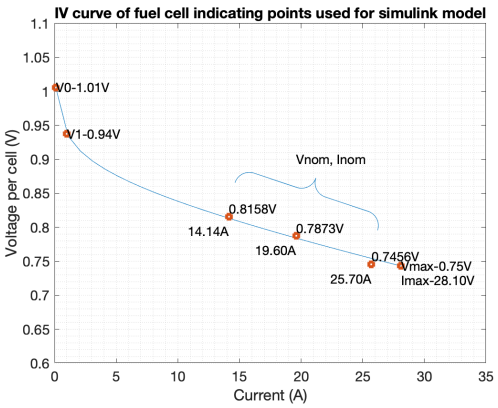

(b) Fuel cell (per cell) [16]

Figure 6.4: Battery and Fuel cell curves showing parameters required by Simulink model

6.3 Results and analysis

Using the sizing methods described above, practical systems were sized for all the three configurations. This chapter presents the results of the simulations performed on Simulink using those sized system parameters. The flight path simulated is Figure 2.10. The results of practical system sizing are tabulated in Table 6.3.

From the table, it can be seen that no system exactly matches the nominal power output as required by theoretical sizing. Further, at this point, there is an option to either size the practical system while maintaining the fuel cell nominal operating power density, or sizing the system to maintain the output power as per theoretical output. The former option was chosen to allow energy and exergy efficiency comparison with the base case (i.e. the existing aircraft). Besides, the selected fuel has a rated power output of 1 kW / stack, while the optimal sizing required the fuel cell to be sized for about 8.5 kW, which is not possible with the selected fuel cell.

E65-FCPEM-BTVTC6-PD416.25-BL01-DC00

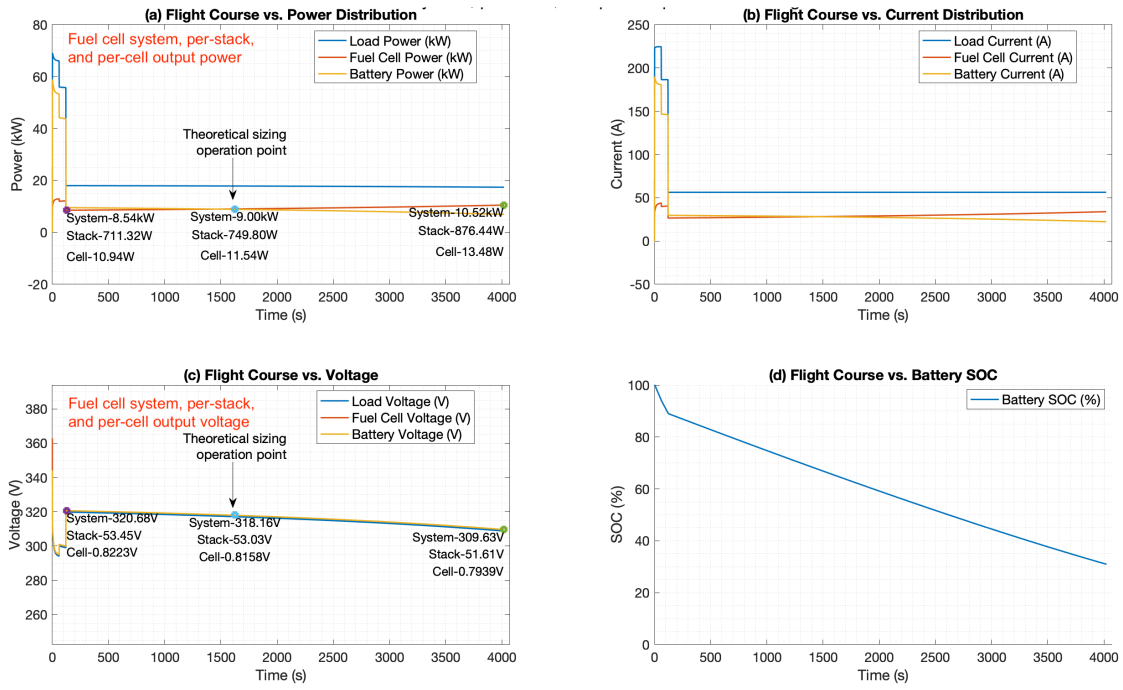

Figure 6.5: Simulink simulation results for power sharing during flight for case FCPEM-BTVTC6-PD416.25-BL01-DC00, indicating fuel cell power and voltage at different points in time during cruise.

For this system, the fuel cell operates nominally at 416.25 W/kg (i.e. at 75% of

its rated power density). Thus to reach the required nominal output power as suggested in Table 5.4, 6 stacks are placed in series along with 2 rows in parallel, making up 6S-2P configuration. The open-circuit voltage of this configuration is 370V, well below the controller peak input voltage. The nominal operating voltage (i.e. system voltage at desired power output) is about 318V, calculated using the Equation 6.7. The required fuel weight is 470g for a 65 minutes cruise, while the selected HES A20 H_2 tank provides a storage capacity of 629g, i.e. 33% more than required. Hence, 1 fuel tank is used.
The number of battery cells in series is 79, and in parallel is 16 (79S-16P). This combination of Sony VTC6 cells provides an open-circuit voltage of 331.8V, which lies between fuel cell open-circuit voltage and fuel cell nominal output voltage. The total energy of the battery pack is 13.65 kWh. The estimated endurance is about 83 mins, 18 minutes higher than the base case. The expected system weight is about 104 kg, about 22 kg lower than the base case. This information is summarized in Table 6.3.

This system was simulated on Simulink, and the results are presented in Figure 6.5. From the figure, following observations can be made:

- The weight estimate of practical system is 102.41 kg, while the weight estimate of theoretically sized system is 104.7 kg. The two are in good agreement, with the difference being $< 2\%$.
- The nominal junction box voltage is about 27V lower than the nominal battery voltage in the base case. This could affect the motor performance, depending on the motor and controller characteristics.
- From Figure 6.5a, it can be noticed that fuel cell output power does not remain constant for the entire flight duration. The fuel cell output power is higher during takeoff and climb phases as the battery voltage dips with high power output.
- As the flight enters cruise mode, the output power from the fuel cell is 8.5 kW, which is less than the designed nominal fuel cell power output. However towards the end of cruise flight, the nominal output power of the fuel cell system increases to 10.5 kW.
- The output power from the fuel cell increases as the battery SOC decreases, and consequently the battery voltage decreases. This effectively implies that the fuel cell is not operating at a constant output voltage and power throughout the flight.

- During cruise flight, the output voltage of the battery and the fuel cell always remain equal.
- The junction box voltage drops by about 10V from the start of flight to the end of flight. This is due to the drop in battery SOC, consequently causing a drop in battery voltage, and change in power distribution.

Fuel cell power variation due to battery configuration: Appendix C contains graphs for systems sized for the same condition, i.e. for PD416.25. The effects of different battery configurations in series and parallel can be observed. The reference case is chosen as battery configuration 79S-16P, which gives and open circuit voltage of 331V. Observations are listed below:

- The effects of the number of cells in series, i.e. the nominal and OCV of battery can be observed in Figure C.1 and Figure C.2. In these figures, the number of cells are 1 less, and 1 more respectively than in the base reference case battery configuration (79S-16P). If the number of cells in series is 1 less, the drop in battery voltage over the cruising duration is about 9V. The fuel cell system power output at the start of cruise flight is more than its theoretical sizing operation point (of 9 kW), and the power output increases to about 10.8 kW by the end of flight, an increase of nearly 133 W/stack. In summary, when number of battery cells in series is decreased, the theoretical sizing operation point is closer to the power output at the start of cruise flight.
- In Figure C.2, it is observed that if the number of cells in series is increased by 1, the trend is opposite than in the previous point. The theoretical sizing operation point shifts more towards end of cruise flight.
- The effects of number of changing the number of cells in parallel is observed in Figure C.3, where number of cells in parallel is decreased by 2 and in Figure C.4 where number of cells in parallel is increased by 2. Decreasing the number of cells in parallel has similar effect to decreasing the cells in series, and the opposite seems to be true for increasing the number of cells in parallel.
- This can be explained as follows: When number of cells in parallel is higher, there is more energy available in the battery pack, and consequently its voltage drop with time (or energy output) is lower. In Figure C.3, the cells in parallel is 14 and the battery voltage drop is about 14.23V between start and end of cruise flight. In Figure C.3, the cells in parallel is 18 and the battery voltage drop is about 8.86V between start and end of cruise flight.

FCPEM-BTVTC6-PD555-BL01-DC00

For this system, the fuel cell operates nominally at 555 W/kg (i.e. at 100% of its rated power density). Thus to reach the required nominal output power as suggested in Table 5.4, 5 stacks are placed in series along with 2 rows in parallel, making up 5S-2P configuration. The open-circuit voltage of this configuration is 309V, well below the controller peak input voltage. The nominal operating voltage (i.e. system voltage at desired power output) is about 255V, calculated using the Equation 6.7. The required fuel weight is 480g for a 65 minutes cruise, while the selected HES A20 H_2 tank provides a storage capacity of 629g, i.e. about 32% more than required. Hence, 1 fuel tank is used.
The number of battery cells in series is 63, and in parallel is 20 (63S-20P). This combination of Sony VTC6 cells provides an open-circuit voltage of 226.8V, which lies between fuel cell open-circuit voltage and fuel cell nominal output voltage. The total energy of the battery pack is 13.61 kWh. The estimated endurance is about 81 mins, 16 minutes higher than the base case. The expected system weight is about 99 kg, about 26 kg lower than the base case This information is summarized in Table 6.3.

This system was simulated on Simulink, and the results are presented in Figure 6.6. Some similar observations can be made:

- The weight estimate of practical system is 99.23 kg, while the weight estimate of theoretically sized system is 99.35 kg. The two are in excellent agreement, with the difference being $< 1\%$.
- The battery nominal voltage is about 90V lower in this case than the base case. This voltage is comparatively much lower than the nominal voltage, and may not be sufficient to run the motor at the required RPM.
- The fuel cell system output power varies from 9.94 kW (993 W/stack) during start of cruise, until about 10.77 kW (1076W/stack) towards the end of cruise flight. This output power is fairly constant when compared to the previous case, where the difference was about 2 kW.

FCPEM-BTVTC6-PD693.75-BL01-DC00

For this system, the fuel cell operates nominally at 693.75 W/kg (i.e. at 125% of its rated power density). Thus to reach the required nominal output power as suggested in Table 5.4, 7 stacks are placed in series along with 1 row in parallel, making up 7S-1P configuration. The open-circuit voltage of this configuration is

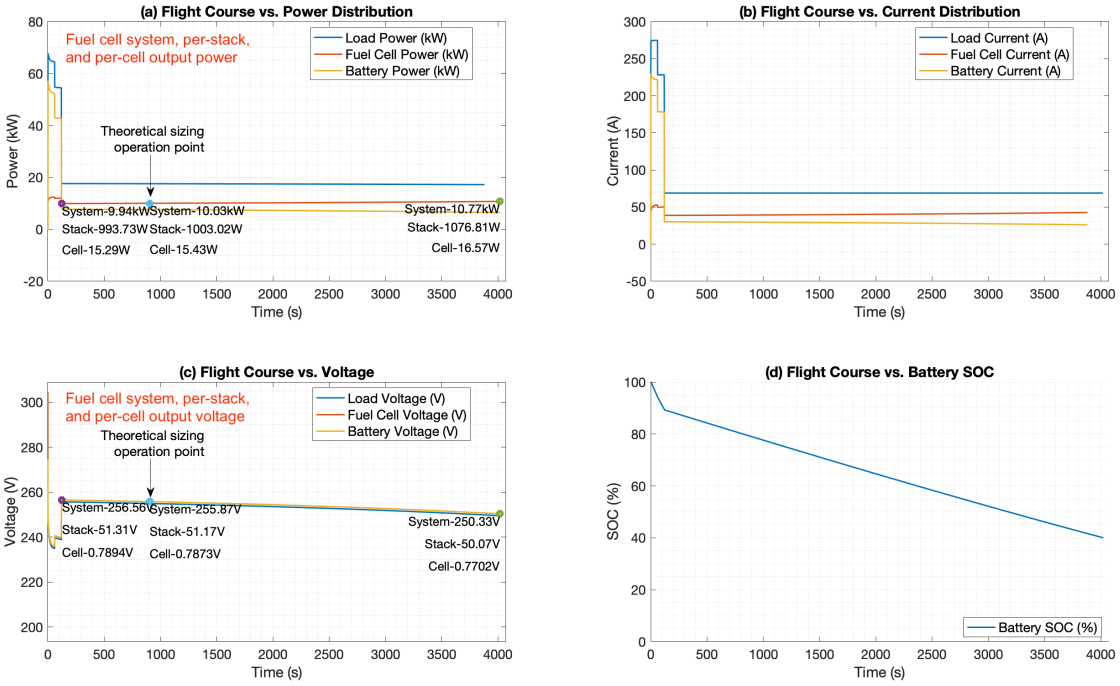

Figure 6.6: Simulink simulation results for power sharing during flight for case FCPEM-BTVTC6-PD555-BL01-DC00 indicating fuel cell power and voltage at different points in time during cruise.

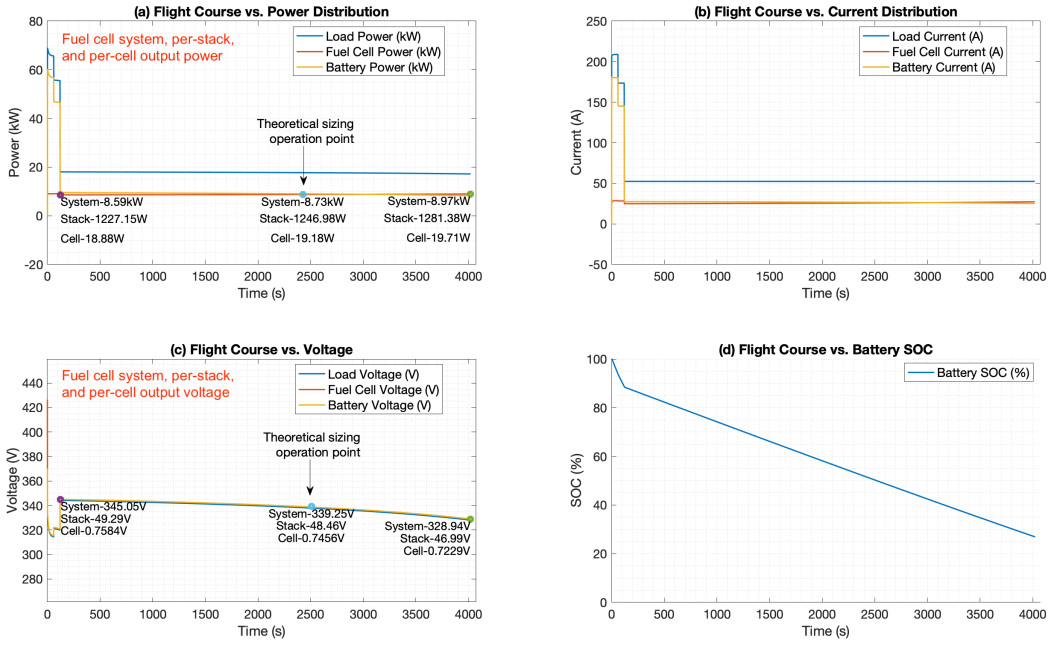

Figure 6.7: Simulink simulation results for power sharing during flight for case FCPEM-BTVTC6-PD693.75-BL01-DC00 indicating fuel cell power and voltage at different points in time during cruise.

432.6V, slightly below the controller peak input voltage. The nominal operating voltage (i.e. system voltage at desired power output) is 339V, calculated using the Equation 6.7. The required fuel weight is 510g for a 65 minutes cruise, while the

selected HES A20 H_2 tank provides a storage capacity of 629g, i.e. about 23% more than required. Hence, 1 fuel tank is used.
The number of battery cells in series is 85, and in parallel is 15 (85S-15P). This combination of Sony VTC6 cells provides an open-circuit voltage of 357V, which lies between fuel cell open-circuit voltage and fuel cell nominal output voltage. The total energy of the battery pack is 13.61 kWh. The estimated endurance is about 80 mins, 15 minutes higher than the base case. The expected system weight is about 94 kg, about 32 kg lower than the base case. This information is summarized in Table 6.3.

This system was simulated on Simulink, and the results are presented in Figure 6.7. Following points can be noted for this configuration:

- The weight estimate of practical system is 94.12 kg, while the weight estimate of theoretically sized system is 96.38 kg. The two are in good agreement, with the difference being about 3%.
- The battery nominal voltage is only about 6V lower in this case than the base case.
- The output power from the fuel cell remains fairly constant from the start until the end of cruise flight, changing by only about 380W (54W/stack).

These three systems are compared on exergy efficiency difference, change in weight, and expected endurance difference in the Figure 6.8.
For all the three designs, the estimated volume of the powerplant is within the budget. However, it should be noted that except for battery pack where the packing density and enclosure volume are taken into account, the volume calculations for all other components only calculate the actual volume occupied by the systems, volume calculation does not account for the clearances required, volume required for enclosures, and for maintaining proper airflow.

6.4 Discussion and summary

In this chapter, three systems were sized practically and analysed on Simulink. It was found that theoretical system sizing determined the system weight fairly accurately. This also proved that a hybrid aircraft powerplant design is possible with commercially available technologies. All the designed powerplants not only proved to be lower in weight than the base aircraft, but also contain higher energy content, thus effectively increasing endurance.
The following can be concluded from practical system sizing:

- All the three practically sized systems weigh under 105 kg, over 20 kg less than the existing system. Systems FCPEM-BTVTC6-PD555-BL01-DC00 and FCPEM-BTVTC6-PD693.25-BL01-DC00 weigh even under 100 kg, at about 99.23 kg and 94.12 kg respectively. From weight distribution in Table 6.3, it can be observed that the weight of battery pack, fuel and fuel tank is nearly the same in all three cases. Only the weight of fuel cell differs in all the three cases. This is because the number of fuel cells is different in each case (12, 10, and 7 in PD416.25, PD555 and PD693.75 respectively).
- Estimated system endurance for all three practically sized systems is at least 15 minutes higher than the existing system endurance of 65 minutes
- All three systems were found to fit in the volume budget of 138 L. However, volume estimations used in practical sizing do not consider and clearances required for air flow and mounting, and also exclude packing density of fuel cell system. Further investigation and CAD modeling is required to ascertain if fitting the systems within given volume is actually possible.
- With the direct hybridization scheme used, the power output from the fuel cell system varies with cruise flight time. It is also higher than theoretical sizing point during takeoff and climb phases. Hence although this hybridization scheme has weight and efficiency benefits, does not provide direct control over the fuel cell output power.
- For systems FCPEM-BTVTC6-PD416.75-BL01-DC00 and FCPEM-BTVTC6-PD693.75-BL01-DC00, the junction box voltage (318V and 339V respectively) at designed fuel cell power output is within the voltage range of existing aircraft (288V to 399V, Table 2.6). However for system FCPEM-BTVTC6-PD555-BL01-DC00, this voltage is lower than the range mentioned above (at 255V), but is still within the motor controller input voltage range (100V to 450V). The effect of lower nominal voltage on motor performance is unknown at this point. Further investigation is required to understand the effect of lower input voltage on motor performance. If required, the motor performance may be compensated by using a gearbox or system voltage can be increased by using a DC-DC converter. However, in either of these cases it is possible that the system mass increases beyond that of PD416.25, and hence the system PD555 might not be the most suitable.
- In the system FCPEM-BTVTC6-PD693.75-BL01-DC00, the fuel cell constantly operates beyond its rated continuous output power. The effects of operating the fuel cell continuously beyond its rated power on the fuel cell lifetime performance is not known and needs further investigation.

6.5 Chapter conclusion

The configuration **FCPEM-BTVTC6-PD416.25-BL01-DC00** is found to be the most suitable fuel cell - battery powerplant system for the Pipistrel Alpha-H_2, with an estimated weight of 102.4 kg, which is about 24 kg lighter that the existing system, and an estimated endurance of 80 minutes, about 15 minutes higher than existing system. The nominal voltage of this configurations also falls within the nominal operating voltage range of the existing aircraft powertrain. The estimated volume of this system (= 129 L) is also within the volume budget (of 138 L), but this needs further investigation. Figure 6.8 and Figure 6.9 compare the key parameters of the three systems analysed in this chapter, and Table 6.3 contains the detailed configuration of all these three systems.

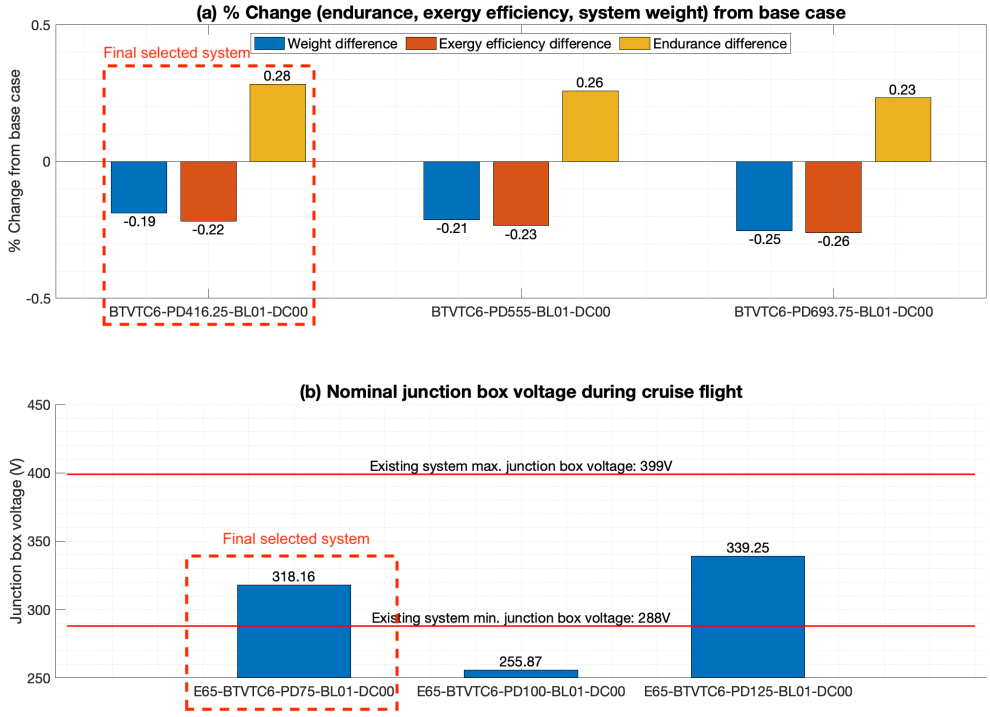

Figure 6.8: (a) Comparing the % change in weight, exergy efficiency, and endurance from the base case for sized systems.
(b) Nominal junction box voltage (at the theoretical sizing point) during cruise flight.

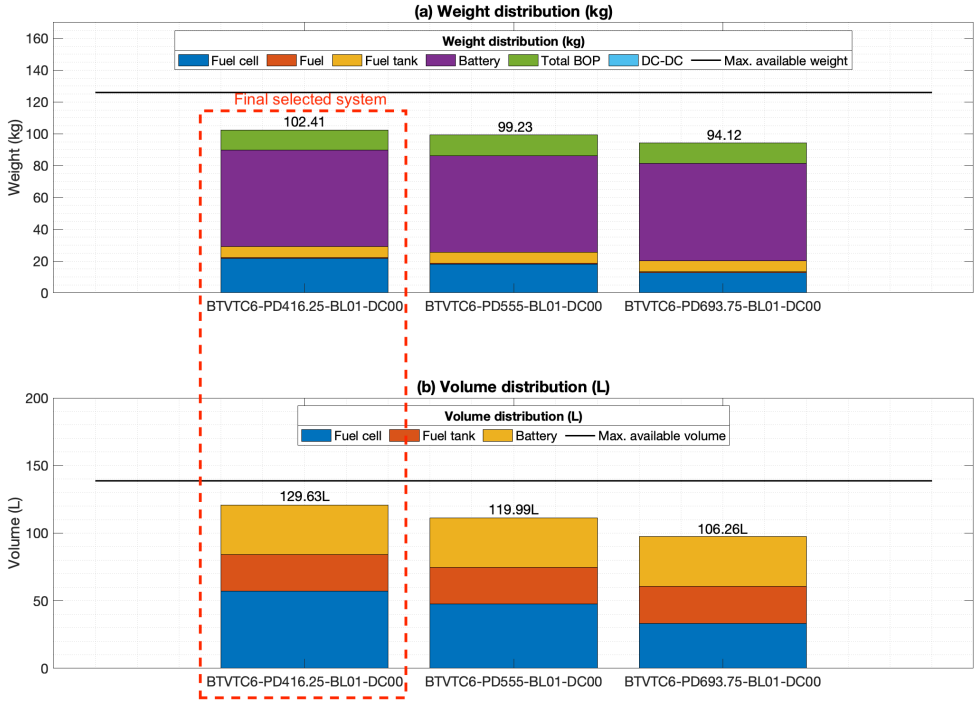

Figure 6.9: (a) Comparing weight distribution for the sized systems. (b) Comparing volume distribution for the sized systems.

Table 6.3: Comparing theoretical and practical system sizing for selected configurations.

	Base case	E65-BTVTC6-PD416.25-BL01-DC00		E65-BTVTC6-PD555-BL01-DC00		E65-BTVTC6-PD693.75-BL01-DC00	
System level		**Theoretical**	**Practical**	**Theoretical**	**Practical**	**Theoretical**	**Practical**
Total weight [kg]	126	104.70	102.41	99.35	99.23	97.07	94.12
Total volume [L]	138.8	99.96	129.63	87.10	119.99	80.68	106.26
Total energy content [kg]	21	21.49	25.67	21.49	25.17	21.49	24.66
Est. endurance [mins]	65	65.00	83.41	65.00	81.81	65.00	80.14
Fuel cell system							
$P_{FC}^{Nominal}[kW]$	-	8.45	9.00	8.45	10.00	8.45	8.75
Vrated [V] at $P_{FC}^{Nominal}$			318.16		255.87		339.25
Weight [kg]	-	20.30	21.60	15.23	18.00	12.80	12.60
BOP weight [kg]	-	2.03	2.16	1.52	1.80	1.28	1.26
λ_{FC}^{Series}	-	-	6.00	-	5.00	-	7.00
$\lambda_{FC}^{Parallel}$	-	-	2.00	-	2.00	-	1.00
Vnom [V]	-	-	318.16	-	255.87	-	339.25
η_{FC}^{Energy}	-	0.5122	0.5122	0.494	0.494	0.467	0.467
Est. volume [L]	-		57.00		47.50		33.25
Fuel tank			HES A20		HES A20		HES A20
Fuel weight [kg]	-	0.47	0.63	0.48	0.63	0.51	0.63
Fuel tank empty weight [kg]	-	5.84	7.00	6.05	7.00	6.41	7.00
Pressure regulator weight [kg]			0.25		0.25		0.25
Fuel tank volume [L]	-	22.73	27.21	23.57	27.21	24.93	27.21
Battery system							
$P_{BATT}[kW]$	65.00	56.50	54.60	56.50	54.43	56.50	55.08
Weight [kg]	126.00	66.14	60.67	66.14	60.48	66.14	61.20
BOP weight [kg]	-	9.92	9.10	9.92	9.07	9.92	9.18
λ_{BATT}^{Series}	96.00	-	79.00	-	63.00	-	85.00
$\lambda_{BATT}^{Parallel}$		-	16.00	-	20.00	-	15.00
OCV [V]	399.00	-	331.80	-	264.60	-	357.00
Crated [Ah]	60.86	-	48	-	60	-	45
Total energy [kWh]	21	12.69	13.65	12.69	13.61	12.69	13.77
Est. volume [L]	138.8	23.53	36.60	23.53	36.49	23.53	36.92

Chapter 7

Conclusion and future work

7.1 Exergy-gravimetric approach

The objective of this Master's thesis was to indicate an exergy-gravimetric approach towards design of a fuel cell - battery hybrid powerplant, and using this to arrive at a mass-minimized configuration for Pipistrel Alpha-H_2. This approach was developed during this Master's thesis, and is summarised below:

- Identify the fuel cell to be used for system sizing, based on specific power density; i.e. selecting the highest specific power density fuel cell. Identify the sources of exergy loss and destruction within the fuel cell.
- For all the identified cases, calculate fuel cell operational efficiency using CycleTempo.
- Identify other variables in the powerplant design. For example: choice of batteries and cruise endurance required.
- Using a mass-minimization function developed in MATLAB, theoretically compute the optimal system weight for all the combination of variables.
- Select configurations resulting in the lowest powerplant weight. Out of these configurations, further eliminate those configurations resulting in higher than available volume budget (of 138 L in this case).
- Practically size systems for the selected configurations; i.e. compute the number of fuel cell stacks and batteries required in series and parallel to achieve the required power and energy. Simulate the system on Simulink to understand the system performance during different flight phases.

The effect of following variables on the optimal system weight was analyzed:

1. **Fuel cell type selection: PEM and SOFC.**

2. **Exergy-gravimetric cases for the fuel cell**
    a. Effect of fuel cell operational power density (and consequently efficiency) on system weight.
    b. Effect of the use of cooling fan in fuel cell on fuel cell efficiency and system weight.
    c. Effect of the use of DC-DC converter on fuel consumption and system weight.
3. **System-level design options**
    a. Aircraft's required cruise endurance: 65 minutes, 110 minutes, 155 minutes.
    b. Effect of the type of battery for hybridization on the optimal system configuration: high power density, high energy density, balanced.
    c. Hybridization condition: only fuel cell provides power during cruise, both battery and fuel cell provide power during cruise flight.

7.2 System sizing

The variables mentioned in the previous section resulted in a total of 225 system configuration options, which were systematically reduced to three using the approach mentioned in the previous section.

- Overall, it was found that even tripling the endurance of existing aircraft is possible within the mass budget (of 126 kg). The most promising configurations make use of the "high power density" cell (A123), along with fuel cell operating at an operational power density of > 416.25 W/kg and without the DC-DC converter. The configuration E155-FCPEM-BTA123-PD693.75-BL01-DC00-COPT is estimated to weigh about 94 kg, i.e. almost 25% lower in weight than existing powerplant.
- For similar endurance requirements and battery hybridization and SOFC system level specific power density, systems hybridized with SOFCs weigh as much as 12% lower than PEM-hybrid systems. If SOFC system level specific power density above 277.5 W/kg can be achieved, an SOFC-hybrid system could weigh 14% to 16% lower than the existing powerplant.
- For optimal configurations, i.e. where fuel cell system and battery system, both provide power during cruise flight, doubling the range requires

additional about 2% weight (about 2.5 kg) for SOFC-hybrid systems, while it requires additional 7% weight (about 8.8 kg) for PEM-hybrid systems. This is because the storage density of propane fuel tanks is 150%, while only 8% for hydrogen tanks. Hence while every kilo of propane adds only about 0.67 kg in fuel tank weight, every kilo of hydrogen adds about 12.8 kg in fuel tank weight. SOFC specific power density of up to 1 kW/kg at stack level has been demonstrated in literature [96], but only up to 120 W/kg has been realized [99]. Thus SOFC-hybrid systems were not considered for practical system sizing.

- Of the PEM-hybrid configurations, only three configurations were estimated to fit within the volume budget (of 138 L). All these configurations provide an estimated endurance of over 80 minutes, i.e. 15 minutes higher than the existing aircraft. These configurations are:
  - System 1: E65-FCPEM-BTVTC6-PD416.25-BL01-DC00
  - System 2: E65-FCPEM-BTVTC6-PD555-BL01-DC00
  - System 3: E65-FCPEM-BTVTC6-PD693.75-BL01-DC00
- With direct hybridization (i.e. without using DC-DC converters), the nominal system voltage at 18kW output power was found to be 318V, 255V and 339V for systems 1, 2, and 3 respectively, as shown in Figure 6.8. The nominal voltage of system 2 is lower than the minimum junction box voltage of the existing aircraft (288V), and the effects of lower junction box voltage on motor performance need to be explored further. For this reason, system 2 is rejected. Furthermore, the fuel cell stacks in system 3 operate beyond their rated continuous output power (of 1000W). The effect of operating the fuel cells beyond their rated continuous output power on the fuel cells needs to be further analysed.

Key takeaway

In conclusion, system 1 (**E65-FCPEM-BTVTC6-PD416.25-BL01-DC00**) was found to be most suitable for hybridizing the aircraft. With an estimated weight of 102 kg, this configuration is about 24 kg lighter than the existing powertrain, and has an endurance of about 80 minutes, i.e. endurance by nearly 15 minutes higher than existing aircraft. The detailed specifications of this system are given in Table 6.3, and its comparison with other practically sized systems is shown in Figure 6.8 and Figure 6.9. Initial calculations suggest that this system, with an estimated volume of 129 L could fit in the given volume budget of 138 L,

however this calculation excludes clearances required for air flow and mounting, and packing density of fuel cells in the volume available, and hence needs to be explored further.

7.3 Future work and recommendations

Due to the limitation imposed by thesis duration, several aspects can be explored further:

- **Exergy-gravimetric analysis**: This thesis work indicates the approach taken towards design of a mass-minimized powerplant while including the "true cost" of energy. This approach can be further extended to include no just the powerplant, but other variables like airframe configurations can be included to arrive at the most suitable configuration for any given mission. Further, this work developed the approach for Exergy-gravimetrics, but the same approach can also be used for different objectives, like cost minimization or mission profile optimization.
- **SOFCs for aerial vehicles**: Using the approach developed in this study, it was found that propane fuelled SOFCs are a viable option for 2-seater aircrafts if their specific power density is more than 277.5 W/kg, proving to be even better than the PEM fuel cells of similar specific power density. The feasibility of having such high specific power density SOFCs should be explored further.
- **Detailing existing powerplant design**:
  - **Volume estimation**: Further calculations and CAD modeling of the systems is required to ascertain if the practically sized systems can fit within the volume budget.
  - **Effect of altitude on fuel cell performance**: The powerplants sized in this thesis assumed the aircraft to be flying at low altitudes. As the flight altitude increases, the pressure and temperature drops, which would affect the aircraft as well as fuel cell performance. To properly design a powerplant for an aircraft and to define its flight envelope, there is further scope for analysing performance sensitivity on altitude.
  - **Flight envelope**: In this master's thesis, the requirements of only a single flight profile was analyzed to determine if there is a possibility to reduce powerplant weight and increase the endurance. This study can be expanded to include multiple flight profiles including the effect of

altitude on performance of both the fuel cell and the aircraft to draw a full flight envelope of the device.

  - **Junction box voltage**: Two of the three systems practically sized had a junction box nominal voltage less than that of the current aircraft. The impact of lower junction box voltage on motor performance needs to be further analyzed. The choice of using a DC-DC converter vs. a motor modification need to be analyzed at a higher level.

- **Fuels**: Only compressed Hydrogen for PEM fuel cells, and propane for SOFCs was explored in this thesis. A further feasibility study of Liquid H_2 fuelled powerplant designs can be explored for PEMs and SOFCs.

Bibliography

[1] Joyce Penner and D.H. Lister. *Aviation and the Global Atmosphere — IPCC*. [ONLINE]: https://www.ipcc.ch/report/aviation-and-the-global-atmosphere-2/.

[2] George Bower. *Tesla Model 3 2170 Energy Density Compared To Bolt, Model S P100D*. [ONLINE]: https://insideevs.com/news/342679/tesla-model-3-2170-energy-density-compared-to-bolt-model-s-p100d/.

[3] *Hermes - High Energy Rechargeable Metal cells for Space*. Tech. rep. Solid Energy Systems, 2019.

[4] The Physics Factbook. *Energy Density of Gasoline - The Physics Factbook*. [ONLINE]: https://hypertextbook.com/facts/2003/ArthurGolnik.shtml.

[5] Rotax GmbH. *Rotax 912 ULS/S - Rotax Aircaft Engines*. [ONLINE]: https://www.flyrotax.com/produkte/detail/rotax-912-uls-s.html.

[6] Energy Education CA. *Energy density vs power density - Energy Education*. [ONLINE]: https://energyeducation.ca/encyclopedia/Energy_density_vs_power_density.

[7] Comas Haynes and Ryan Miller. "ExergoGravimetric Design for Increased SOFC Power Density". In: (2013), pp. 1–9.

[8] Frano Barbir. "PEM Fuel Cells - Theory and Practice". In: (2005).

[9] Andrew L. Dicks and David A.J. Rand. *Fuel cell systems explained*. John Wiley & Sons Ltd., 2018. ISBN: 9781118706978.

[10] G.F. Hundy et al. "Air and Water Vapour Mixtures". In: *Refrigeration, Air Conditioning and Heat Pumps* (Jan. 2016), pp. 301–312. DOI: 10.1016/B978-0-08-100647-4.00019-X.

[11] Mark G. Lawrence. "The Relationship between Relative Humidity and the Dewpoint Temperature in Moist Air: A Simple Conversion and Applications". In: *Bulletin of the American Meteorological Society* 86.2 (Feb. 2005), pp. 225–234. ISSN: 0003-0007. DOI: 10.1175/BAMS-86-2-225.

[12] Ryan P. O'Hayre. *Fuel cell fundamentals*. Vol. 2nd ed. 2006, p. 409. ISBN: 9788578110796. DOI: 10.1017/CBO9781107415324.004.

[13] Torsten Berning, Ned Djilali, and D.M. Lu. "Three-dimensional computational analysis of transport phenomena in a PEM fuel cell". In: *Journal of Power Sources* 106 (2001), pp. 284–294.

[14] Zhan Gao et al. "A perspective on low-temperature solid oxide fuel cells". In: *Energy & Environmental Science* 9.5 (May 2016), pp. 1602–1644. ISSN: 1754-5692. DOI: 10.1039/C5EE03858H.

[15] Intelligent Energy Limited. *Our Products / UAVs | Intelligent Energy*. 2019. [ONLINE]: https://www.intelligent-energy.com/our-products/uavs/.

[16] Harshwardhan Thakar. *Private communication*. 2019. [ONLINE]: https://www.hes.sg/aerostak.

[17] Jingming Liang and Zefeng Wu. "Simulation and Optimization of Air-Cooled PEMFC Stack for Lightweight Hybrid Vehicle Application". In: *Mathematical Problems in Engineering* 2015 (Oct. 2015), pp. 1–11. ISSN: 1024-123X. DOI: 10.1155/2015/738207.

[18] Syed Mushahid Hussain Hashmi. *Cooling Strategies for PEM FC*. Tech. rep. 2010.

[19] Bent Sørensen et al. "Fuel cells". In: *Hydrogen and Fuel Cells* (Jan. 2018), pp. 107–220. DOI: 10.1016/B978-0-08-100708-2.00003-5.

[20] *ZERO EMISSION HEAVY DUTY MOTIVE MODULES*. Tech. rep. Ballard Power Systems, 2019.

[21] Hydrogenics. *Hydrogen Products and Solutions | Hydrogenics*. 2019. [ONLINE]: https://www.hydrogenics.com/hydrogen-products-solutions/.

[22] Powercell SE. *PowerCell MS-30 10-30 kW PEM Fuel Cell System*. Tech. rep. Powercell Sweden, 2019.

[23] Louis Schlapbach and Andreas Züttel. "Hydrogen-storage materials for mobile applications". In: *Nature* 414.6861 (Nov. 2001), pp. 353–358. ISSN: 0028-0836. DOI: 10.1038/35104634.

[24] Trygve Riis et al. *Hydrogen Storage-Gaps and Priorities*. Tech. rep. 2005.

[25] D. K. Ross. "Hydrogen storage: The major technological barrier to the development of hydrogen fuel cell cars". In: *Vacuum* 80.10 (2006), pp. 1084–1089. ISSN: 0042207X. DOI: 10.1016/j.vacuum.2006.03.030.

[26] *Compressed hydrogen storage | MAHYTEC*. 2019. [ONLINE]: http://www.mahytec.com/en/products/compressed-hydrogen-storage/.

[27] *Hydrogen Products - Hexagon Lincoln*. 2017. [ONLINE]: https://www.hexagonlincoln.com/hydrogen/hydrogen-products.

[28] Viking Cylinders. *Viking Cylinders® Lightweight Propane Tank | ZAP*. 2019. [ONLINE]: https://www.zapshrinkwrap.com/product/viking-cylinders-lightweight-propane-tank/.

[29] A123 Systems. *Nanophosphate® High Power Lithium Ion Cell ANR26650M1-B*. 2012. [ONLINE]: https://www.batteryspace.com/prod-specs/6610.pdf.

[30] *Sony VTC6 Battery Technical Information*. 2015. [ONLINE]: https://www.kronium.cz/uploads/SONY_US18650VTC6.pdf.

[31] R.W. De Doncker, D.M. Divan, and M.H. Kheraluwala. "A three-phase soft-switched high power density DC/DC converter for high power applications". In: *Conference Record of the 1988 IEEE Industry Applications Society Annual Meeting*. IEEE, pp. 796–805. DOI: 10.1109/IAS.1988.25153.

[32] Giulio Romeo, Ileana Moraglio, and Carlo Novarese. "ENFICA-FC: Preliminary Survey & Design of 2-Seat Aircraft Powered by Fuel Cells Electric Propulsion". In: September (2012), pp. 1–15. DOI: 10.2514/6.2007-7754.

[33] Tame-Power. *DC/DC energy converters | Buck, Boost or Bidirectional | Tame-Power*. [ONLINE]: https://www.tame-power.com/en/dc-dc-converters/dcdc-non-isolated-converters.

[34] Zekalabs. *DC/DC 15kW, 450V*. [ONLINE]: https://www.zekalabs.com/products/isolated-power-converters/dc-dc-isolated-converter-15kw-450v.

[35] Andrej Bernard Horvat and Pipistrel d.o.o. "Private communication". In: *Light-Sport* 2.April (2019), pp. 1–94.

[36] FAA. *Recommended standard traffic patterns and practices for aeronautical operations at airports without control towers*. Tech. rep. Federal Aviation Administration.

[37] Mohammad H Sadraey. *AIRCRAFT DESIGN Aerospace Series List Design and Analysis of Composite Structures: With applications to aerospace Structures*. John Wiley & Sons, Ltd., 2013. ISBN: 9781119953401.

[38] P. V. Aravind. *EXERGY ANALYSIS*. Tech. rep.

[39] Aurelien Du Pasquier et al. "A comparative study of Li-ion battery, supercapacitor and nonaqueous asymmetric hybrid devices for automotive applications". In: *Journal of Power Sources* 115.1 (Mar. 2003), pp. 171–178. ISSN: 0378-7753. DOI: 10.1016/S0378-7753(02)00718-8.

[40] Marc Rosen et al. "Using Exergy to Understand and Improve the Efficiency of Electrical Power Technologies". In: *Entropy* 11.4 (Nov. 2009), pp. 820–835. ISSN: 1099-4300. DOI: 10.3390/e11040820.

[41] Martin H. Weik and Martin H. Weik. "Maintenance Manual". In: *Computer Science and Communications Dictionary* 00 (2006), pp. 969–969. DOI: 10.1007/1-4020-0613-6{_}10968.

[42] D. Guida and M. Minutillo. "Design methodology for a PEM fuel cell power system in a more electrical aircraft". In: *Applied Energy* 192 (2017), pp. 446–456. ISSN: 03062619. DOI: 10.1016/j.apenergy.2016.10.090.

[43] Giulio Romeo et al. "A Fuel Cell Based Propulsion System for General Aviation Aircraft: The ENFICA-FC Experience". In: *SAE International Journal of Aerospace* (2011). ISSN: 1946-3901. DOI: 10.4271/2011-01-2522.

[44] Giulio Romeo et al. "Enfica-Fc : Design , Realization and Flight Test of All Electric 2-Seat Aircraft Powered By Fuel Cells". In: *27Th International Congress of the Aeronautical Sciences* (2010).

[45] P. Rathke et al. "Antares DLR-H2 Flying Test Bed for Development of Aircraft Fuel Cell Systems". In: *ECS Transactions* 51.1 (2013), pp. 229–241. ISSN: 1938-6737. DOI: 10.1149/05101.0229ecst.

[46] Johannes Schirmer et al. "Fuel Cell Systems for Aircraft Application & Antares DLR-H2 All-Electric Flying Testbed". In: January (2013), pp. 1–9. DOI: 10.2514/6.2013-936.

[47] Elena Bataller-Planes et al. "Power balance of a hybrid power source in a power plant for a small propulsion aircraft". In: *IEEE Transactions on Power Electronics* (2009). ISSN: 08858993. DOI: 10.1109/TPEL.2009.2022943.

[48] Nieves Lapeña-Rey et al. “First Fuel-Cell Manned Aircraft”. In: *Journal of Aircraft* 47.6 (2010), pp. 1825–1835. ISSN: 0021-8669. DOI: 10.2514/1.42234.

[49] Tom Koehler. *A green machine Boeing makes history with flights of Fuel Cell Demonstrator Airplane*. Tech. rep. Boeing Frontiers, 2009.

[50] Akira Nishizawa et al. “Fuel cell and Li-ion battery direct hybridization system for aircraft applications”. In: *Journal of Power Sources* 222 (2013), pp. 294–300. ISSN: 03787753. DOI: 10.1016/j.jpowsour.2012.09.011.

[51] Jan Becker et al. “Design of a Safe and Reliable Li-ion Battery System for Applications in Airborne System”. In: *52nd Aerospace Sciences Meeting*. Reston, Virginia: American Institute of Aeronautics and Astronautics, Jan. 2014. ISBN: 978-1-62410-256-1. DOI: 10.2514/6.2014-0380.

[52] Yong Song Chen, Sheng Miao Lin, and Boe Shong Hong. “Experimental study on a passive fuel Cell/Battery hybrid power system”. In: *Energies* 6.12 (2013), pp. 6413–6422. ISSN: 19961073. DOI: 10.3390/en6126413.

[53] Remzi Can Samsun et al. “A battery-fuel cell hybrid auxiliary power unit for trucks: Analysis of direct and indirect hybrid configurations”. In: *Energy Conversion and Management* 127 (Nov. 2016), pp. 312–323. ISSN: 0196-8904. DOI: 10.1016/J.ENCONMAN.2016.09.025.

[54] Asimptote. *Cycle-Tempo*. [ONLINE]: http://www.asimptote.nl/software/cycle-tempo/.

[55] K.P. Adzakpa et al. “Transient air cooling thermal modeling of a PEM fuel cell”. In: *Journal of Power Sources* 179.1 (Apr. 2008), pp. 164–176. ISSN: 0378-7753. DOI: 10.1016/J.JPOWSOUR.2007.12.102.

[56] Yuyao Shan and Song Y. Choe. “A high dynamic PEM fuel cell model with temperature effects”. In: *Journal of Power Sources* (2005). ISSN: 03787753. DOI: 10.1016/j.jpowsour.2004.12.033.

[57] Toyoaki Matsuura et al. “Degradation phenomena in PEM fuel cell with dead-ended anode”. In: *International Journal of Hydrogen Energy* (2013). ISSN: 03603199. DOI: 10.1016/j.ijhydene.2013.06.096.

[58] Aboubakr M. Abdullah et al. “Temperature gradients measurements within a segmented H2/air PEM fuel cell”. In: *Journal of Power Sources* (2007). ISSN: 03787753. DOI: 10.1016/j.jpowsour.2007.07.044.

[59] Jintae Kim et al. “Degradation modeling and operational optimization for improving thelifetime of high-temperature PEM (proton exchange membrane) fuel cells”. In: *Energy* (2014). ISSN: 03605442. DOI: 10.1016/j.energy.2013.08.053.

[60] M. Tohidi, S. H. Mansouri, and H. Amiri. “Effect of primary parameters on the performance of PEM fuel cell”. In: *International Journal of Hydrogen Energy*. 2010. DOI: 10.1016/j.ijhydene.2010.03.112.

[61] Yaliang Tang et al. “Stresses in Proton Exchange Membranes Due to Hygro-Thermal Loading”. In: *Journal of Fuel Cell Science and Technology* (2006). ISSN: 1550624X. DOI: 10.1115/1.2173666.

[62] S. M. Rahgoshay et al. “Thermal investigation of a PEM fuel cell with cooling flow field”. In: *Energy* (2017). ISSN: 03605442. DOI: 10.1016/j.energy.2017.05.151.

[63] Uwe Beuscher, Simon J.C. Cleghorn, and William B. Johnson. “Challenges for PEM fuel cell membranes”. In: *International Journal of Energy Research* (2005). ISSN: 0363907X. DOI: 10.1002/er.1142.

[64] Faysal Tiss, Ridha Chouikh, and Amenallah Guizani. “Dynamic modeling of a PEM fuel cell with temperature effects”. In: *International Journal of Hydrogen Energy*. 2013. DOI: 10.1016/j.ijhydene.2012.09.101.

[65] Yuyao Shan and Song Y. Choe. “Modeling and simulation of a PEM fuel cell stack considering temperature effects”. In: *Journal of Power Sources* (2006). ISSN: 03787753. DOI: 10.1016/j.jpowsour.2005.09.053.

[66] A.V. Anantaraman and C.L. Gardner. “Studies on ion-exchange membranes. Part 1. Effect of humidity on the conductivity of Nafion®”. In: *Journal of Electroanalytical Chemistry* 414.2 (Jan. 1996), pp. 115–120. ISSN: 1572-6657. DOI: 10.1016/0022-0728(96)04690-6.

[67] M. Casciola et al. “On the decay of Nafion proton conductivity at high temperature and relative humidity”. In: *Journal of Power Sources* 162.1 (Nov. 2006), pp. 141–145. ISSN: 0378-7753. DOI: 10.1016/J.JPOWSOUR.2006.06.023.

[68] Hyunchul Ju, Hua Meng, and Chao-Yang Wang. “A single-phase, non-isothermal model for PEM fuel cells”. In: *International Journal of Heat and Mass Transfer* 48.7 (Mar. 2005), pp. 1303–1315. ISSN: 0017-9310. DOI: 10.1016/J.IJHEATMASSTRANSFER.2004.10.004.

[69] Jaewan Park and Xianguo Li. “Effect of flow and temperature distribution on the performance of a PEM fuel cell stack”. In: *Journal of Power Sources* 162.1 (Nov. 2006), pp. 444–459. ISSN: 0378-7753. DOI: 10.1016/J.JPOWSOUR.2006.07.030.

[70] Lin Wang et al. “A parametric study of PEM fuel cell performances”. In: *International Journal of Hydrogen Energy* 28.11 (2003), pp. 1263–1272. ISSN: 03603199. DOI: 10.1016/S0360-3199(02)00284-7.

[71] S.O. O. Mert, I. Dincer, and Z. Ozcelik. “Performance investigation of a transportation PEM fuel cell system”. In: *International Journal of Hydrogen Energy* 37.1 (Jan. 2012), pp. 623–633. ISSN: 03603199. DOI: 10.1016/j.ijhydene.2011.09.021.

[72] Ankit Rohatgi. *WebPlotDigitizer*. 2019. [ONLINE]: https://automeris.io/WebPlotDigitizer%0A%0A.

[73] MATLAB. *Find minimum of constrained nonlinear multivariable function - MATLAB fmincon*. [ONLINE]: https://www.mathworks.com/help/optim/ug/fmincon.html.

[74] K. C. Neyerlin et al. “Study of the Exchange Current Density for the Hydrogen Oxidation and Evolution Reactions”. In: *Journal of The Electrochemical Society* 154.7 (2007), B631. ISSN: 00134651. DOI: 10.1149/1.2733987.

[75] K. T. Adjemian et al. “Silicon Oxide Nafion Composite Membranes for Proton-Exchange Membrane Fuel Cell Operation at 80-140°C”. In: *Journal of The Electrochemical Society* 149.3 (2002), A256. ISSN: 00134651. DOI: 10.1149/1.1445431.

[76] Sandip Dutta, Sirivatch Shimpalee, and J. W. Van Zee. “Numerical prediction of mass-exchange between cathode and anode channels in a PEM fuel cell”. In: *International Journal of Heat and Mass Transfer* (2001). ISSN: 00179310. DOI: 10.1016/S0017-9310(00)00257-X.

[77] Trung V. Nguyen and R White. “A Water and Heat Management Model for Proton-Exchange-Membrane Fuel Cells”. In: *Journal of Electrochemical Society* 140.8 (1993), pp. 2178–2186. ISSN: 00134651. DOI: 10.1149/1.2220792.

[78] Donald T. Sawyer et al. *Electrochemistry for chemists*. Wiley, 1995, p. 505. ISBN: 9780471594680.

[79] U.S. Department of Energy. “Fuel cell handbook”. In: *Choice Reviews Online* 26.11 (2013), pp. 26–6292. ISSN: 0009-4978. DOI: 10.5860/choice.26-6292.

[80] Duke University. *What's a good value for R-squared?* [ONLINE]: https://people.duke.edu/~rnau/rsquared.htm.

[81] Shou-Shing Hsieh, Bing-Shyan Her, and Yi-Ji Huang. "Effect of pressure drop in different flow fields on water accumulation and current distribution for a micro PEM fuel cell". In: *Energy Conversion and Management* 52.2 (Feb. 2011), pp. 975–982. ISSN: 0196-8904. DOI: 10.1016/J.ENCONMAN.2010.08.025.

[82] CoolerMaster. *MasterFan Pro 120 Air Flow | Cooler Master*. [ONLINE]: https://www.coolermaster.com/catalog/coolers/case-fan/masterfan-pro-120-af/.

[83] Theo Woudstra and TU Delft. *Private communication*. 2019.

[84] Jürgen Stumper et al. "In-situ methods for the determination of current distributions in PEM fuel cells". In: *Electrochimica Acta* 43.24 (Aug. 1998), pp. 3773–3783. ISSN: 0013-4686. DOI: 10.1016/S0013-4686(98)00137-6.

[85] Xiqiang Yan et al. "The study on transient characteristic of proton exchange membrane fuel cell stack during dynamic loading". In: *Journal of Power Sources* 163.2 (Jan. 2007), pp. 966–970. ISSN: 0378-7753. DOI: 10.1016/J.JPOWSOUR.2006.09.075.

[86] Robert T. Balmer. "Vapor and Gas Power Cycles". In: *Modern Engineering Thermodynamics* (Jan. 2011), pp. 447–534. DOI: 10.1016/B978-0-12-374996-3.00013-0.

[87] Hasan K. Atiyeh et al. "Experimental investigation of the role of a microporous layer on the water transport and performance of a PEM fuel cell". In: *Journal of Power Sources* 170.1 (June 2007), pp. 111–121. ISSN: 0378-7753. DOI: 10.1016/J.JPOWSOUR.2007.04.016.

[88] Sandip Mazumder and James Vernon Cole. "Rigorous 3-D Mathematical Modeling of PEM Fuel Cells". In: *Journal of The Electrochemical Society* 150.11 (Nov. 2003), A1503. ISSN: 00134651. DOI: 10.1149/1.1615608.

[89] Zhihao Zhang et al. "An improved dynamic model considering effects of temperature and equivalent internal resistance for PEM fuel cell power modules". In: *Journal of Power Sources* 161.2 (Oct. 2006), pp. 1062–1068. ISSN: 0378-7753. DOI: 10.1016/J.JPOWSOUR.2006.05.030.

[90] Rong-Jong Wai et al. "High-Efficiency DC-DC Converter With High Voltage Gain and Reduced Switch Stress". In: *IEEE Transactions on Industrial Electronics* 54.1 (Feb. 2007), pp. 354–364. ISSN: 0278-0046. DOI: 10.1109/TIE.2006.888794.

[91] M. Nymand and M.A.E. Andersen. "High-Efficiency Isolated Boost DC–DC Converter for High-Power Low-Voltage Fuel-Cell Applications". In: *IEEE Transactions on Industrial Electronics* 57.2 (Feb. 2010), pp. 505–514. ISSN: 0278-0046. DOI: 10.1109/TIE.2009.2036024.

[92] Joey Hoogendoorn. *Fuel Cell and Battery Hybrid System Optimization: Towards Increased Range and Endurance*. 2018. [ONLINE]: https://repository.tudelft.nl/islandora/object/uuid%3A6e274095-9920-4d20-9e11-d5b76363e709.

[93] Oliver Gröger, Hubert A. Gasteiger, and Jens-Peter Suchsland. "Review—Electromobility: Batteries or Fuel Cells?" In: *Journal of The Electrochemical Society* 162.14 (Jan. 2015), A2605–A2622. ISSN: 0013-4651. DOI: 10.1149/2.0211514jes.

[94] P. V. Aravind and TU Delft. *Private communication*. 2019.

[95] Ulf Bossel. *SOLID OXIDE FUEL CELLS FOR TRANSPORTATION*. Tech. rep. 2005, pp. 3–4.

[96] Thomas L. Cable and Stephen W. Sofie. "A symmetrical, planar SOFC design for NASA's high specific power density requirements". In: *Journal of Power Sources* 174.1 (Nov. 2007), pp. 221–227. ISSN: 0378-7753. DOI: 10.1016/J.JPOWSOUR.2007.08.110.

[97] Binghe Liu et al. "Mechanical integrity of 18650 lithium-ion battery module: Packing density and packing mode". In: *Engineering Failure Analysis* 91 (Sept. 2018), pp. 315–326. ISSN: 1350-6307. DOI: 10.1016/J.ENGFAILANAL.2018.04.041.

[98] Olivier Tremblay et al. "Experimental Validation of a Battery Dynamic Model for EV Applications". In: *World Electric Vehicle Journal* 3.2 (June 2009), pp. 289–298. ISSN: 2032-6653. DOI: 10.3390/wevj3020289.

[99] Adaptive Energy LLC. *D350XR | Fuel Cell Energy | Portable Power | Adaptive Energy | United States*. [ONLINE]: https://www.adaptiveenergyllc.com/d350xr.

Appendix A

Exergy flow diagrams

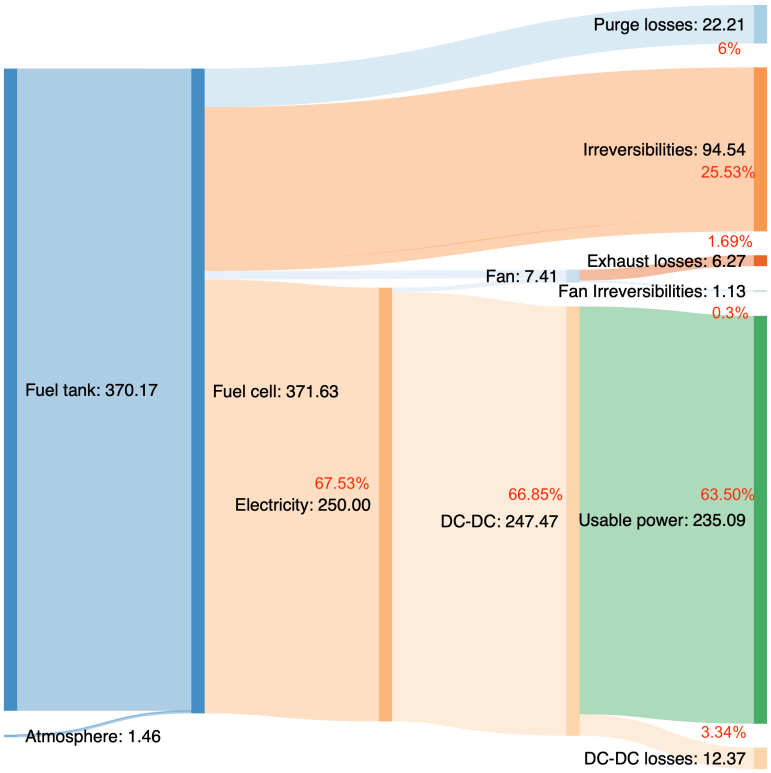

Figure A.1: Exergy flow diagram for fuel cell operating at 25% of rated power density.

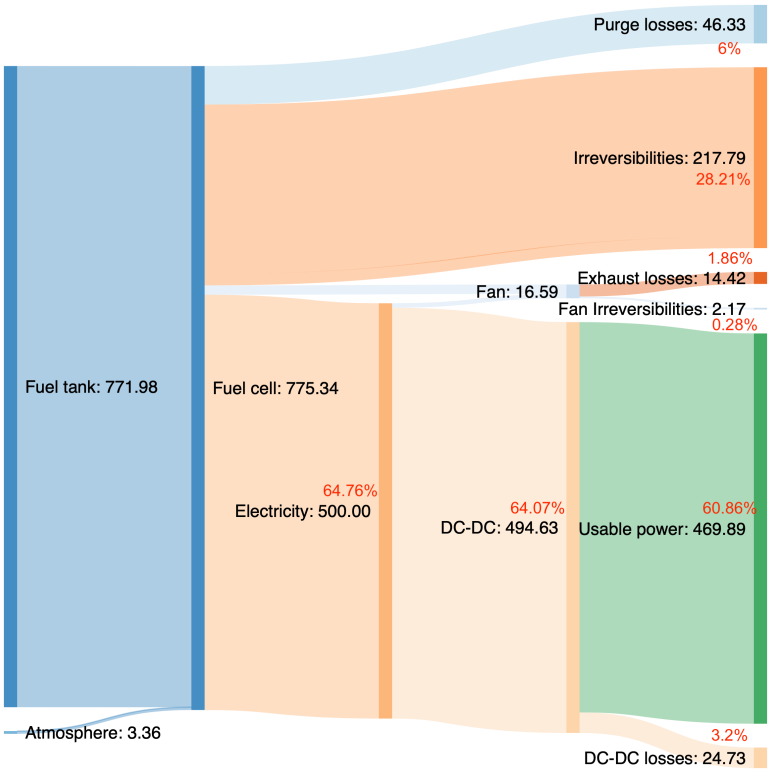

Figure A.2: Exergy flow diagram for fuel cell operating at 50% of rated power density.

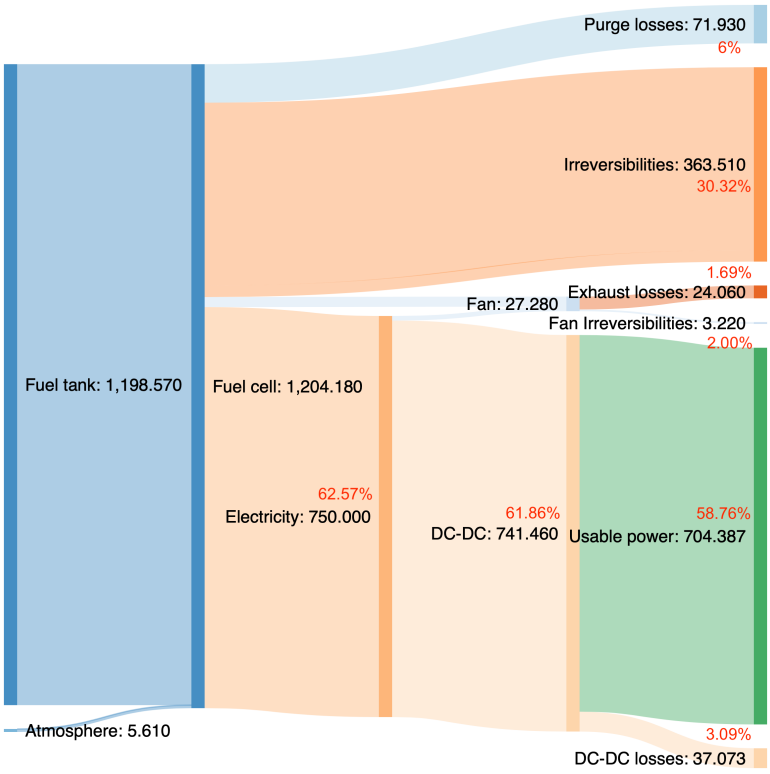

Figure A.3: Exergy flow diagram for fuel cell operating at 75% of rated power density.

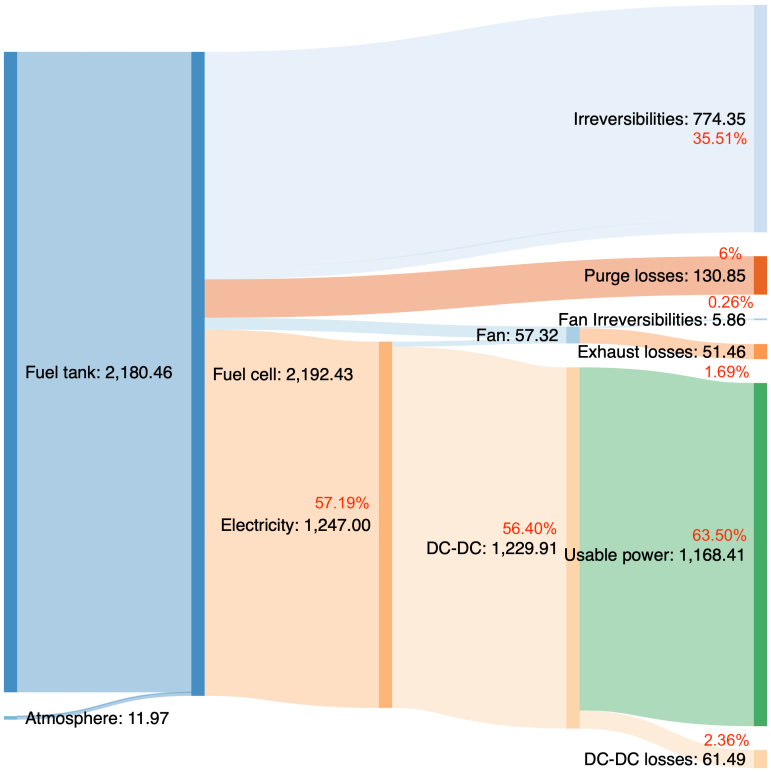

Figure A.4: Exergy flow diagram for fuel cell operating at 125% of rated power density.

Appendix B

Theoretical system sizing results

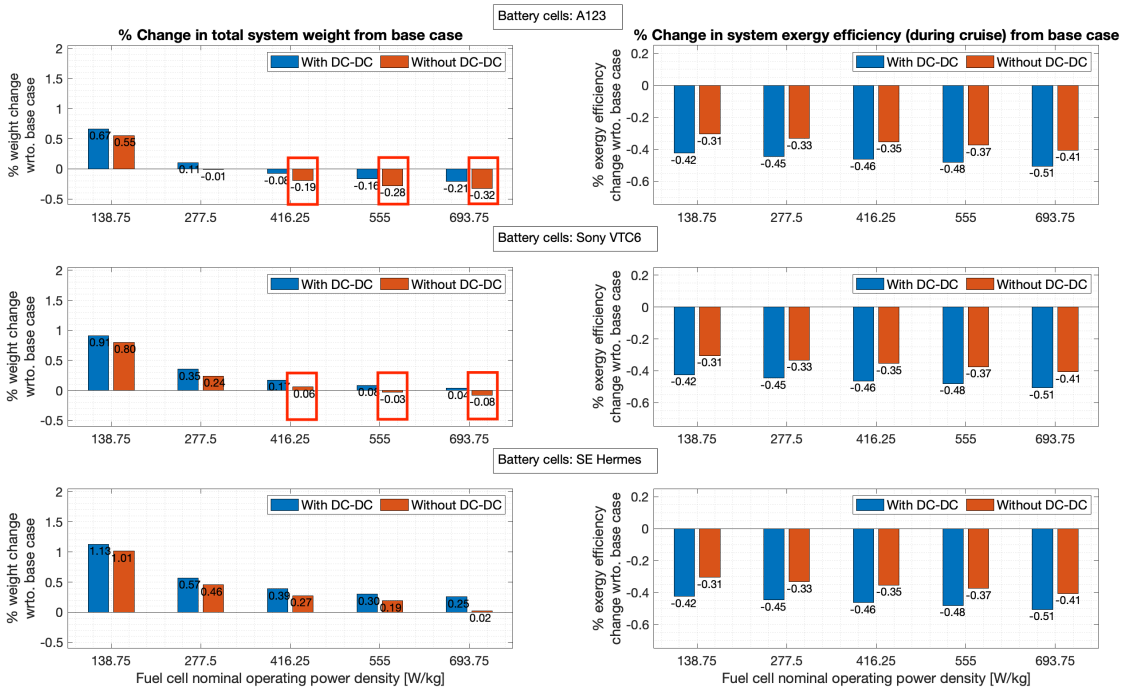

Figure B.1: Weight and exergy efficiency comparison against base case for E110-FCPEM-BL01-DC(Variable)-PD(Variable)-BT(Variable)-CFCCruise.

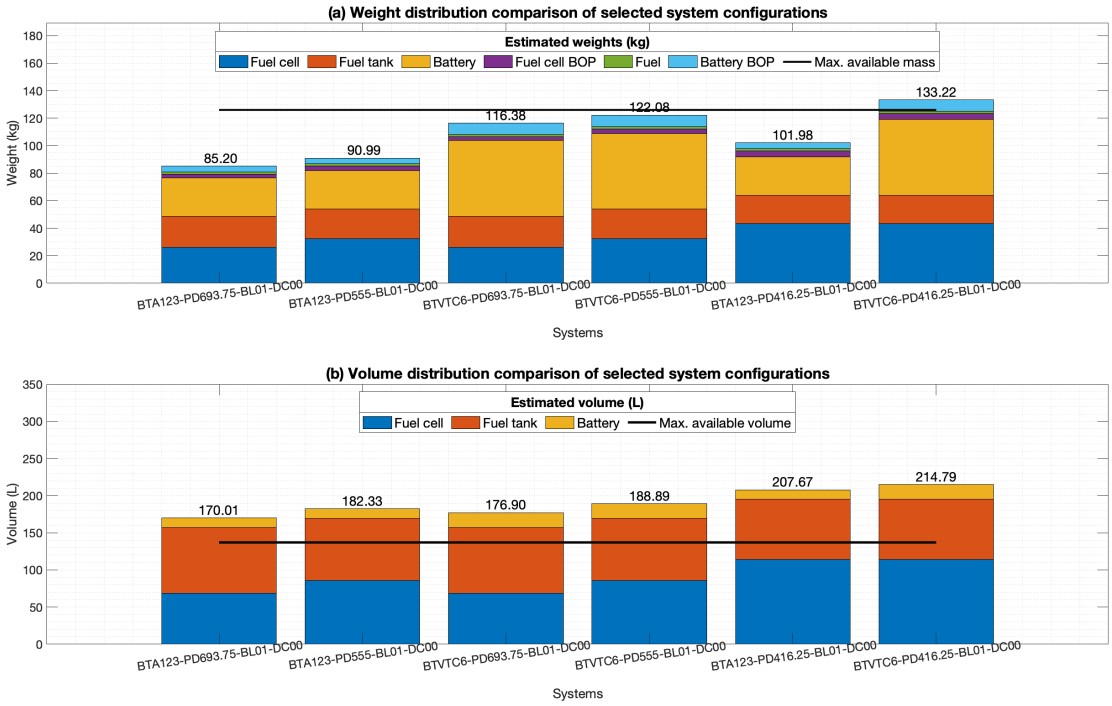

Figure B.2: Weight and volume distribution of the six lowest weight combinations for the case: E110-FCPEM-BL01-DC(Variable)-PD(Variable)-BT(Variable)-CFCCruise

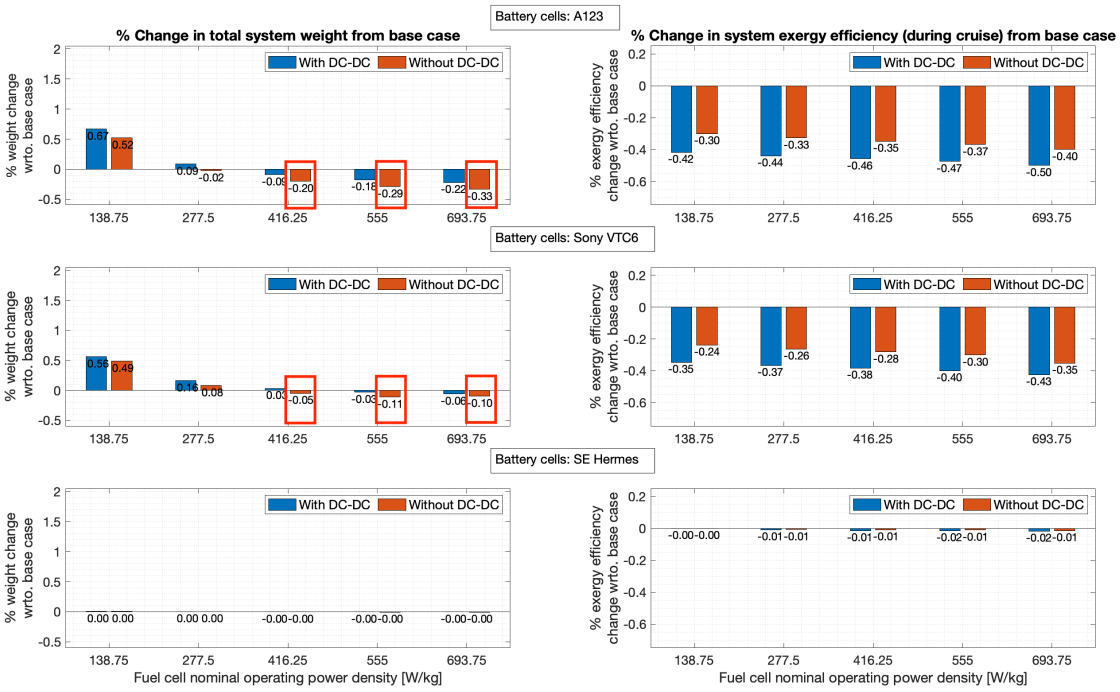

Figure B.3: Weight and exergy efficiency comparison against base case for E110-FCPEM-BL01-DC(Variable)-PD(Variable)-BT(Variable)-COPT.

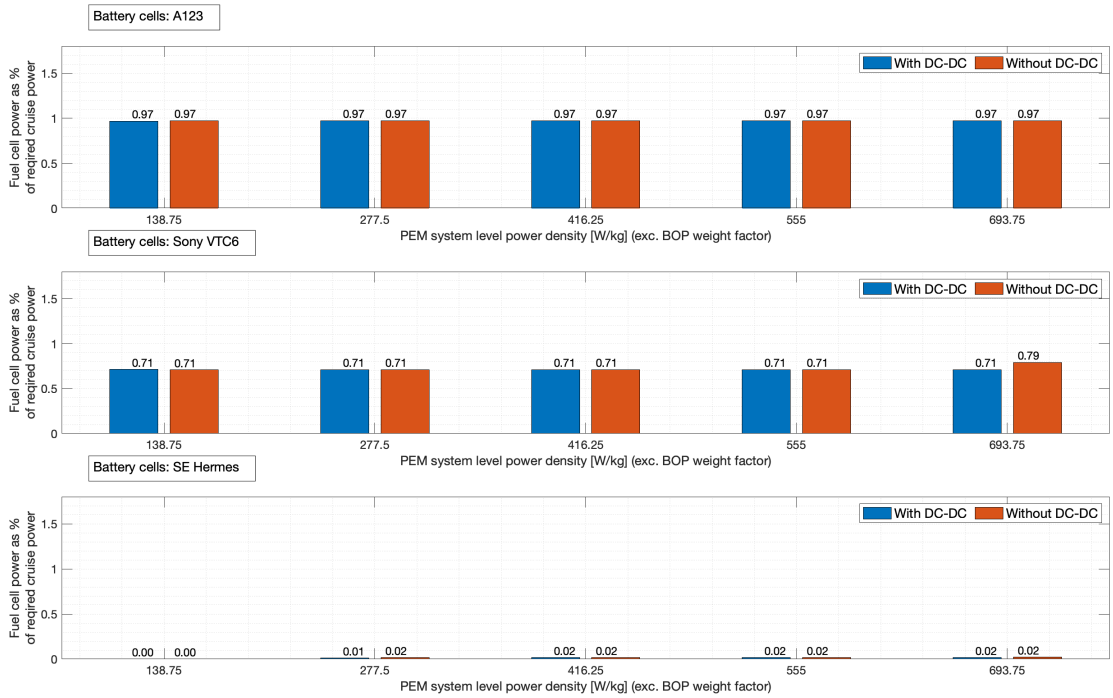

Figure B.4: Comparison of degree of hybridization for all the sized systems for case: E110-FCPEM-BL01-DC(Variable)-PD(Variable)-BT(Variable)-COPT.

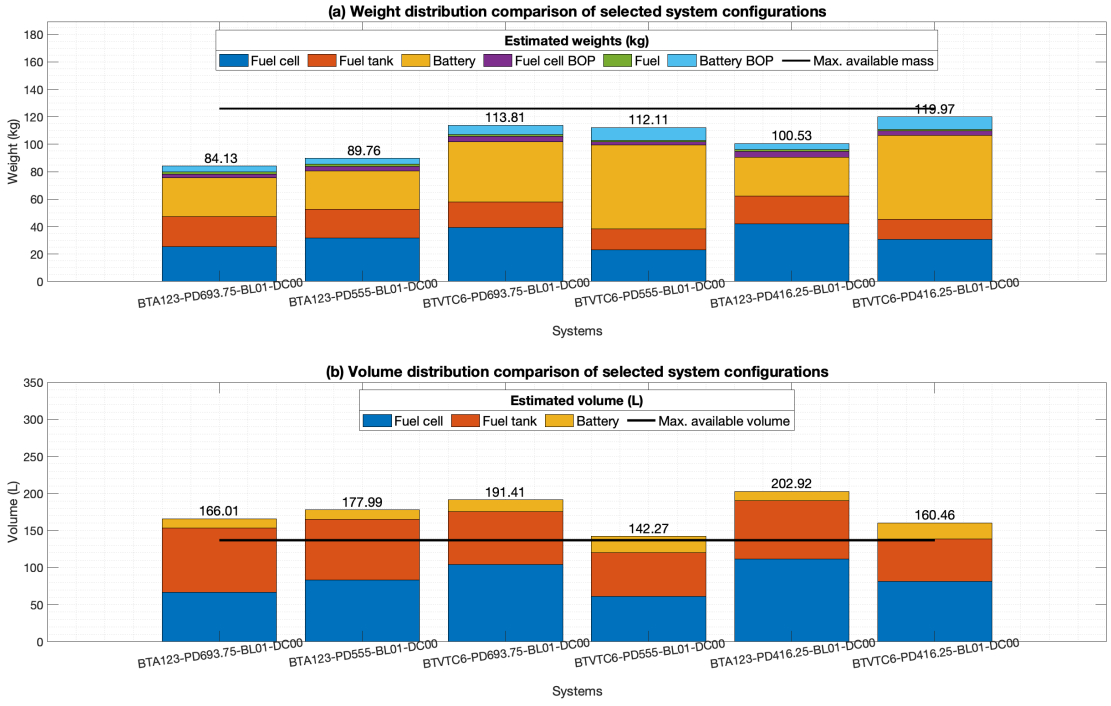

Figure B.5: Weight and volume distribution of the six lowest weight combinations for the case: E110-FCPEM-BL01-DC(Variable)-PD(Variable)-BT(Variable)-COPT.

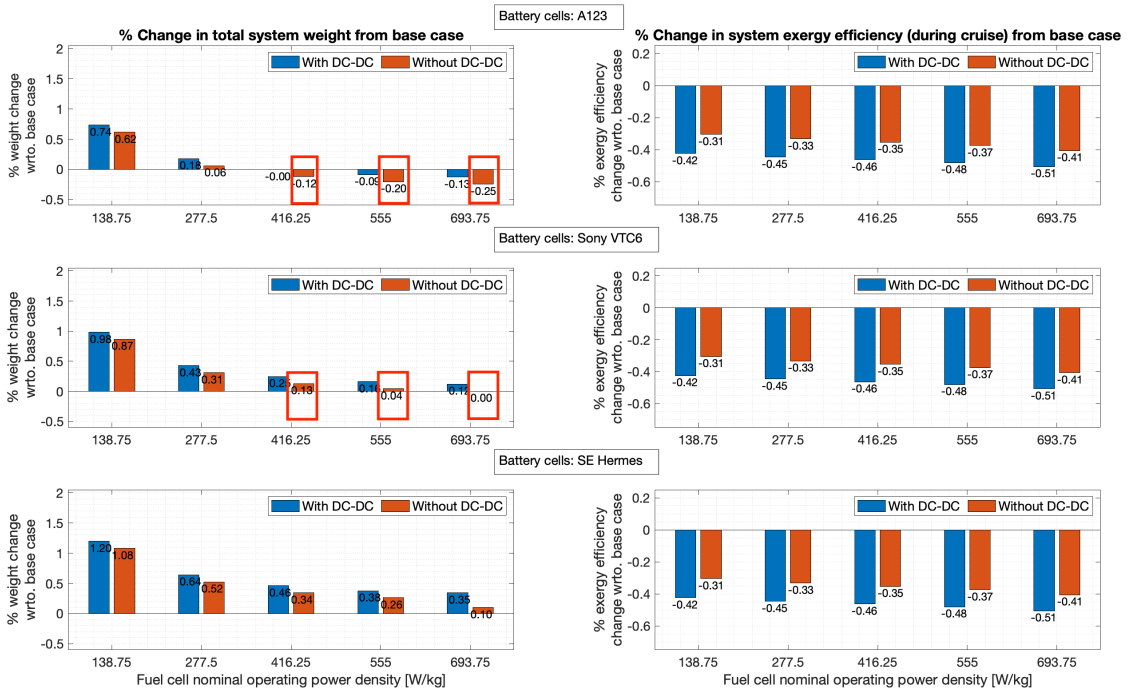

Figure B.6: Weight and exergy efficiency comparison against base case for E155-FCPEM-BL01-DC(Variable)-PD(Variable)-BT(Variable)-CFCCruise.

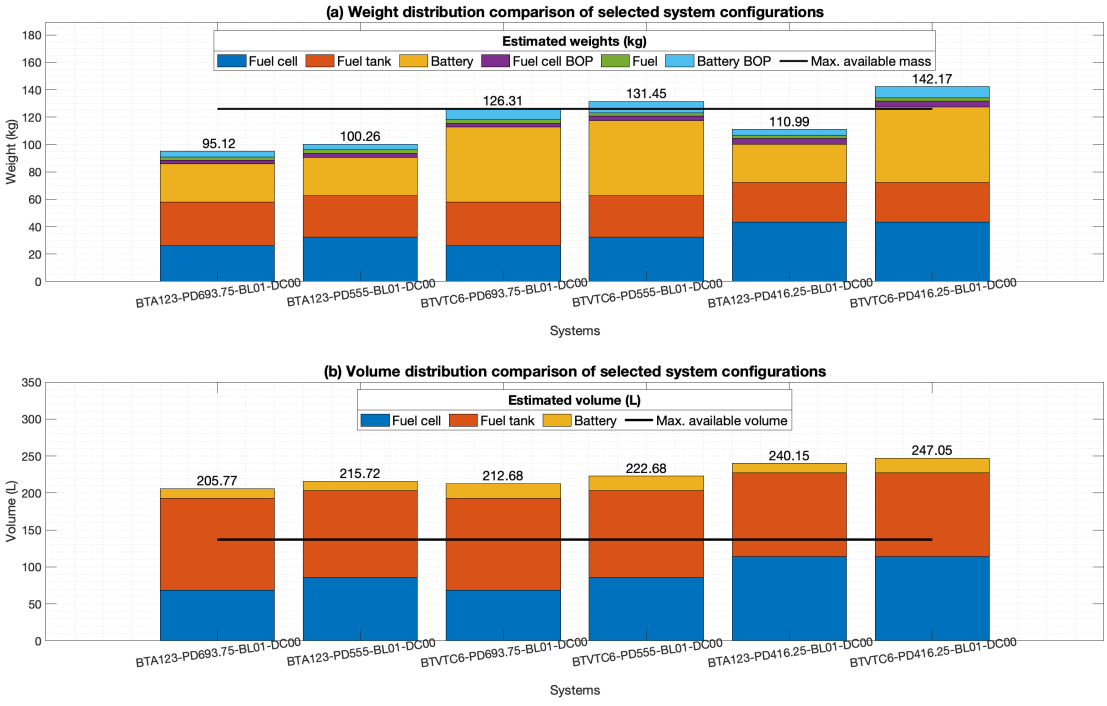

Figure B.7: Weight and volume distribution of the six lowest weight combinations for the case: E155-FCPEM-BL01-DC(Variable)-PD(Variable)-BT(Variable)-CFCCruise

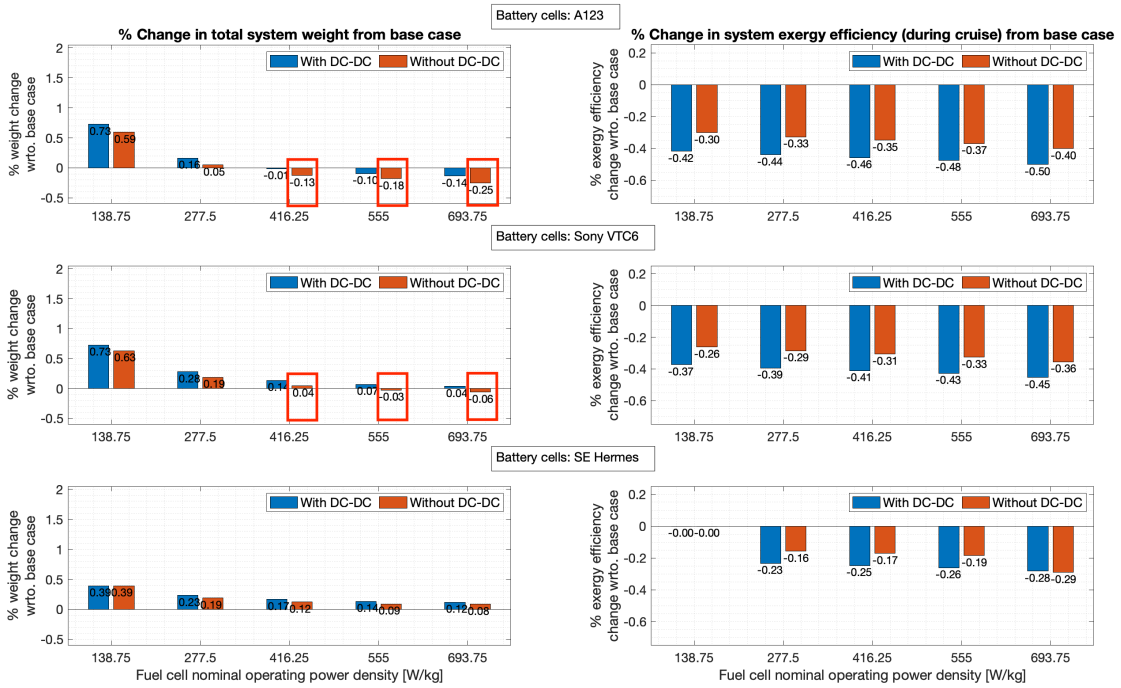

Figure B.8: Weight and exergy efficiency comparison against base case for E155-FCPEM-BL01-DC(Variable)-PD(Variable)-BT(Variable)-COPT.

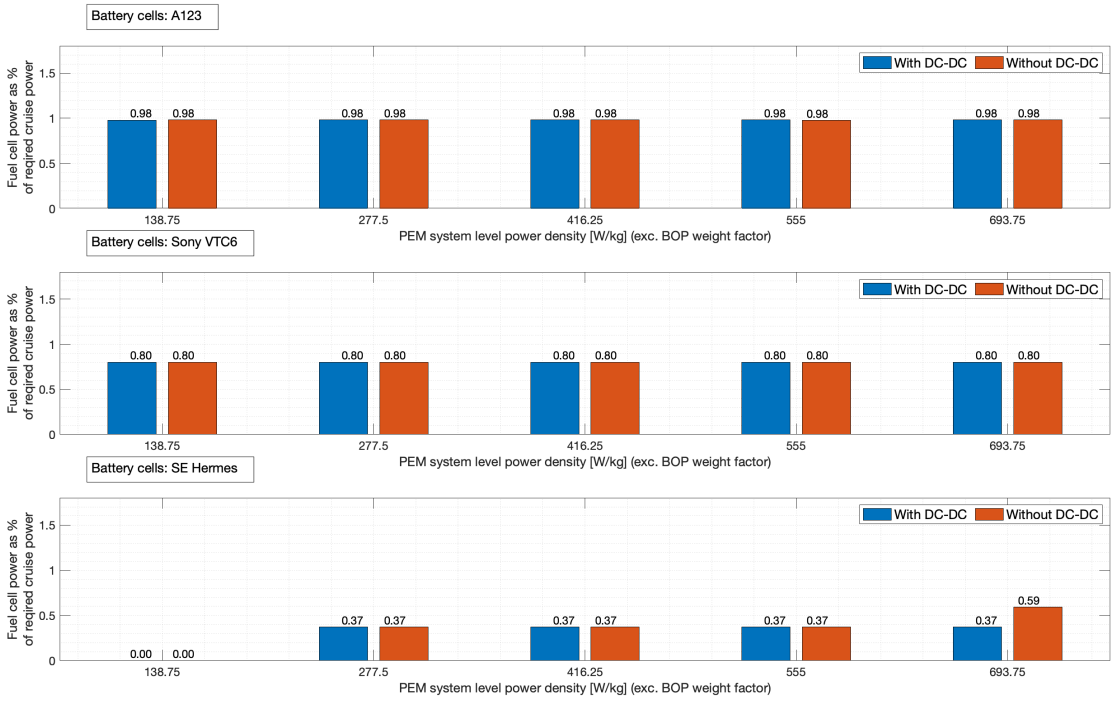

Figure B.9: Comparison of degree of hybridization for all the sized systems for case: E155-FCPEM-BL01-DC(Variable)-PD(Variable)-BT(Variable)-COPT.

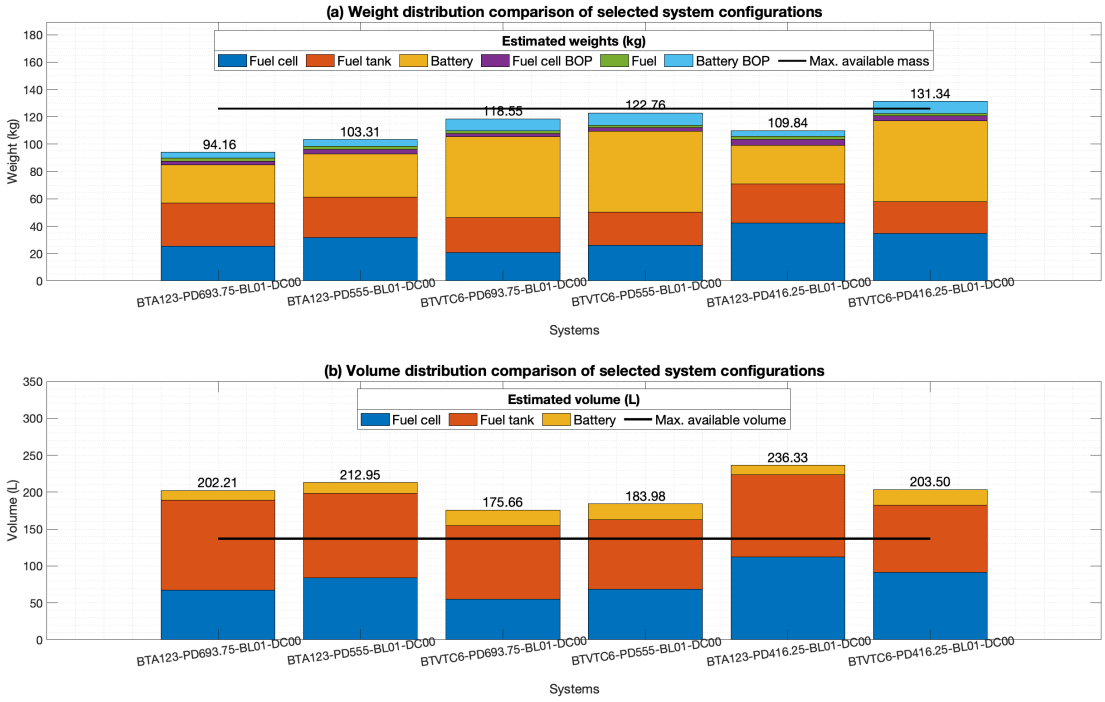

Figure B.10: Weight and volume distribution of the six lowest weight combinations for the case: E155-FCPEM-BL01-DC(Variable)-PD(Variable)-BT(Variable)-COPT.

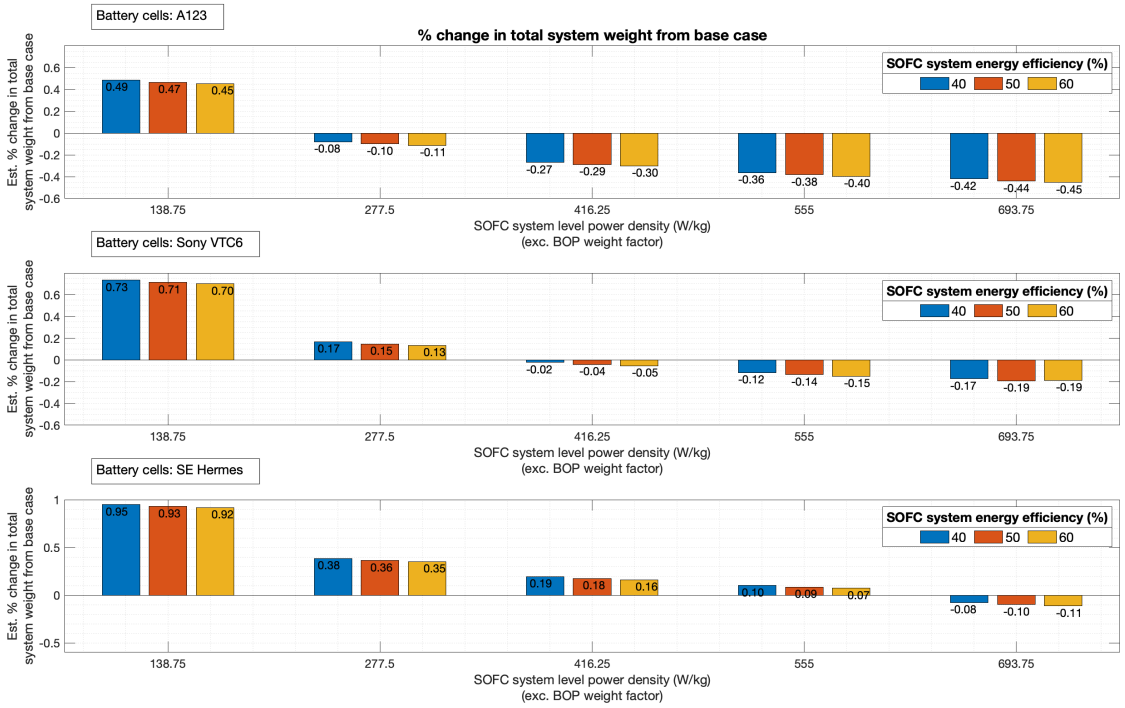

Figure B.11: Weight comparison against base case for E110-FCSOFC-PD(Variable)-BT(Variable)-CFCCruise

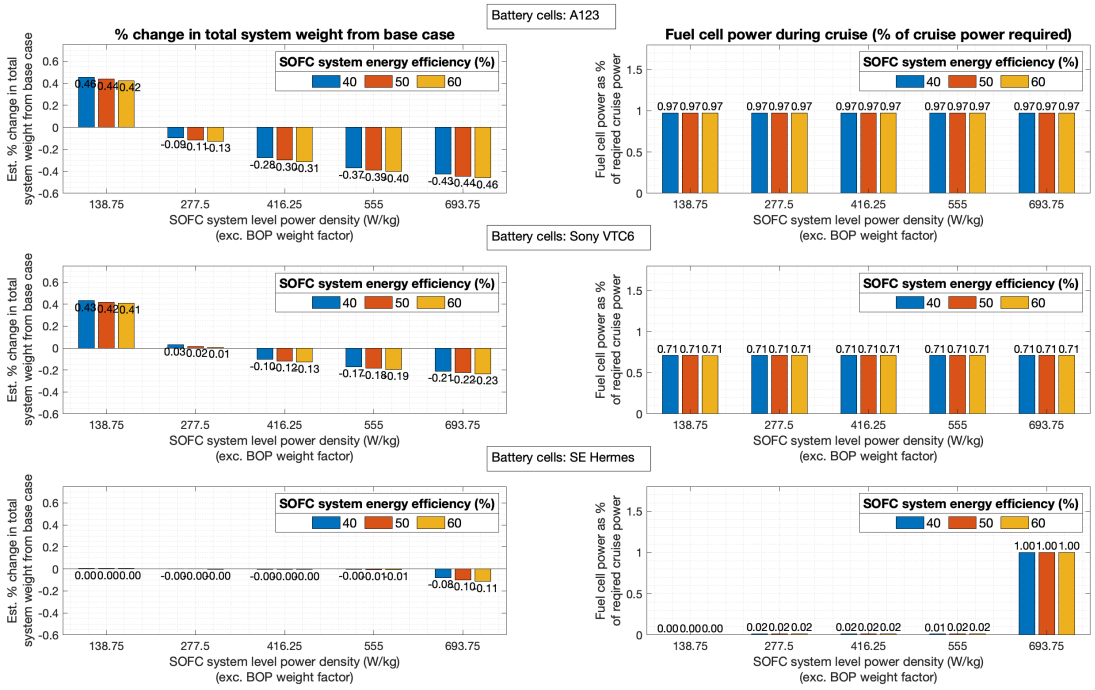

Figure B.12: Weight comparison and degree of hybridization for E110-FCSOFC-PD(Variable)-BT(Variable)-COPT

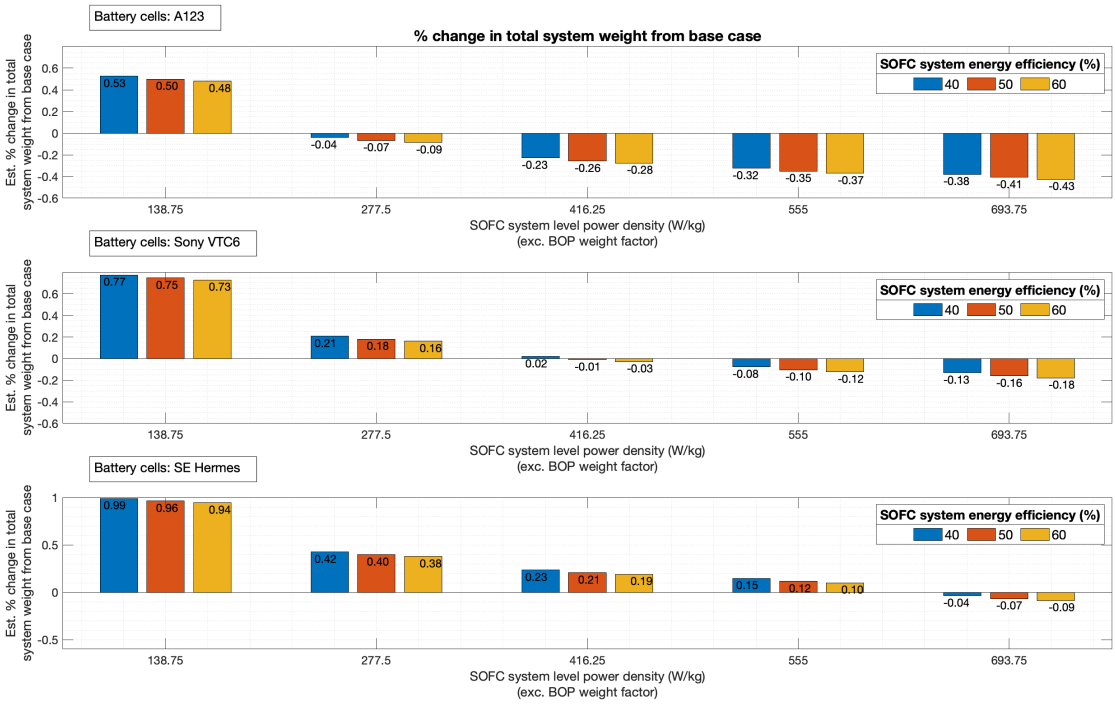

Figure B.13: Weight comparison against base case for E155-FCSOFC-PD(Variable)-BT(Variable)-CFCCruise

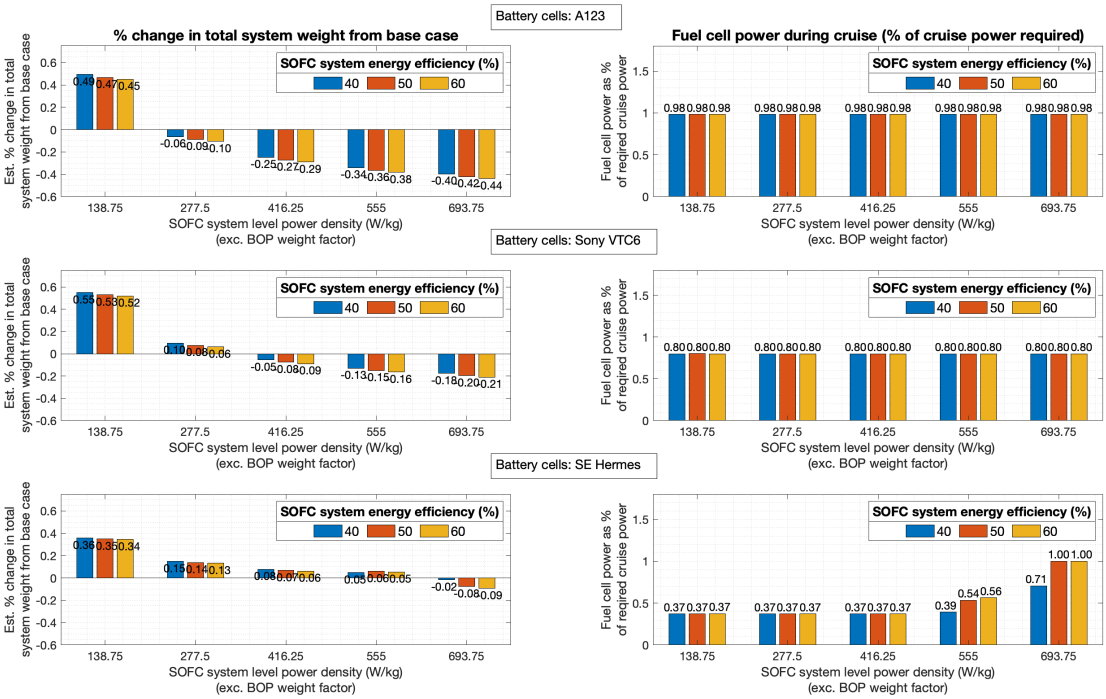

Figure B.14: Weight comparison and degree of hybridization for E155-FCSOFC-PD(Variable)-BT(Variable)-COPT

Appendix C

Effect of battery configuration on fuel cell power output

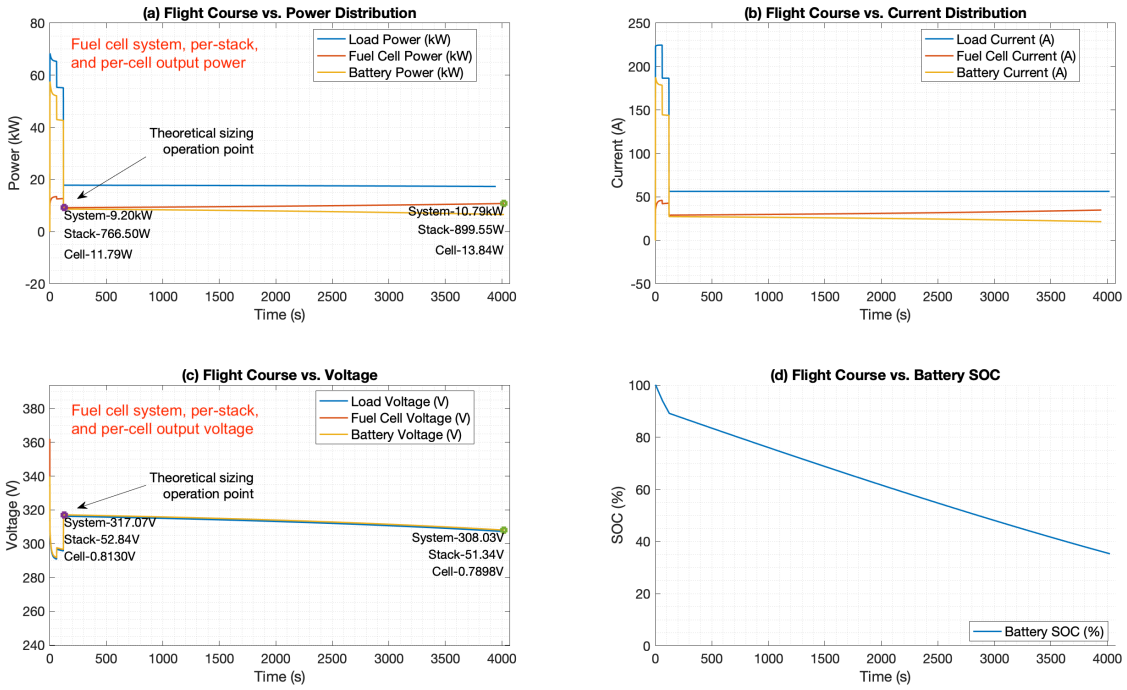

Figure C.1: Simulink simulation for battery configuration: 78S-16P for PD416.25 indicating fuel cell power and voltage at different points in time during cruise.

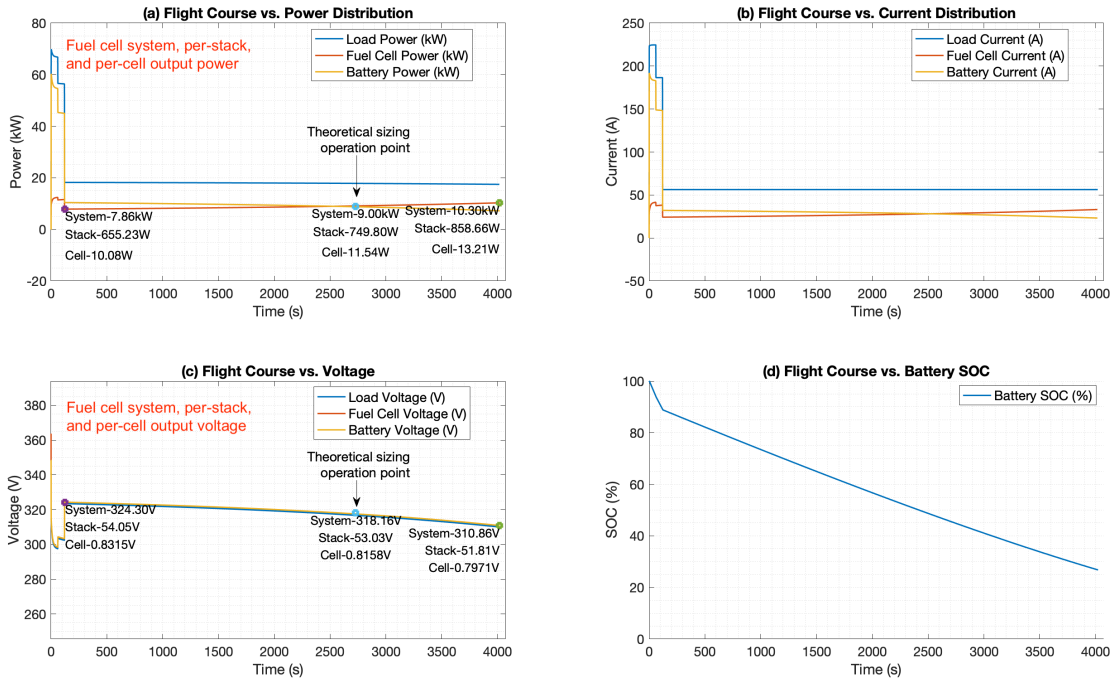

Figure C.2: Simulink simulation for battery configuration: 80S-16P for PD416.25 indicating fuel cell power and voltage at different points in time during cruise.

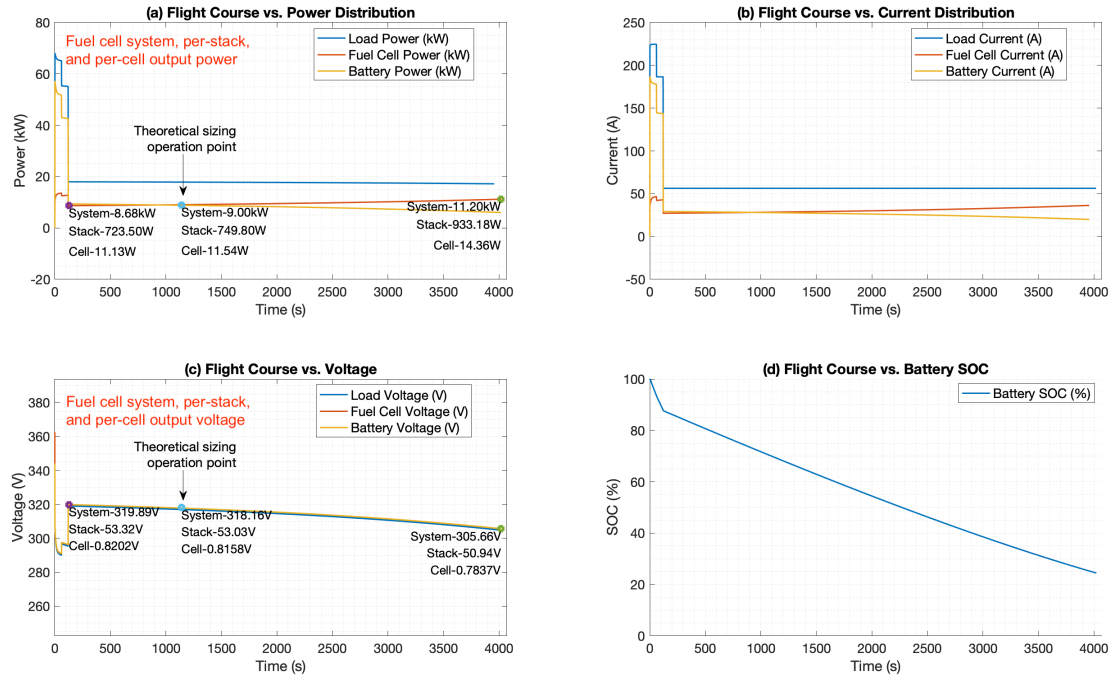

Figure C.3: Simulink simulation for battery configuration: 78S-14P for PD416.25 indicating fuel cell power and voltage at different points in time during cruise.

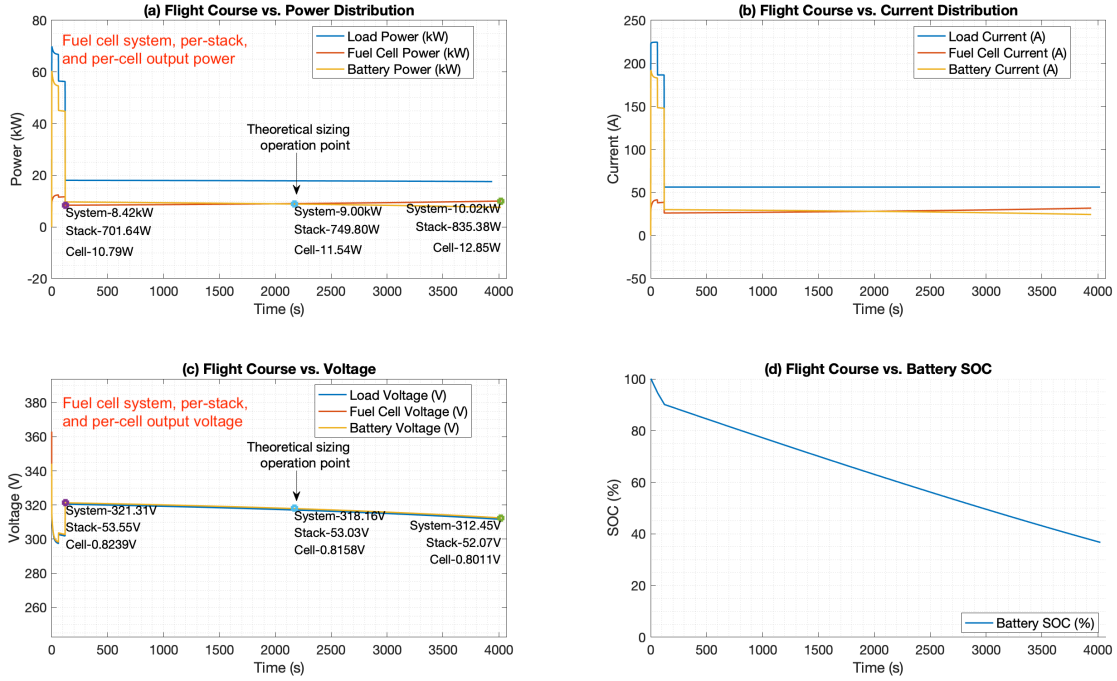

Figure C.4: Simulink simulation for battery configuration: 78S-18P for PD416.25 indicating fuel cell power and voltage at different points in time during cruise.